

**Geometrical and geological analysis of photogrammetrically
measured deformed sediments of the fjord zone,
central East Greenland**

Hans-Jørgen Bengaard

September 1989

Open File Series

The Open File Series consists of un-edited reports and maps that are made available quickly in limited numbers to the public. They are a non-permanent form of publication that may be cited as sources of information. Certain reports may be replaced later by edited versions.

Citation form

Open File Series Grønlands Geologiske Undersøgelse

conveniently abbreviated to:

Open File Ser. Grønlands geol. Unders.

GGU's Open File Series består af uredigerede rapporter og kort, som publiceres hurtigt og i et begrænset antal. Disse publikationer er midlertidige og kan anvendes som kildemateriale. Visse af rapporterne vil evt. senere blive erstattet af redigerede udgaver.

ISSN 0903-7322

GRØNLANDS GEOLOGISKE UNDERSØGELSE

Open File Series No. 89/6

Geometrical and geological analysis of photogrammetrically
measured deformed sediments of the fjord zone,
central East Greenland

Hans-Jørgen Bengaard

September 1989

| CONTENTS | P. | |
|----------|---|----|
| 1 | Abstract | 7 |
| 2 | Introduction | 9 |
| 3 | Mathematical modelling of folded surfaces | 13 |
| 3.1 | Fold segments | 13 |
| 3.2 | Conepoint calculation | 14 |
| 3.3 | Projection onto profile plane | 16 |
| 3.4 | Fitting of a polynomium to the profile of a folded surface | 19 |
| 3.5 | Calculation of line length shortening | 22 |
| 3.6 | Deformation mechanism model | 23 |
| 3.7 | Construction of new folded surface | 29 |
| 3.8 | Deformation mechanism analysis | 30 |
| 3.9 | Strain ellipse calculation | 35 |
| 4 | Detailed photoinvestigation of the western part of Ella Ø, using mathematical models | 39 |
| 4.1 | The Eleonore Bugt anticline in the 'D' fault block | 42 |
| 4.2 | The Eleonore Bugt anticline in the 'X' fault block | 48 |
| 4.3 | The Central syncline | 49 |
| 5 | Photo-interpretation of the Eleonore Bay Group of the Fjord Zone, central East Greenland | 53 |
| 5.1 | Introduction | 53 |
| 5.2 | Stratigraphy and photo-geological characteristics of the rocks of the area | 53 |
| 5.3 | Ages of the rocks of the photo-interpreted area | 54 |
| 6 | Structural analysis of photo-interpreted area | 67 |
| 6.1 | Introduction | 67 |
| 6.2 | Upper Ordovician structures | 70 |
| 6.2.1 | Basal décollement zone | 71 |
| 6.2.2 | Folds of general north-south axial direction | 71 |
| 6.2.2.1 | The Border syncline | 71 |
| 6.2.2.2 | The Kap Alfred anticline | 71 |
| 6.2.2.3 | The Nunatakletscher anticline | 73 |
| 6.2.2.4 | The Central syncline | 73 |
| 6.2.2.5 | The Erimitdal syncline | 74 |
| 6.2.2.6 | The Eleonore Bugt anticline | 74 |
| 6.2.2.7 | The Agardh Bjerg anticline | 75 |
| 6.2.2.8 | The Gletscherpas syncline | 75 |
| 6.2.2.9 | The Brogetdal anticline | 75 |
| 6.2.3 | East-west striking faults | 75 |
| 6.2.4 | Low angle tension faults | 76 |
| 6.3 | Discussion of the Upper Ordovician deformation | 77 |
| 6.3.1 | General westward translation of the Eleonore Bay Group | 77 |
| 6.3.2 | Dynamic models for the translation | 79 |
| 6.4 | Devonian deformation | 82 |
| 6.4.1 | Fault system associated with the eastern margin of the Eleonore Bay Group in the new area | 82 |
| 6.4.2 | Devonian structures associated with the western margin of the Gauss basin | 85 |
| 6.5 | Deep-seated fractures | 88 |

| | | |
|-------|---|----|
| 7 | Summary and conclusions | 93 |
| 7.1 | Mathematical modelling of folded surfaces | 93 |
| 7.2 | Computer implementation of the mathematical models | 94 |
| 7.3 | Photo-interpretation of an area of folded sediments | 94 |
| 7.4 | Structural analysis of the photo-interpreted area | 95 |
| 7.4.1 | Upper Ordovician structures | 95 |
| 7.4.2 | Devonian structures | 95 |
| 7.4.3 | Deep-seated fractures | 96 |
| | Acknowledgements | 97 |
| | References | 99 |

1. ABSTRACT

A mathematical modelling of folded surfaces has been developed. It involves the splitting of individual folds into approximately conical or cylindrical segments, projection of the surfaces of each fold segment onto a profile plane perpendicular to the fold axis, and approximation of each surface projection with a polynomial. When the surfaces have been modelled, best fitting deformation parameters for the fold segment can be calculated, assuming a simple deformation history for the fold. This involves first flexural slip folding, thereafter similar folding, and lastly homogeneous compression.

Computer programs have been developed that allow use of this modelling on folded surfaces measured via the Kern PG2 stereo restitution instrument of the Grønlands Geologiske Undersøgelse.

An area of Upper Proterozoic to Lower Palaeozoic sediments in central East Greenland, folded during the Caledonian orogeny, has been photo-interpreted and structurally analysed. Major north-south directed folds, east-west striking faults, and west-dipping low-angle tension faults are thought to be related to a westward translation of the sediment packet of at least 25 km during the Upper Ordovician. It is concluded, that the driving force behind the translation was gravity.

Major faulting in the western part of the area is related to a basement uplift of Middle Devonian age. En échelon folds, slides and crescent-shaped faults in the north-eastern part of the area may be related to dextral strike-slip faulting along the margin of the future Gauss Basin. Together these movements formed the relief present during the deposition of the Upper Middle Devonian Vilddal Supergroup.

2. INTRODUCTION

This paper is the final report of the project 'geometrical and geological analysis of photogrammetrically measured folded surfaces', carried out at the photogrammetric laboratory of the Grønlands Geologiske Undersøgelse and financed by the Carlsberg Foundation by a grant for two and a half years.

The photogrammetric laboratory of the Grønlands Geologiske Undersøgelse, led by H.F. Jepsen, was in 1977 equipped with a Kern PG2 stereo restitution instrument. With this instrument stereo models can be set up from vertical air photos, and precise topographic mapping of the features visible in the models can be done by tracing them with a measuring mark. The PG2 instrument was coupled to a HP 9825 table computer via a digitizer, making tape file storage of the resulting map lines possible. A project was carried out, which resulted in the establishment of computer routines for the calculation of the orientation of a plane surface from the coordinates of points, measured on the surface via the PG2 instrument. Other routines allowed the calculation of bed thicknesses between two planes, calculation of fold axes from differently oriented planes etc. (Jepsen & Dueholm, 1978). Thus at this stage topographic and photogeological mapping, storage of data, and computer treatment of photogrammetrically measured plane surfaces was possible.

In 1984 the table computer was replaced by a HP 1000 minicomputer, and a project involving the author was planned, with the aim of treating non-plane surfaces, measured via the PG2 instrument. The author had shortly before finished his M.Sc. degree with a dissertation on the geology of East Greenland north of 70° N, and it was decided to use an area here as test area for the routines, and to couple the project with a photo-interpretation and structural analysis of a part of this area. The part selected was the fjord zone of central East Greenland shown on fig. 2.1. This figure also gives the place names used in this paper. This part of the fjord zone, measuring ca. 200 x 50 km, is occupied by an up to 16 000 m thick sequence of Upper Proterozoic to Lower Ordovician sediments, folded during the Caledonian orogeny. This sedimentary sequence, comprising the Eleonore Bay Group, the Tillite Group and Cambro-Ordovician sediments, is well differentiated into 'bed groups' and formations, which are generally well distinguishable photogrammetrically through their different colours and

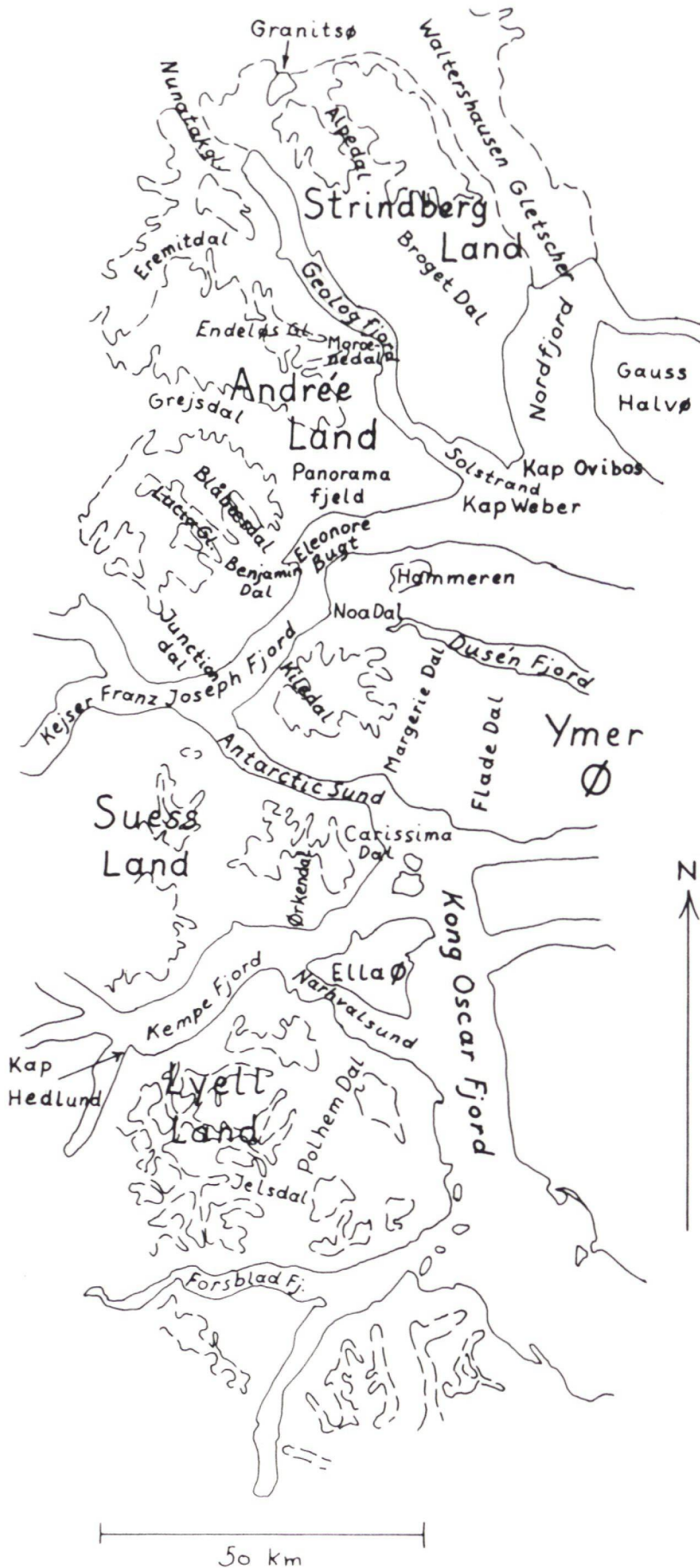


Fig. 2.1
Name map of the photo-interpreted area

weathering characteristics. Most of the area is well exposed, and is covered by geological maps on a scale of 1:250 000, made by the Danish Expeditions to East Greenland under the leadership of Lauge Koch in the period 1926 to 1958 (Koch & Haller, 1971).

The Danish Geodetic Institute was in 1985 covering a large part of central East Greenland with vertical air photos with a photo scale of 1:150000, taken by super-wideangle cameras. Photos covering the fjord zone became available during 1986 with ca. 40 stereo models covering the area of interest.

Much of the project time was taken up by developing the mathematical models for treatment of folded surfaces, and implementing them in the form of computer programs. In all ca. 700 pages of computer programs have been written. The mathematical model used is described in section 3 of this report; the computer programs are not described, but are available from the Grønlands Geologiske Undersøgelse on request.

In the summer of 1986, the author had the opportunity to visit a part of the fjord zone of central East Greenland, accompanying J.L. Petersen, who was then working on the project 'The use of structural and spectral enhancement of remote sensing data in ore prospecting'. This project was carried out at the IMSOR Institute of the Technical University of Denmark, and entailed the detailed mapping of the Noa Dal area of north-western Ymer Ø. Here the upper part of the Eleonore Bay Group, the Tillite Group and most of the Cambro-Ordovician sediments are exposed, and the first-hand impressions gained of this part of the stratigraphy was of great value for the later photo-interpretation.

In the summer of 1987 the project was suspended for 2 months while the author was given a leave to participate in geological mapping in West Greenland for Grønlands Geologiske Undersøgelse. This was necessitated by the sudden illness of a colleague.

In the spring of 1988 the programming was so far finished that the photo-interpretation and structural analysis of the fjord zone could start. This was planned to take place during the summer of 1988, but a major instrument breakdown in the photogrammetric laboratory caused a delay of 2-3 months, so that the interpretation was not finished until the end of 1988. Section 5 of this report treats the photo-interpretation.

The western part of Ella Ø was selected for a detailed analysis of the folding, using 1:50 000 air photos. This analysis is treated in section 4,

which also shows how the computer programs work. The amount of interpretation and boundary mapping necessary to produce a satisfactory geological map of the fjord zone left little time for a more detailed treatment of individual folds, so the structural analysis of the whole photo-interpreted area is mainly based on the geological map resulting from the photo-interpretation. This regional structural analysis is treated in section 6.

3. MATHEMATICAL MODELLING OF FOLDED SURFACES

3.1 Fold segments

The mathematical model for folded surfaces used by the program treats folds as two-dimensional forms, by projecting them onto a profile plane perpendicular to the fold axis. It further treats them as single forms, i. e. isolated synforms and anti-forms. To be projected, a fold must not be too far from a cylindrical or conical form.

In nature, folded surfaces are generally deformed into series of antiforms and synforms, that vary in profile along their length in a non-cylindrical way. To be treated by the program, they must therefore be divided into smaller units; a folded area must be divided first into individual syn- and antiforms, and each of these again divided into approximately cylindrical or conical

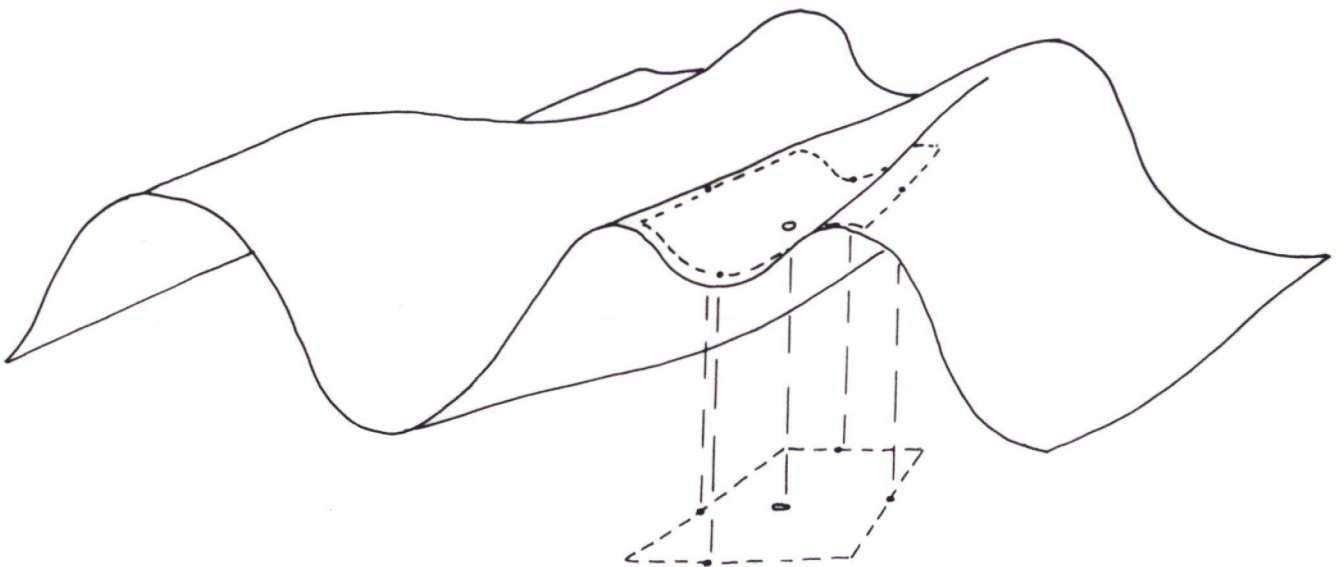


Fig. 3.1

A surface folded into irregular folds. The limits of an approximately conical fold segment is shown.

fold segments. This is done by the user of the program by selecting four "limitpoints" for each fold segment; two of these limit it against neighbouring segments along the hinge of the fold, the two other limits it against neighbouring syn- or antiforms. The interval defined by the latter two limitpoints may be narrowed during the later treatment of the segment, and may consequently be chosen fairly wide.

Furthermore, the user must select a "centerpoint" for the fold segment; this will define the position of the projection plane. Also an axialplane and either a fold axis or a "conepoint" must be selected, to define the projection parameters. In the program, axialplane and foldaxis/conepoint can be estimated by the user, or be selected from those calculated from measurements in the photogrammetrical model. Planes and foldaxes are calculated with the routines developed by Jepsen & Dueholm (1978). Conepoints are calculated from calculated planes in the way described below.

3.2 Conepoint calculation

A conical fold is here defined by its profile in a specific plane and by its "conepoint"; The folded surface is generated by a line passing through the conepoint and moving along the profile. The "opening angle", traditionally used for description of conical folds, is not used here, since it varies across the fold profile.

For a packet of folded surfaces, each surface should in principle have its own conepoint, since otherwise all bed thicknesses would decrease to zero at the conepoint. For simplicity, however, only one conepoint is used; consequently the conical fold model is imprecise away from the profile plane.

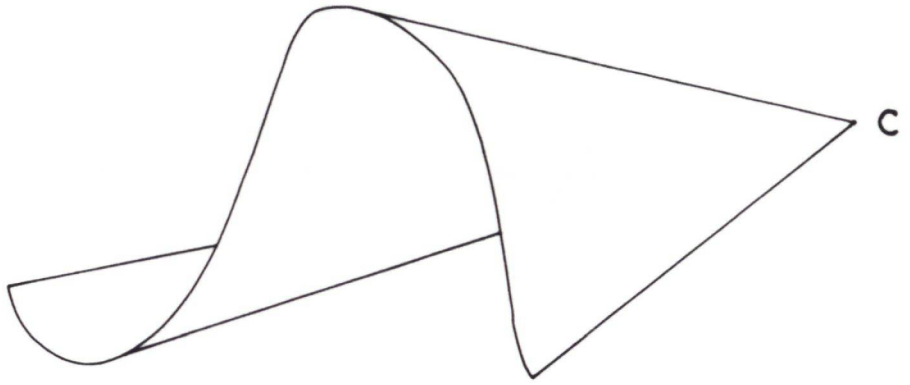


Fig. 3.2
A conical fold with conepoint at C.

The conepoint is calculated as the point that has the smallest weighted square distance to a number of planes calculated for the fold segment. At least three planes are necessary, in which case the conepoint is their intersection. If more than 3 planes are used, then if the i 'th plane is given by the equation

$a_i x + b_i y + c_i z + d_i = 0$, where (a_i, b_i, c_i) is a unit vector, then the distance from the plane to the conepoint (X, Y, Z) is $v_i = \pm(a_i X + b_i Y + c_i Z + d_i)$ and the weighted square distance to the plane $p_i v_i^2 = p_i \cdot (a_i X + b_i Y + c_i Z + d_i)^2$, where p_i is the weight given the plane. If n planes are used, the sum to be minimized is $\sum_{i=1}^n p_i v_i^2$. The condition for minimum is

$$\frac{\delta \sum p v^2}{\delta X} = 2 \cdot \sum (p \cdot ((aX + bY + cZ + d) \cdot a)) = 0$$

$$\frac{\delta \sum p v^2}{\delta Y} = 2 \cdot \sum (p \cdot ((aX + bY + cZ + d) \cdot b)) = 0$$

$$\frac{\delta \sum p v^2}{\delta Z} = 2 \cdot \sum (p \cdot ((aX + bY + cZ + d) \cdot c)) = 0$$



$$\begin{pmatrix} \sum pa^2 & \sum pba & \sum pca \\ \sum pab & \sum pb^2 & \sum pcb \\ \sum pac & \sum pbc & \sum pc^2 \end{pmatrix} \cdot \begin{pmatrix} X \\ Y \\ Z \end{pmatrix} + \begin{pmatrix} \sum pda \\ \sum pdb \\ \sum pdc \end{pmatrix} = \begin{pmatrix} 0 \\ 0 \\ 0 \end{pmatrix}$$

$$\Downarrow$$

$$\begin{pmatrix} X \\ Y \\ Z \end{pmatrix} = \begin{pmatrix} \sum pa^2 & \sum pba & \sum pca \\ \sum pab & \sum pb^2 & \sum pcb \\ \sum pac & \sum pbc & \sum pc^2 \end{pmatrix}^{-1} \begin{pmatrix} -\sum pda \\ -\sum pdb \\ -\sum pdc \end{pmatrix}$$

In practice, the calculation is done iteratively, as the weight function used is dependant on the position of the cone-point. A first cone-point is calculated with each plane weighted inversely to the variance found during the calculation of the plane. This cone-point is then used as the starting point for an iterative calculation, with each plane weighted inversely to the variance of the distance from the plane to the last cone-point. The variance is calculated from the covariance matrix of the plane:

$$V = (X, Y, Z) \cdot \begin{pmatrix} V_a & \text{Cov}_{ba} & \text{Cov}_{ca} \\ \text{Cov}_{ab} & V_b & \text{Cov}_{cb} \\ \text{Cov}_{ac} & \text{Cov}_{bc} & V_c \end{pmatrix} \cdot \begin{pmatrix} X \\ Y \\ Z \end{pmatrix} + V_d$$

where (X, Y, Z) is the last cone-point and (a, b, c, d) are the parameters of the plane.

3.3 Projection onto profile plane

For each fold, a local coordinate system is set up with the profile plane (which is per definition perpendicular to the fold axis) as the x-z plane, the axialplane as the y-z plane and origo at the user defined centerpoint of the fold. All further calcu-

lations on the surfaces of the fold is done in this coordinate system, in which no overturned flanks occur. Also several of the shear directions of the simple folding mechanism model described later are parallel to the axes of this coordinate system. The transformation parameters from the UTM coordinate system to the local coordinate system are derived as shown below:

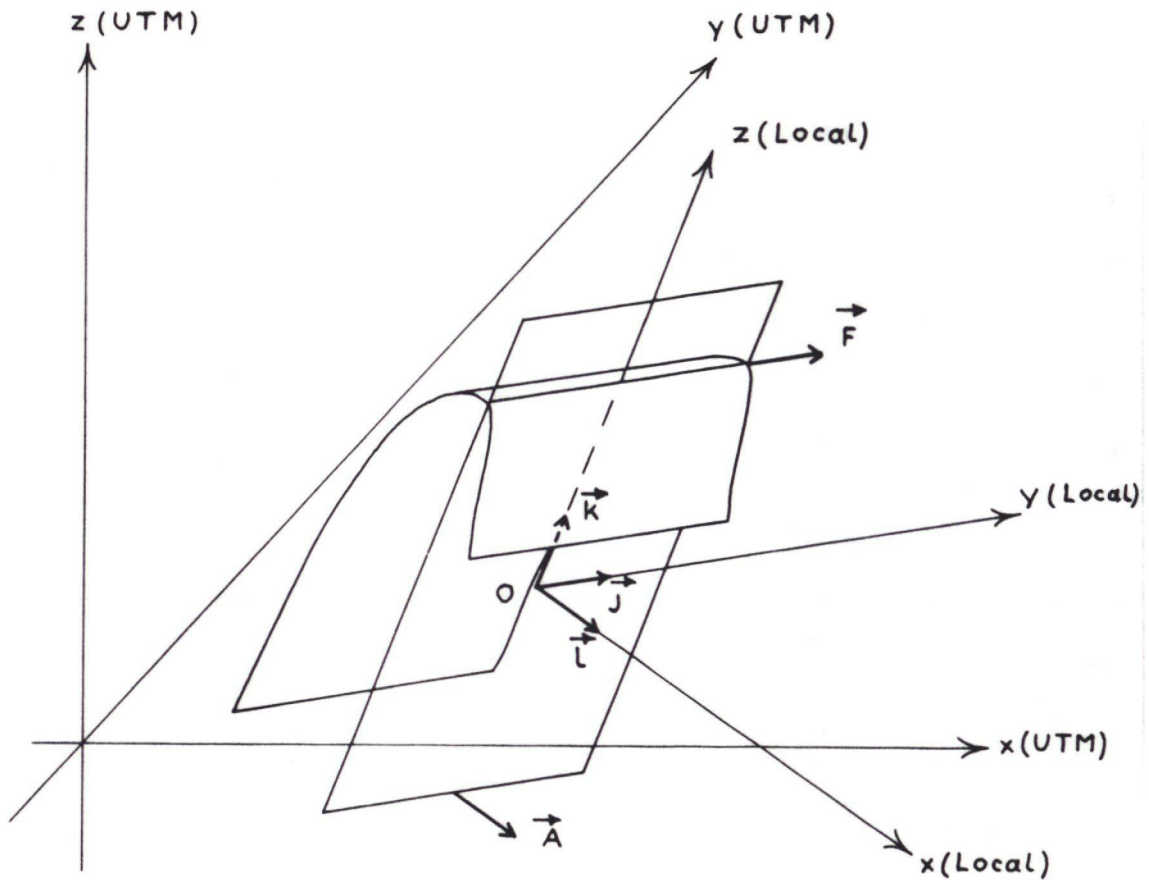


Fig. 3.3

The local coordinate system for a fold in relation to the UTM coordinate system.

For the fold has been selected a centerpoint "O" = (o_1, o_2, o_3) , an axialplane given by the normalised equation $ax + by + cz + d = 0$, and either a foldaxis given by the unit vector $\vec{F} = (f_1, f_2, f_3)$ or a conepoint "C" = (c_1, c_2, c_3) . All

this is in the UTM coordinate system. Then a unit vector $\vec{j} = (j_1, j_2, j_3)$ parallel to the y-axis of the local coordinate system will be either $\pm\vec{F}$ or $\pm(C \vec{z} - O)/|C \vec{z} - O|$. By convention the sign is chosen, that gives a downward pointing vector ($j_3 < 0$). A unit vector $\vec{k} = (k_1, k_2, k_3)$ parallel to the z-axis of the local coordinate system will be $\pm(\vec{j} \times \vec{A})/|\vec{j} \times \vec{A}|$, where $\vec{A} = (a, b, c)$. Here the sign is chosen, that gives an upward pointing vector ($k_3 > 0$). A unit vector $\vec{i} = (i_1, i_2, i_3)$ parallel to the x-axis of the local coordinate system will be $\vec{j} \times \vec{k}$. The coordinate transformations between the UTM coordinate system and the local coordinate system for the fold is then given by

$$L = \begin{pmatrix} i_1 & i_2 & i_3 \\ j_1 & j_2 & j_3 \\ k_1 & k_2 & k_3 \end{pmatrix} \cdot (U - O) \text{ and } U = \begin{pmatrix} i_1 & j_1 & k_1 \\ i_2 & j_2 & k_2 \\ i_3 & j_3 & k_3 \end{pmatrix} \cdot L + O.$$

Here U and L are the coordinates of a point in the UTM resp. the local coordinate system.

In the local coordinate system, the profile plane is the x-z plane, and projection onto it of points for a cylindrical fold is trivial, since the fold axis by definition is parallel to the y-axis. For a conical fold, the projection of a point (x, y, z) will be $(x \cdot s, 0, z \cdot s)$ where $s = y_c / (y_c - y)$ and y_c is the local y-coordinate of the conepoint. This will by definition always lie on the y-axis of the local coordinate system.

In the program, the point projection resulting from the axialplane and fold axis/conepoint chosen by the user is shown on the terminals graph screen; the user may then repeatedly change the axialplane and fold axis/conepoint and have the resulting projection shown, until a satisfactory result is reached.

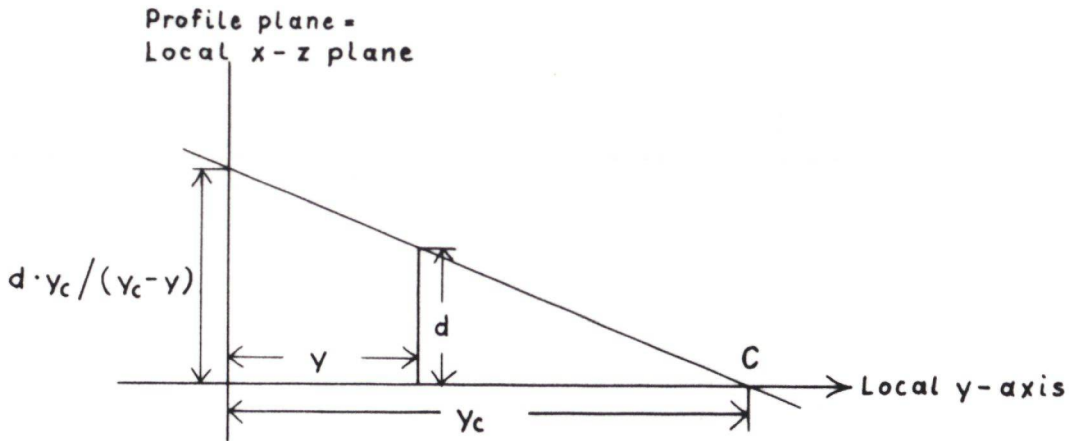


Fig. 3.4
Projection of a point P onto the profile plane of a conical fold with conepoint at C.

3.4 Fitting of a polynomial to the profile of a folded surface

When the points measured on a folded surface have been projected onto the x-z plane of the local coordinate system of a fold segment, they will lie on a curve describing the fold profile, provided the fold segment is reasonably cylindrical or conical, and the proper projection parameters have been found. The last step in the description of the surface is now to find a function that describes this curve. The function type used in the program is a polynomial, whose coefficients are calculated by the least square method, so that the sum of the weighted square vertical distance from the measured points to the polynomial is minimised. It would be more correct to minimise the perpendicular distances, but that would make the coefficient calculation very complicated. The coefficients are calculated as shown below:

The polynomial is given by the equation

$z = a_0 + a_1x + a_2x^2 + \dots + a_nx^n$. The vertical distance from a point $(x, 0, z)$ to the polynomial is

$v = a_0 + a_1x + a_2x^2 + \dots + a_nx^n - z$, and the weighted square distance is $p \cdot v^2 = p \cdot (a_0 + a_1x + a_2x^2 + \dots + a_nx^n - z)^2$.

The sum to be minimised for m points is

$$\sum_{i=1}^m (p_i \cdot v_i^2) = \sum_{i=1}^m (p_i \cdot (a_0 + a_1x_i + a_2x_i^2 + \dots + a_nx_i^n - z_i)^2)$$

The condition for minimum is

$$\frac{\delta \sum p v^2}{\delta a_0} = 2 \cdot \sum (p \cdot (a_0 + a_1x + a_2x^2 + \dots + a_nx^n - z)) = 0$$

$$\frac{\delta \sum p v^2}{\delta a_1} = 2 \cdot \sum (p \cdot (a_0 + a_1x + a_2x^2 + \dots + a_nx^n - z) \cdot x) = 0$$

$$\frac{\delta \sum p v^2}{\delta a_2} = 2 \cdot \sum (p \cdot (a_0 + a_1x + a_2x^2 + \dots + a_nx^n - z) \cdot x^2) = 0$$

⋮

$$\frac{\delta \sum p v^2}{\delta a_n} = 2 \cdot \sum (p \cdot (a_0 + a_1x + a_2x^2 + \dots + a_nx^n - z) \cdot x^n) = 0$$

⇓

$$\begin{pmatrix} a_0 \\ a_1 \\ a_2 \\ \vdots \\ a_n \end{pmatrix} = \begin{pmatrix} \sum p & \sum px & \sum px^2 & \dots & \sum px^n \\ \sum px & \sum px^2 & \sum px^3 & \dots & \sum px^{n+1} \\ \sum px^2 & \sum px^3 & \sum px^4 & \dots & \sum px^{n+2} \\ \vdots & \vdots & \vdots & \vdots & \vdots \\ \sum px^n & \sum px^{n+1} & \sum px^{n+2} & \dots & \sum px^{2n} \end{pmatrix}^{-1} \cdot \begin{pmatrix} -\sum pz \\ -\sum pzx \\ -\sum pzx^2 \\ \vdots \\ -\sum pzx^n \end{pmatrix}$$

or, with the abbreviations used in the following

$$A = N^{-1} \cdot C.$$

The mean spread of the points around the fitted surface is

$s_0 = \sqrt{\sum (pv^2) / (m - n)}$. The sum $\sum pv^2$ may be calculated thus:

$$\sum pv^2 = \sum (p \cdot (a_0 + a_1x + a_2x^2 + \dots + a_nx^n - z)^2) =$$

$$\sum (p \cdot (a_0 + a_1x + a_2x^2 + \dots + a_nx^n)^2) + \sum pz^2$$

$$- 2 \cdot \sum (p \cdot (za_0 + za_1x + za_2x^2 + \dots + za_nx^n)) =$$

$$A \cdot N \cdot A + \sum pz^2 - 2 \cdot A \cdot C.$$

When s_0 is known, the covarians matrix for the coefficients can be calculated as $COV = s_0^2 \cdot N^{-1}$.

Since z is a linear function of the coefficients:

$$z = (a_0, a_1, a_2, \dots, a_n) \cdot (1, x, x^2, \dots, x^n)$$

the error on z is

$$s_z^2 = (1, x, x^2, \dots, x^n) \cdot COV \cdot (1, x, x^2, \dots, x^n).$$

Since very large potencies of x are used in the calculations, it is impractical to use x directly, as this would cause overflow or underflow during the computer calculations. To circumvent this problem, x is multiplied by a "scale factor". This is a potency of 10, chosen such that the largest absolute value of x multiplied by the scale factor will lie between 5 and 0.5. With the use of a scale factor the polynomium fitting the surface becomes $z = (a_0 + a_1(x \cdot s) + a_2(x \cdot s)^2 + \dots + a_n(x \cdot s)^n)/s$, where "s" is the scale factor.

The points available for surface fitting include all the points measured for the surface within the user selected limits of the fold. These should be selected rather wide laterally, so that a fairly broad profile of points can be used for surface fitting. In the program, the user may select any interval in this profile as a "computation interval"; only the points within this will be used for surface fitting. He may further change the weight of points within selected parts of the profile, thereby increasing the significance of some points (e. g. those in the hinge region of the fold) and decreasing the significance of others (e. g. points that can be seen to lie far away from a realistic surface). He may also within limits select the number of terms of the fitting polynomium (the present maximum is 15 terms).

When a satisfactory fit has been reached, a "definition in-

interval" must be chosen. This must lie within the computation interval; thereby an evt. area of bad fit near the margins of this interval can be skipped. The definition interval is regarded as the valid interval of the surface, when this is used for further computations. It is important, that the interval is chosen, so that the surface represents a single form, i. e. a single synform or antiform.

3.5 Calculation of line length shortening

Given a polynomium $z = P(x)$ describing a folded surface, the shortening between two points on the surface (x_1, z_1) and (x_2, z_2) , where $z_1 = P(x_1)$ and $z_2 = P(x_2)$, can be calculated.

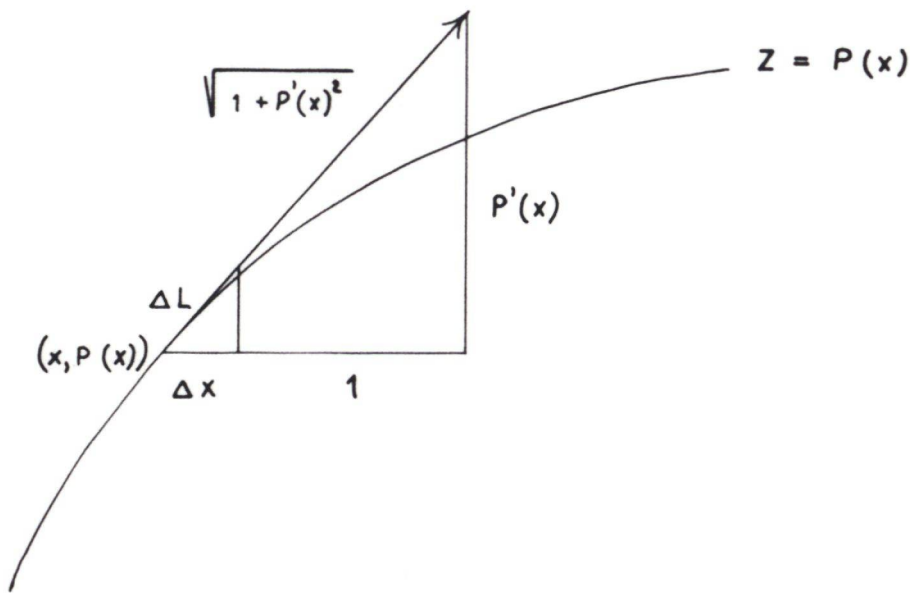


Fig. 3.5

Calculation of line length of a surface profile approximated by the polynomium $z = P(x)$.

The direct distance between the two points is

$D = \sqrt{(x_1 - x_2)^2 + (z_1 - z_2)^2}$, and the distance along the surface

is the line length along the polynomium between x_1 and x_2

$$L = \int_{x_1}^{x_2} \sqrt{1 + P'(x)^2} dx. \text{ The shortening is then calculated as } D/L.$$

The standard deviation s_L on the line length along the polynomium may be calculated from the covariance matrix COV of the coefficients of P:

$$P'(x) = a_1 + 2a_2x + 3a_3x^2 + \dots + na_nx^{n-1} =$$

$$(0, 1, 2x, 3x^2, \dots, nx^{n-1}) \cdot (a_0, a_1, a_2, a_3, \dots, a_n)$$

$$s_{P'(x)}^2 = (0, 1, 2x, \dots, nx^{n-1}) \cdot \text{COV} \cdot (0, 1, 2x, \dots, nx^{n-1})$$

$$\Delta L = \sqrt{1 + P'(x)^2} \cdot \Delta x$$

$$s_{\Delta L}^2 = s_{P'(x)}^2 \cdot \frac{\delta \Delta L}{\delta P'(x)} \cdot \Delta x = s_{P'(x)}^2 \cdot \frac{P'(x)}{\sqrt{1 + P'(x)^2}} \cdot \Delta x$$

$$s_L^2 = \int_{x_1}^{x_2} s_{P'(x)}^2 \cdot \frac{P'(x)}{\sqrt{1 + P'(x)^2}} dx$$

For a conical fold away from the profile plane (the x-z plane of the local coordinate system) the shortening and standard deviation must be multiplied by $(y_c - y)/y_c$, where y is the local y-coordinate of that profile plane, where the shortening is wanted, and y_c is the local y-coordinate of the conepoint of the fold.

3.6 Deformation mechanism model

For construction and analysis of folded surfaces, a simple fold model is used, where the fold first undergoes pure flexural slip folding, and thereafter pure similar folding and pure homogeneous compression perpendicular to the axialplane. The sequence of the last two deformational mechanism is unimportant for the calculations. The spatial relationship between points on

two folded surfaces is calculated as shown below:

A folded surface has a shape described by the polynomial P so that a point on it has the coordinates $(x, z) = (x, P(x))$. The tangent to the surface at this point is $(1, P'(x))$.

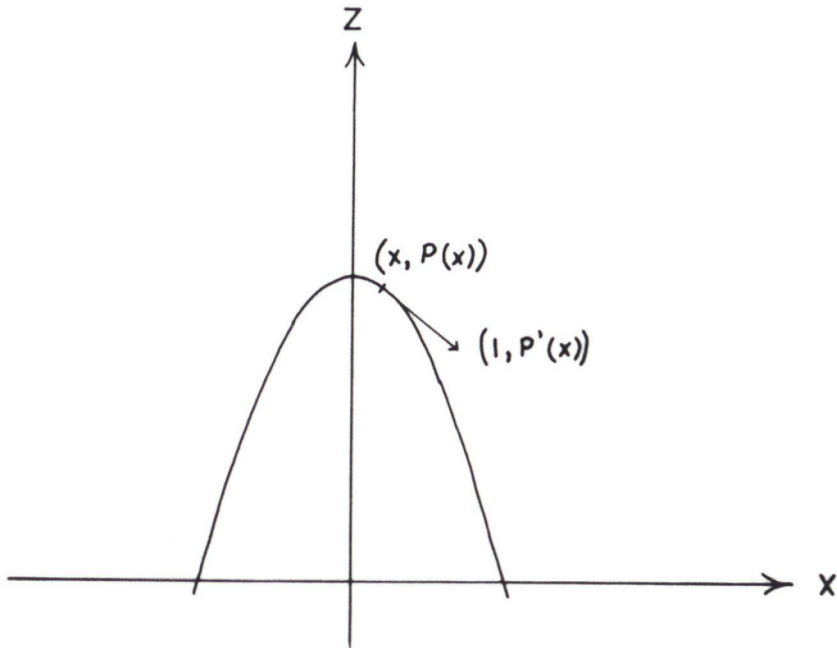


Fig. 3.6a

A folded surface approximated by the polynomial $z = P(x)$.

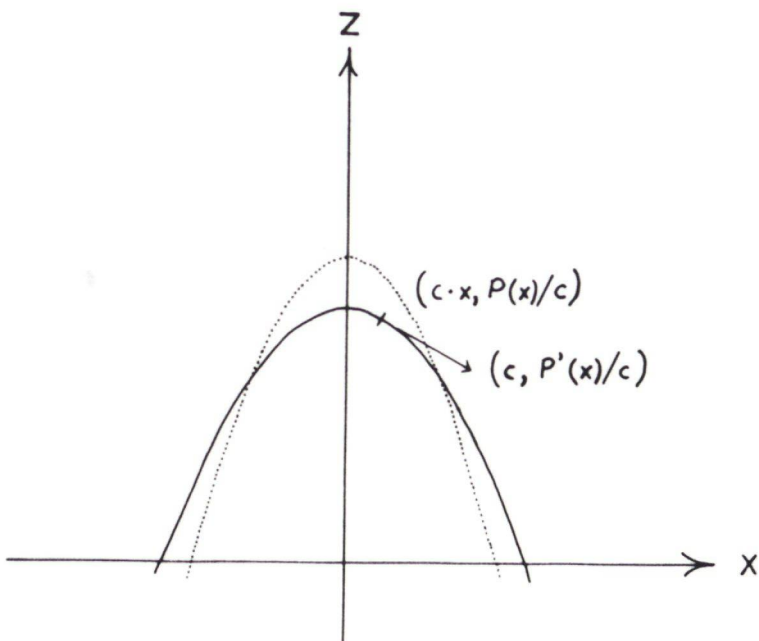


Fig. 3.6b

The surface after removal of homogeneous compression.

The amount of homogeneous compression in the folding mechanism is "c". After removal of homogeneous compression the coordinates of the point is $(x \cdot c, P(x)/c)$ and the tangent is $(c, P'(x)/c)$.

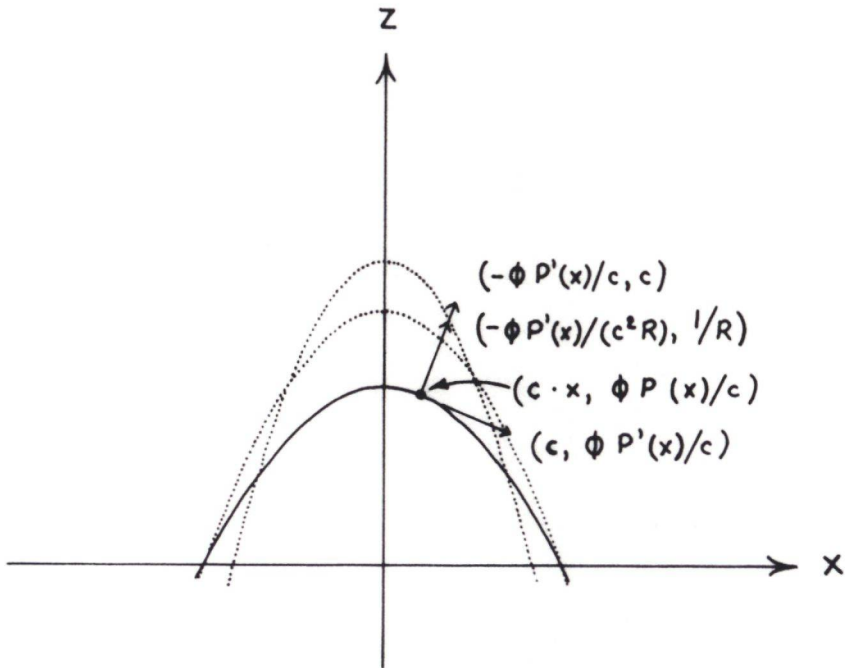


Fig. 3.6c

The surface after removal of similar folding.

The proportion of flexural slip in the folding mechanism is called " ϕ ", so the proportion of similar folding is $1 - \phi$. After removal of the similar folding, the coordinates of the point is $(x \cdot c, \phi \cdot P(x)/c)$ and the tangent is $(c, \phi \cdot P'(x)/c)$. An upward pointing vector perpendicular to the tangent is now $(-\phi \cdot P'(x)/c, c)$. The length of this vector is $\sqrt{c^2 + (\phi \cdot P'(x)/c)^2} = c \cdot R$, where $R = \sqrt{1 + (\phi \cdot P'(x)/c^2)^2}$. Thus an upward pointing unit vector perpendicular to the tangent is $(-\phi \cdot P'(x)/(c^2 \cdot R), 1/R)$, and the coordinates of a point on a surface at distance "d" from the original ("basal") surface is $(x \cdot c - \phi \cdot P'(x) \cdot d/(c^2 \cdot R), \phi \cdot P(x)/c + d/R) = (S \cdot c, \phi \cdot P(x)/c + d/R)$, where $S = x - \phi \cdot P'(x) \cdot d/(c^3 \cdot R)$.

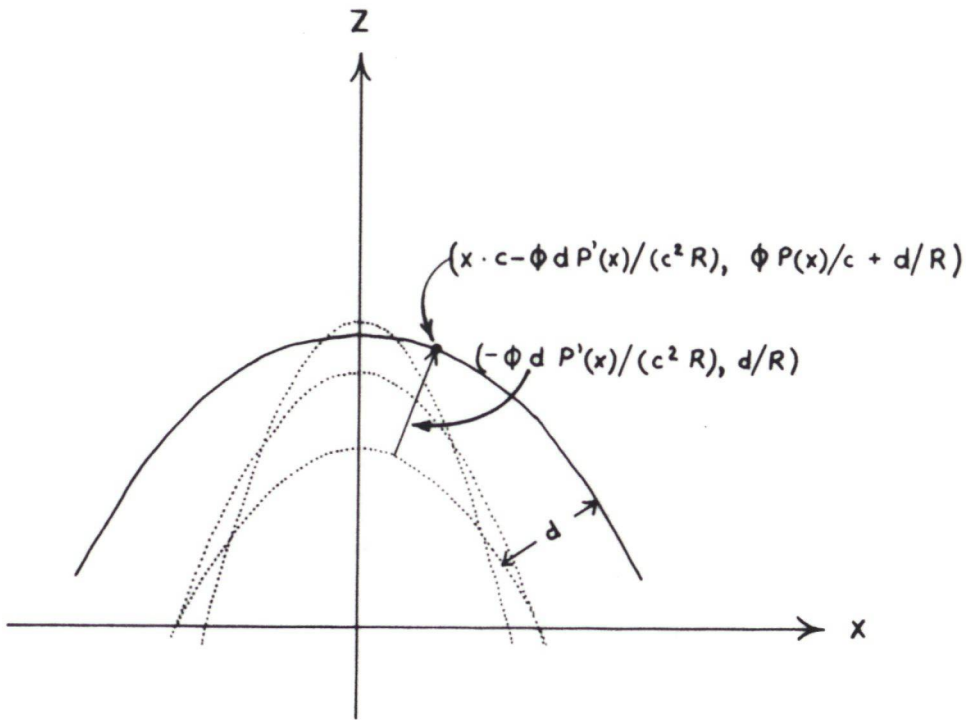


Fig. 3.6d

A new surface at an undeformed distance 'd' from the old surface.

After similar folding, the coordinates of the new point is $(S \cdot c, \phi \cdot P(x)/c + d/R + (1 - \phi) \cdot P(S)/c)$.

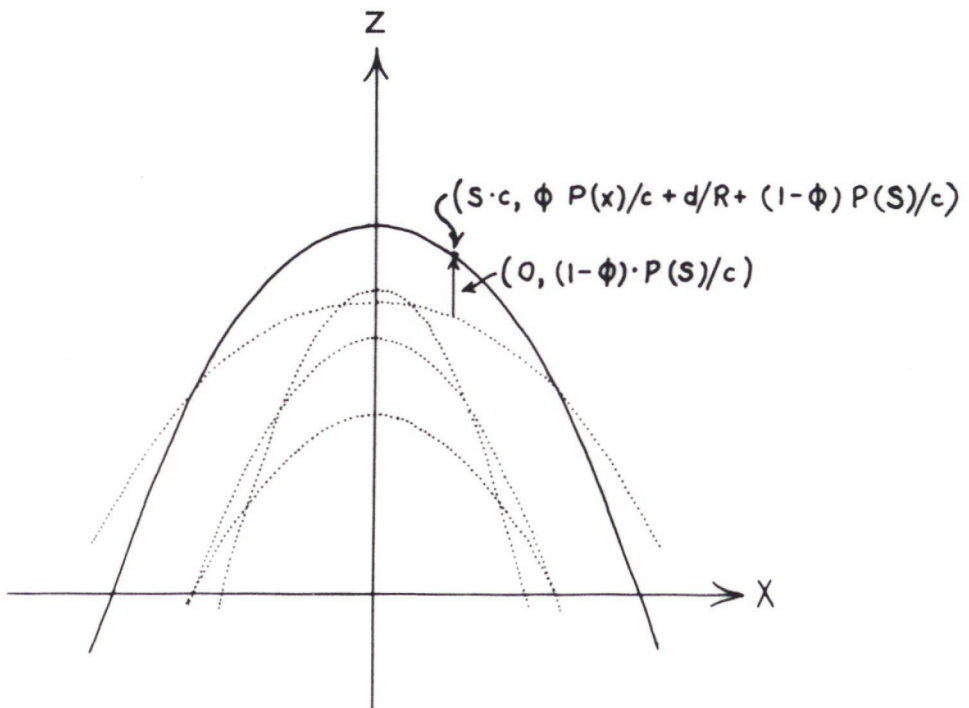


Fig. 3.6e

The new surface with similar folding added.

After homogeneous compression, the coordinates of the new point is $(S, \phi \cdot P(x) + d \cdot c/R + (1 - \phi) \cdot P(S))$.

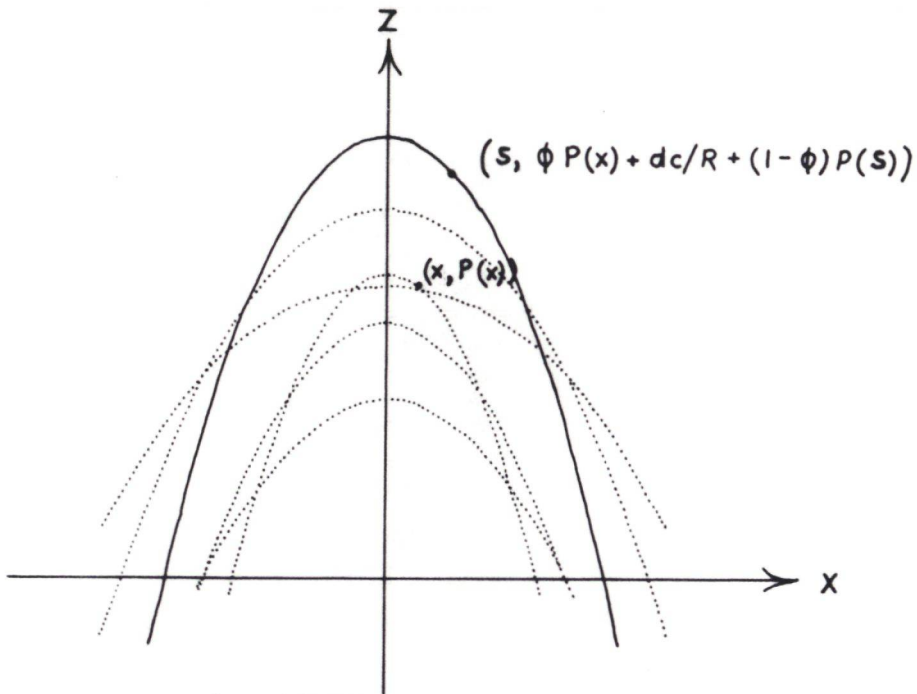


Fig. 3.6f

The new surface with homogeneous compression added.

To sum up: given a folded surface $z = P(x)$, folded with a homogeneous compression "c" and a proportion of flexural slip folding " ϕ "; then from a point $(x, P(x))$ on this surface may be calculated a point on an other surface at an undeformed distance "d" from the first surface. The coordinates of this new point is $(S, \phi \cdot P(x) + d \cdot c/R + (1 - \phi) \cdot P(S))$, where

$$S = x - \phi \cdot P'(x) \cdot d / (c^3 \cdot R) \text{ and } R = \sqrt{1 + (\phi \cdot P'(x) / c^2)^2}.$$

This fold model becomes too simple, if more than two folded surfaces are involved, as may be seen from the example below.

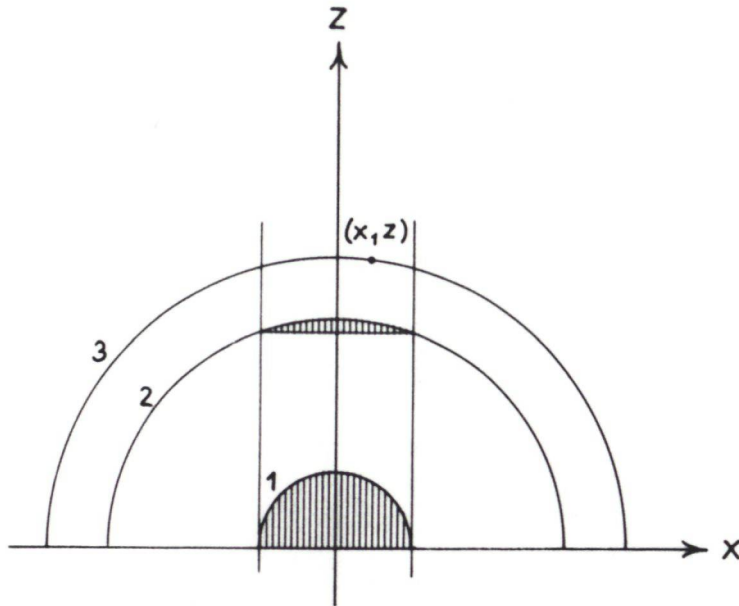


Fig. 3.7

Three surfaces after flexural slip folding, but before similar folding. The surface '3' will receive different amounts of similar folding if surface '1' resp. surface '2' is used as 'guiding surface'.

Here 3 surfaces, numbered 1, 2 and 3, are shown after deformation by flexural slip, but before similar folding and homogeneous compression. It may be seen, that the point (x, z) on surface 3 will receive a different amount of similar folding if surface 1 resp. surface 2 is used as base of calculation.

To circumvent this problem, a "guiding surface" is used. This is a surface, whose shape defines the similar folding for a whole packet of folded surfaces. If the polynomial for the guiding surface is $z = G(x)$, then the above derived formula will be changed to:

$(x, P(x))$ on the basal surface corresponds to

$(S, P(x) + d \cdot c/R + (1 - \phi) \cdot (G(S) - G(x)))$ where

$S = x - d \cdot (P'(x) - (1 - \phi) \cdot G'(x)) / (c^3 \cdot R)$ and

$R = \sqrt{1 + ((P'(x) - (1 - \phi) \cdot G'(x)) / c^2)^2}$

In principle, the similar folding for a packet of surfaces may assume any shape, independent of the shape of any surface af-

ter flexural slip folding. The calculation of a best fitting independent guiding surface would, however, be very complicated and has not been attempted.

3.7 Construction of new folded surface

Using the formulas for calculation of new points, a new surface may be constructed from a basal surface $z = P(x)$ and an evt. guiding surface $z = G(x)$. In practice, this is done by calculating an appropriate number of points for the new surface, and thereafter fitting a polynomial to them, in the same way as for measured points. When the new surface lies inside the basal surface, space problems may arise, if the folding mechanism includes flexural slip folding. These problems are circumvented by skipping all new points, that lies at the opposite side of the axialplane relative to their "mother point".

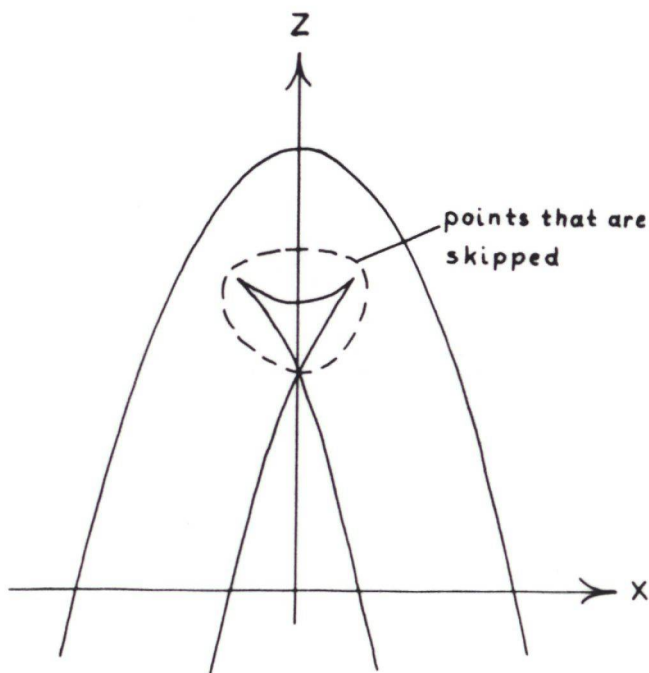


Fig. 3.8

Space problems in the core of a fold. Skipped points are not used for calculation of polynomial coefficients for the new surface.

3.8 Deformation mechanism analysis

Given a folded surface $z = P(x)$ and evt. a guiding surface $z = G(x)$, points for an other surface may be calculated using arbitrary values of c , d and ϕ . The purpose of the deformation mechanism analysis is to find a set of deformation mechanism parameters c , d and ϕ so that the sum of the squared distances to a measured surface $z = M(x)$ is minimised.

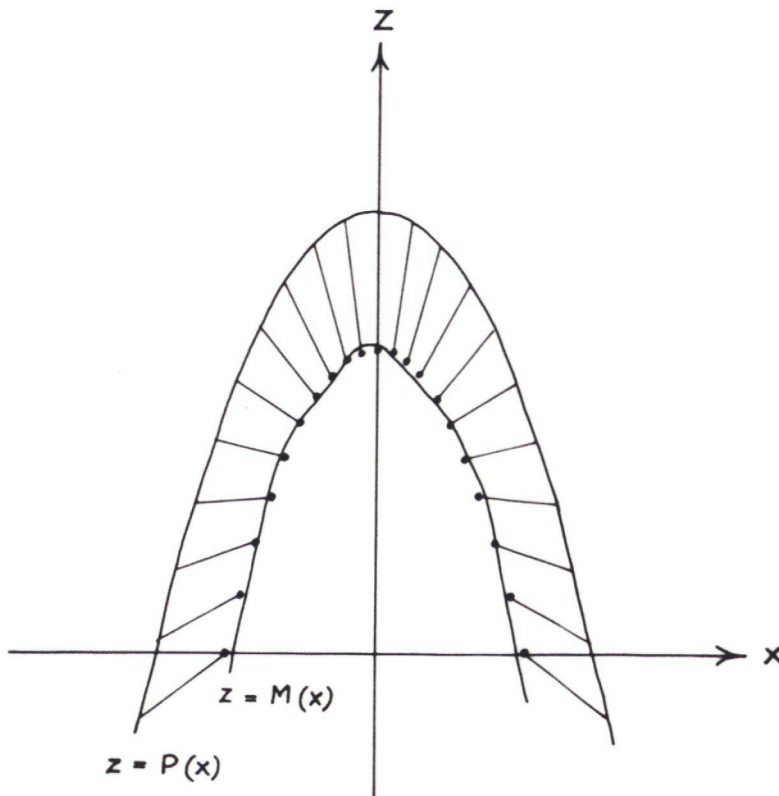


Fig. 3.9

Points calculated from the surface $z = P(x)$ for a given set of deformation mechanism parameters are compared to the surface $z = M(x)$.

The analysis may also be carried out for a packet of folded surfaces; here deformation mechanism parameters may be found for each pair of neighbouring surfaces. In this case, only one "c" can be found, since "c" according to the simple fold model used must be the same all over the fold. If a single guiding surface

is assumed for the fold, " ϕ " will also be the same for the whole fold and only one " ϕ " value can be found; otherwise an individual " ϕ " value may be found for each surface pair.

Fixed "d" values may be used for the calculations, if reliable "d" values are known from other sources.

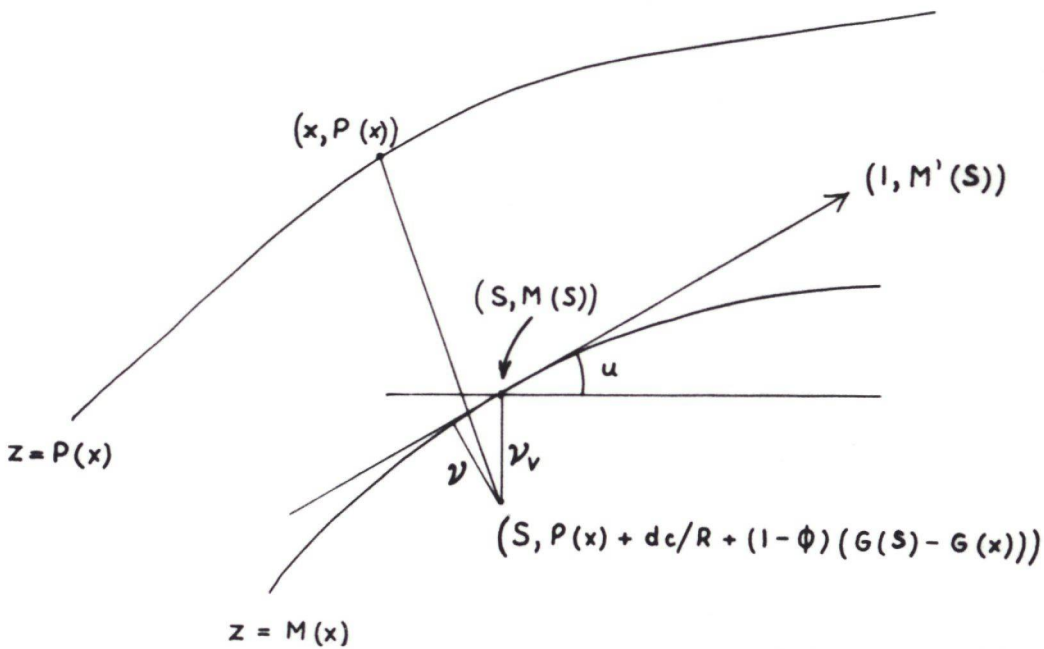


Fig. 3.10
Calculation of distance from a calculated point to the surface $z = M(x)$.

The vertical distance between a calculated point and the measured surface is

$$v_v = P(x) + \frac{d \cdot c}{R} + (1 - \phi) \cdot (G(S) - P(x)) - M(x).$$

The perpendicular distance cannot be easily calculated; the distance to the tangent to the measured surface is used as an approximation instead:

$$v = v_v \cdot \cos u = v_d / \sqrt{1 + \text{tg}^2 u} = v_d / \sqrt{1 + M'(S)^2}$$

The sum to be minimised thus becomes

$$\sum_{j=1}^m \sum_{i=1}^n v_{ij}^2 = \sum_{j=1}^m \sum_{i=1}^n \left((P_j(x_i) + \frac{d_j \cdot c}{R} + (1 - \phi_j) \cdot (G_j(S) - P_j(x_i)) - M_j(S)) \cdot \frac{1}{\sqrt{1 + M_j'(S)^2}} \right)^2$$

where there is summed over n calculated point for each of m pairs of surfaces.

v is not a linear function of c , d and ϕ , and in order to use linear regression it is approximated with the first degree Taylor row $v \approx v(c_0, d_0, \phi_0) + \frac{\delta v(c_0, d_0, \phi_0)}{\delta c} \cdot \Delta c + \frac{\delta v(c_0, d_0, \phi_0)}{\delta d} \cdot \Delta d + \frac{\delta v(c_0, d_0, \phi_0)}{\delta \phi} \cdot \Delta \phi$

or, with a shorter notation

$$v \approx v_0 + \frac{\delta v_0}{\delta c} \cdot \Delta c + \frac{\delta v_0}{\delta d} \cdot \Delta d + \frac{\delta v_0}{\delta \phi} \cdot \Delta \phi$$

Here c_0 , d_0 and ϕ_0 are estimated deformation mechanism parameters. Normal linear regression can be used on this approximation, and a set of corrections Δc , Δd and $\Delta \phi$ calculated. The corrected deformation mechanism parameters can then be used for calculation of a new set of corrections; this procedure is repeated until further corrections does not give significantly smaller deviations between calculated points and measured surfaces.

For a single pair of surfaces the corrections are calculated as

$$\begin{pmatrix} \Delta c \\ \Delta d \\ \Delta \phi \end{pmatrix} = \begin{pmatrix} \sum \frac{\delta v_0}{\delta c} \frac{\delta v_0}{\delta c} & \sum \frac{\delta v_0}{\delta c} \frac{\delta v_0}{\delta d} & \sum \frac{\delta v_0}{\delta c} \frac{\delta v_0}{\delta \phi} \\ \sum \frac{\delta v_0}{\delta c} \frac{\delta v_0}{\delta d} & \sum \frac{\delta v_0}{\delta d} \frac{\delta v_0}{\delta d} & \sum \frac{\delta v_0}{\delta d} \frac{\delta v_0}{\delta \phi} \\ \sum \frac{\delta v_0}{\delta c} \frac{\delta v_0}{\delta \phi} & \sum \frac{\delta v_0}{\delta d} \frac{\delta v_0}{\delta \phi} & \sum \frac{\delta v_0}{\delta \phi} \frac{\delta v_0}{\delta \phi} \end{pmatrix}^{-1} \cdot \begin{pmatrix} - \sum v_0 \frac{\delta v_0}{\delta c} \\ - \sum v_0 \frac{\delta v_0}{\delta d} \\ - \sum v_0 \frac{\delta v_0}{\delta \phi} \end{pmatrix}$$

For m pairs of surfaces the corrections are calculated as

$$\left(\begin{array}{cccccccc} \Delta c, & \Delta d_1, & \Delta d_2, & \dots & \Delta d_m, & \Delta \phi_1, & \Delta \phi_2, & \dots & \Delta \phi_m \end{array} \right) =$$

$$\left[\begin{array}{cccccccc} \sum \frac{\delta v_0}{\delta c} \frac{\delta v_0}{\delta c} & \sum \frac{\delta v_0}{\delta c} \frac{\delta v_0}{\delta d_1} & \sum \frac{\delta v_0}{\delta c} \frac{\delta v_0}{\delta d_2} & \dots & \sum \frac{\delta v_0}{\delta c} \frac{\delta v_0}{\delta d_m} & \sum \frac{\delta v_0}{\delta c} \frac{\delta v_0}{\delta \phi_1} & \sum \frac{\delta v_0}{\delta c} \frac{\delta v_0}{\delta \phi_2} & \dots & \sum \frac{\delta v_0}{\delta c} \frac{\delta v_0}{\delta \phi_m} \\ \sum \frac{\delta v_0}{\delta d_1} \frac{\delta v_0}{\delta c} & \sum \frac{\delta v_0}{\delta d_1} \frac{\delta v_0}{\delta d_1} & 0 & \dots & 0 & \sum \frac{\delta v_0}{\delta d_1} \frac{\delta v_0}{\delta \phi_1} & 0 & \dots & 0 \\ \sum \frac{\delta v_0}{\delta d_2} \frac{\delta v_0}{\delta c} & 0 & \sum \frac{\delta v_0}{\delta d_2} \frac{\delta v_0}{\delta d_2} & \dots & 0 & 0 & \sum \frac{\delta v_0}{\delta d_2} \frac{\delta v_0}{\delta \phi_2} & \dots & 0 \\ \dots & \dots \\ \sum \frac{\delta v_0}{\delta d_m} \frac{\delta v_0}{\delta c} & 0 & 0 & \dots & \sum \frac{\delta v_0}{\delta d_m} \frac{\delta v_0}{\delta d_m} & 0 & 0 & \dots & \sum \frac{\delta v_0}{\delta d_m} \frac{\delta v_0}{\delta \phi_m} \\ \sum \frac{\delta v_0}{\delta \phi_1} \frac{\delta v_0}{\delta c} & \sum \frac{\delta v_0}{\delta \phi_1} \frac{\delta v_0}{\delta d_1} & 0 & \dots & 0 & \sum \frac{\delta v_0}{\delta \phi_1} \frac{\delta v_0}{\delta \phi_1} & 0 & \dots & 0 \\ \sum \frac{\delta v_0}{\delta \phi_2} \frac{\delta v_0}{\delta c} & 0 & \sum \frac{\delta v_0}{\delta \phi_2} \frac{\delta v_0}{\delta d_2} & \dots & 0 & 0 & \sum \frac{\delta v_0}{\delta \phi_2} \frac{\delta v_0}{\delta \phi_2} & \dots & 0 \\ \dots & \dots \\ \sum \frac{\delta v_0}{\delta \phi_m} \frac{\delta v_0}{\delta c} & 0 & 0 & \dots & \sum \frac{\delta v_0}{\delta \phi_m} \frac{\delta v_0}{\delta d_m} & 0 & 0 & \dots & \sum \frac{\delta v_0}{\delta \phi_m} \frac{\delta v_0}{\delta \phi_m} \end{array} \right)^{-1}$$

$$\left(-\sum v_0 \frac{\delta v_0}{\delta c}, -\sum v_0 \frac{\delta v_0}{\delta d_1}, -\sum v_0 \frac{\delta v_0}{\delta d_2}, \dots, -\sum v_0 \frac{\delta v_0}{\delta d_m}, -\sum v_0 \frac{\delta v_0}{\delta \phi_1}, -\sum v_0 \frac{\delta v_0}{\delta \phi_2}, \dots, -\sum v_0 \frac{\delta v_0}{\delta \phi_m} \right)$$

The d 's and ϕ 's for different pairs of surfaces are uncorrelated; this give rise to the many 0's in the matrix.

For the calculation of the partial derivates serves:

$$T_2 = P'(x) - (1 - \phi) \cdot G'(x)$$

$$T_3 = T_2 / c^2$$

$$T_4 = \frac{1}{\sqrt{1 + M'(S)^2}}$$

$$T_5 = P(x) + \frac{d \cdot c}{R} + (1 - \phi) \cdot (G(S) - G(x)) - M(S)$$

$$T_6 = \frac{M'(S) \cdot M''(S)}{\sqrt{(1 + M'(S)^2)^3}}$$

$$\frac{\delta v}{\delta c} = T_4 \cdot \left(d \cdot \left(R - c \cdot \frac{\delta R}{\delta c} \right) / R^2 + (1 - \phi) \cdot G'(S) \cdot \frac{\delta S}{\delta c} - M'(S) \cdot \frac{\delta S}{\delta c} \right) - T_5 \cdot T_6 \cdot \frac{\delta S}{\delta c}$$

$$\frac{\delta S}{\delta c} = d \cdot T_3 \cdot \left(3R + c \cdot \frac{\delta R}{\delta c} \right) / (c^2 \cdot R^2)$$

$$\frac{\delta R}{\delta c} = - 2 \cdot (T_3)^2 / (R \cdot c)$$

$$\frac{\delta v}{\delta d} = T_4 \cdot \left(\frac{c}{R} + (1 - \phi) \cdot G'(S) \cdot \frac{\delta S}{\delta d} - M'(S) \cdot \frac{\delta S}{\delta d} \right) - T_5 \cdot T_6 \cdot \frac{\delta S}{\delta d}$$

$$\frac{\delta S}{\delta d} = - T_3 / (c \cdot R)$$

$$\begin{aligned} \frac{\delta v}{\delta \phi} = & T_4 \cdot \left(-(d \cdot c \cdot \frac{\delta R}{\delta \phi}) / R^2 + (1 - \phi) \cdot G'(S) \cdot \frac{\delta S}{\delta \phi} \right. \\ & \left. - (G(S) - G(x)) - M'(S) \cdot \frac{\delta S}{\delta \phi} \right) - T_5 \cdot T_6 \cdot \frac{\delta S}{\delta \phi} \end{aligned}$$

$$\frac{\delta S}{\delta \phi} = - d \cdot (R \cdot G'(x) - T_2 \cdot \frac{\delta R}{\delta \phi}) / (c^3 \cdot R^2)$$

$$\frac{\delta R}{\delta \phi} = T_3 \cdot G'(x) / (c^2 \cdot R)$$

When a set of corrections (Δc , Δd , $\Delta \phi$) has been calculated, they are added to the initial estimated deformation mechanism parameters (c_0 , d_0 , ϕ_0), producing a new set of parameters; from these a new set of corrections are calculated, added etc. in an iterative fashion. The iteration is stopped, when the corrections does not give a significantly smaller deviation between calculated points and measured surface.

There are some problems connected with the use of this iterative method:

1. If the first estimated deformation mechanism parameters are far from the true values, the iteration may not converge but "run wild". It must then be repeated with better start values. (i. e. better start values for "d"; the start value for "c" is computed from the "d" start values in the hinge zone of the fold, where the main strain is that caused by homogeneous compression, and the start value for " ϕ " is always set to 0.5 by the program).

In order to reduce the tendency for the iteration to "run wild", only a fraction (presently 1/4) of the corrections are ap-

plied to the estimates; this makes the iteration proceed rather slow, however.

2. The iteration finds deformation mechanism parameters corresponding to a deviation minimum. Since the deviation is a non-linear function of the deformation mechanism parameters, several such minima may exist, and the minimum found may not be global.

3.9 Strain ellipse calculation

When the deformation mechanism parameters for two neighbouring surfaces are known, the strain ellipse at any point (x, z) between the surfaces can be calculated. The first step is to find the position of the point in the fold at the stage of deformation, when only flexural slip deformation had occurred. This is done by finding a solution (x_0, d) to the equation

$$(x, z) = (S, P(x_0) + d \cdot c/R + (1 - \Phi) \cdot (G(S) - G(x_0)))$$

where P is the polynomial for one of the surfaces, G is the polynomial for the guiding surface,

$$S = x_0 - d \cdot (P'(x_0) - (1 - \Phi) \cdot G'(x_0)) / (c^3 \cdot R), \text{ and}$$

$$R = \sqrt{1 + ((P'(x_0) - (1 - \Phi) \cdot G'(x_0)) / c^2)^2}$$

Φ is the proportion of flexural slip folding, and c is the homogeneous compression.

The point $(x_0, P(x_0))$ has received the same flexural slip deformation as (x, z) (see figure).

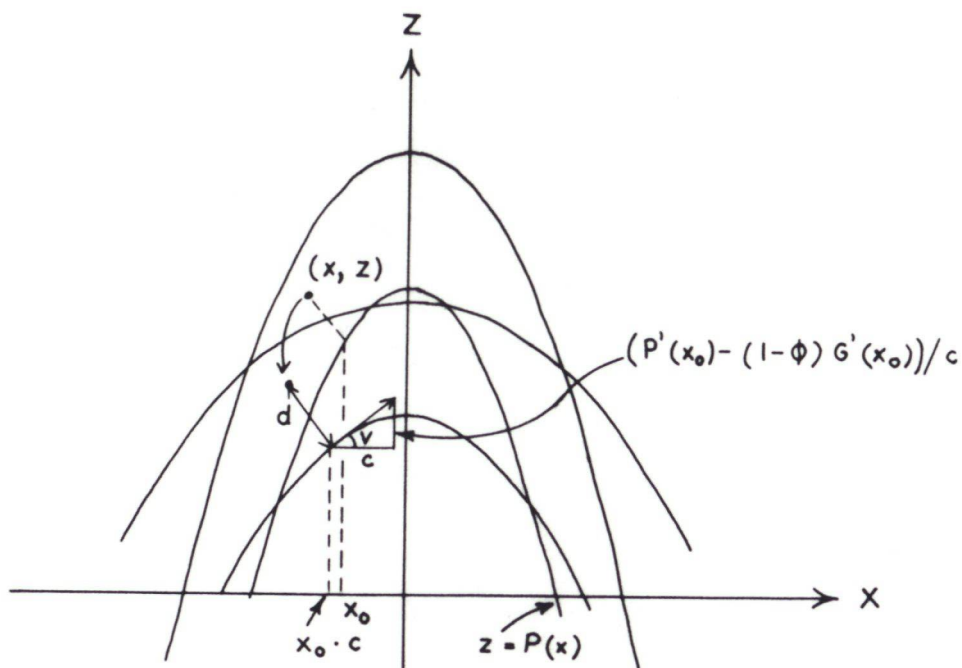


Fig. 3.11

Calculation of shear resulting from flexural slip folding for the point (x, z) .

The flexural slip deformation will result in a simple shear parallel to the surface of magnitude

$$v = \arctan \left(\frac{P'(x_0) - (1 - \phi) \cdot G'(x_0)}{c^2} \right).$$

The deformation matrix corresponding to this shear is

$$M_{\text{flex}} = \begin{pmatrix} 1 & -v \\ 0 & 1 \end{pmatrix}$$

The flexural slip folding also rotates the surface. The matrix corresponding to this rotation is

$$M_{\text{rot}} = \begin{pmatrix} \cos v & \sin v \\ -\sin v & \cos v \end{pmatrix}$$

The similar folding results in a simple shear strain of magnitude

$$\gamma = (1 - \phi) \cdot G'(x) / c^2$$

The deformation matrix corresponding to this shear is

$$M_{\text{sim}} = \begin{pmatrix} 1 & 0 \\ -\gamma & 1 \end{pmatrix}$$

The homogeneous compression results in a pure shear parallel to the x and z local coordinate axes. The deformation matrix corresponding to this shear is

$$M_{\text{comp}} = \begin{pmatrix} c & 0 \\ 0 & 1/c \end{pmatrix}$$

The deformation matrix for the whole deformation is

$$M_{\text{def}} = M_{\text{comp}} \cdot M_{\text{sim}} \cdot M_{\text{rot}} \cdot M_{\text{flex}} = \begin{pmatrix} m_{11} & m_{12} \\ m_{21} & m_{22} \end{pmatrix}$$

so that any small vector close to (x, z) will be deformed $(x', z') \rightarrow (m_{11} \cdot x' + m_{12} \cdot z', m_{21} \cdot x' + m_{22} \cdot z')$ and the original unit circle at (x, z)

$$x^2 + z^2 = 1 \rightarrow (m_{11}^2 + m_{21}^2) \cdot x^2 + (m_{12}^2 + m_{22}^2) \cdot z^2 + 2 \cdot (m_{11}m_{12} + m_{21}m_{22}) \cdot xz = 1.$$

This is the equation of the strain ellipse. It can be written as a quadratic form

$$(x, z) \cdot \begin{pmatrix} m_{11}^2 + m_{21}^2 & m_{11}m_{12} + m_{21}m_{22} \\ m_{11}m_{12} + m_{21}m_{22} & m_{12}^2 + m_{22}^2 \end{pmatrix} \cdot (x, z) - 1 = 0.$$

With a proper rotation of the coordinate system this may be reduced to

$$\lambda_1 x^2 + \lambda_2 z^2 = 1 \text{ or } \frac{x^2}{(1/\sqrt{\lambda_1})^2} + \frac{z^2}{(1/\sqrt{\lambda_2})^2} = 1,$$

where λ_1 and λ_2 are the eigenvalues of the matrix of the quadratic form. λ_1 and λ_2 can be calculated as

$$\lambda = ((m_{11}^2 + m_{21}^2) + (m_{12}^2 + m_{22}^2)) \pm \sqrt{((m_{11}^2 + m_{21}^2) - (m_{12}^2 + m_{22}^2))^2 + 4 \cdot (m_{11}m_{12} + m_{21}m_{22})^2} / 2$$

From the largest eigenvalue λ_1 , resulting from the addition of the square root in the formula above, can be calculated the length of the short axis of the strain ellipse $= 1/\sqrt{\lambda_1}$. Correspondingly the length of the long axis is $1/\sqrt{\lambda_2}$. The angle be-

tween the long axis and the x-axis of the local fold coordinate system is $\arctan ((\lambda_2 - (m_{11}^2 + m_{21}^2))/(m_{11}m_{12} + m_{21}m_{22}))$.

4. DETAILED PHOTOINVESTIGATION OF THE WESTERN PART OF ELLA Ø, USING MATHEMATICAL MODELS

The western part of Ella Ø was selected for a detailed analysis of the folding, using the computer implementation of the mathematical modelling of folded surfaces described in section 3. Ella Ø is made up of folded sediments of the Eleonore Bay Group, Tillite Group and the Cambro-Ordovician sequence; the lowest exposed bed is bed group 16 of the Limestone-dolomite series of the Eleonore Bay Group, the highest exposed is the Lower Ordovician Narhvalsund Formation. The folded sediments are overlain with an angular discordance by Middle Devonian continental clastic sediments. The island has been mapped earlier by Poulsen & Rasmussen (1951) and Eha (1953).

Two folds are present on the island, namely the Central syncline and the Eleonore Bugt anticline. The Central syncline crosses the high western spur of the island, called Bastionen, while the Eleonore Bugt anticline crosses the central part of the island from the peninsula Kap Oswald to the bay Antiklinalbugt. These folds can be followed for ca. 150 km in the fjord zone, see section 6.2.2. The central and eastern part of Ella Ø is cut by many south-east striking faults, and an east-west striking fault. These faults may have been active during the folding (see section 6.2.3).

The photoinvestigation was carried out using three stereo models 1:50 000, supplied by two stereo models 1:150 000 to cover some steep cliffs that fell in the 'dead angle' of the 1:50 000 models. The eastern part of the area investigated, comprising the eastern flank of the Eleonore Bay anticline, is very well exposed. The central part, with the western flank of the Eleonore Bugt anticline, is less well exposed; the beds could be traced on the ground, but the precise position of their boundaries was difficult to locate on the photos, and no bed orientations could be measured. The western part of the area, comprising Bastionen with the Central syncline, is again well exposed, but the steep fjord walls of the Bastionen were difficult to see in the stereo instrument, and the north wall lies in deep shadow. The result of the photo-interpretation is reproduced here as a geological map 1:50 000, covering western Ella Ø (plate IV).

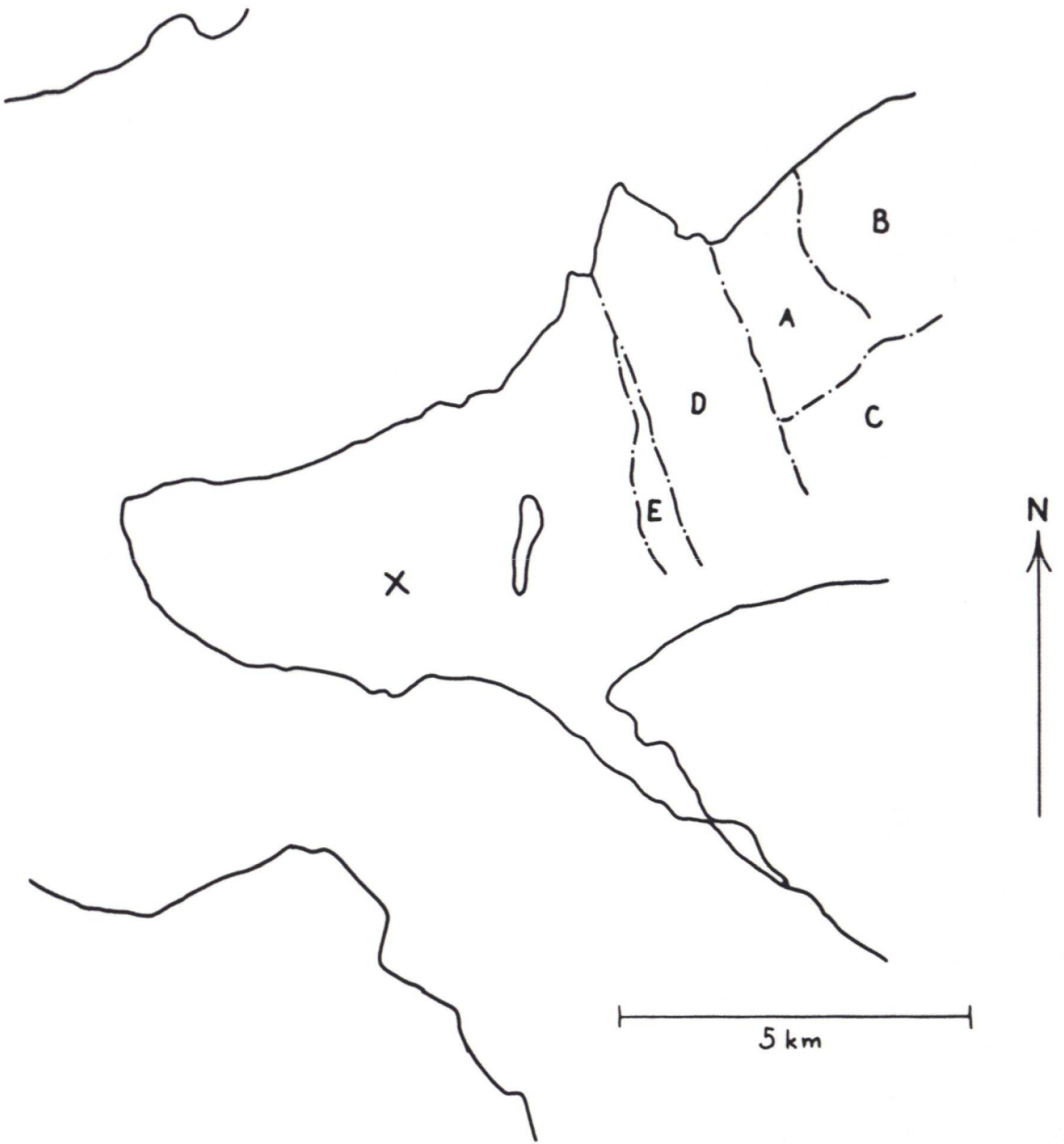


Fig. 4.1

Subdivision of western Ella ϕ into fault blocks.

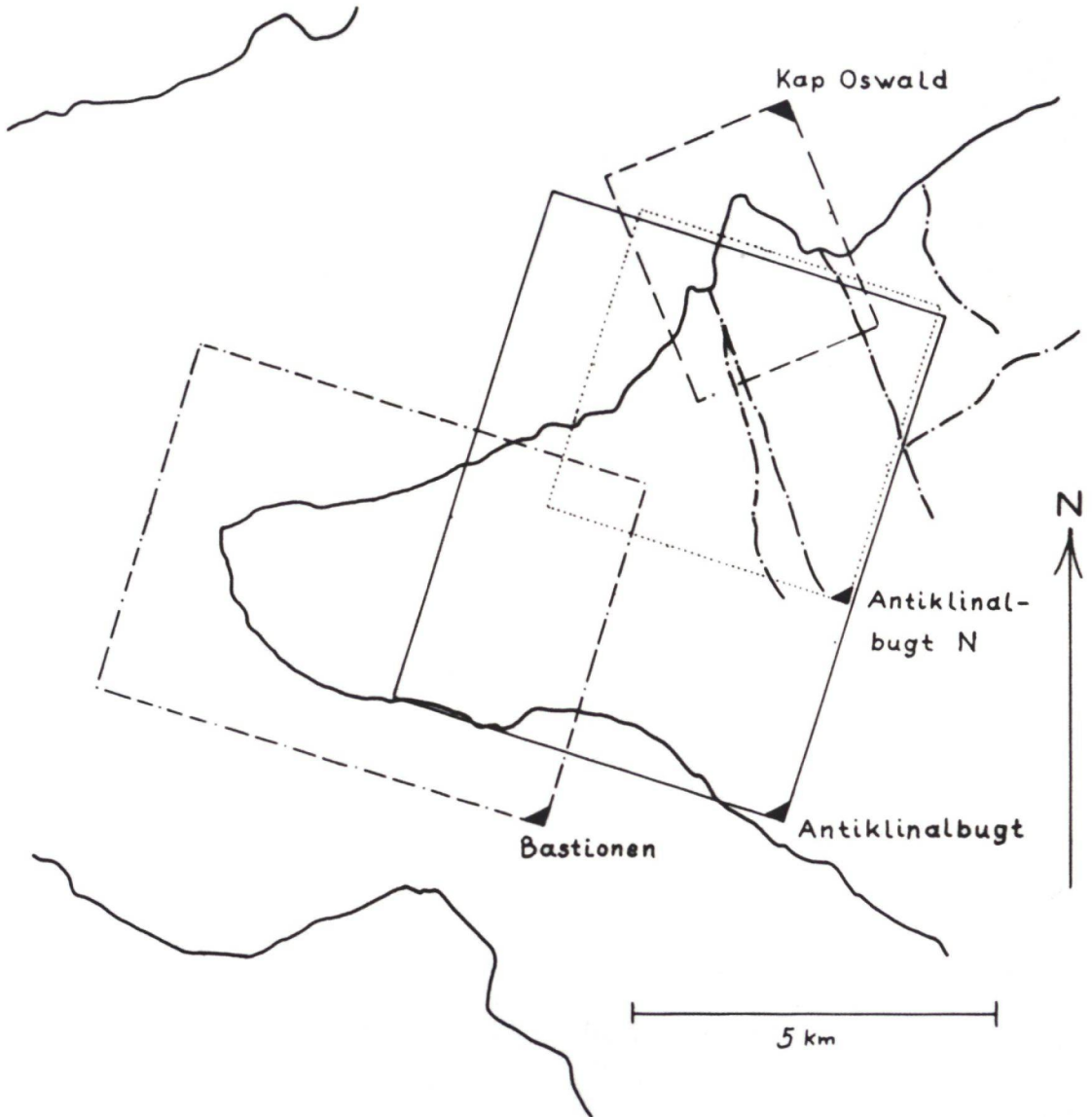


Fig. 4.2

Limits of fold segments defined for western Ella Ø.

The area was split into 6 fault blocks, labelled 'A', 'B', 'C', 'D', 'E', and 'X', (fig. 4.1). Only the 'D' and 'X' blocks contain fold hinges.

4.1. The Eleonore Bugt anticline in the 'D' fault block

Here a single fold segment, labelled "KAP OSWALD" was defined with the limits shown on fig. 4.2. Whether the segment is really cylindrical or conical cannot be determined due to the lack of relief in the area covered by the segment. Several bed orientations could be measured, and two almost similar fold axes calculated (fig. 4.3); one of these, with an orientation

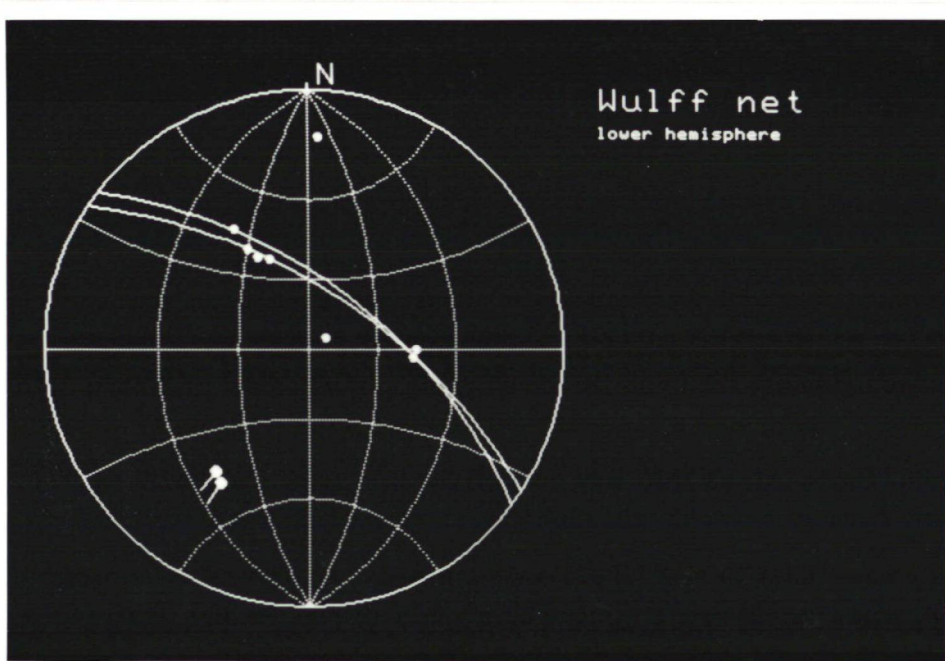


Fig. 4.3

Wulff net with measured beddingplane orientations and calculated fold axes for the KAP OSWALD fold segment.

of 213-29 was selected as fold axis of the segment. No axial plane could be measured; an estimate of 15-80 E was used as axial plane for the segment, since the Eleonore Bugt anticline generally has steeply east-dipping axial planes. The projection of the measured surface points on a profile plane perpendicular to the fold axis, resulting from this fold axis and axial plane, is shown on fig. 4.4. This projection, and all the following fold projections, shows the fold looking down the axis and rotated so that the axial plane is shown vertical. It is clear that the dip of the axial plane is wrong; the projection after the necessary corrections is shown on fig.

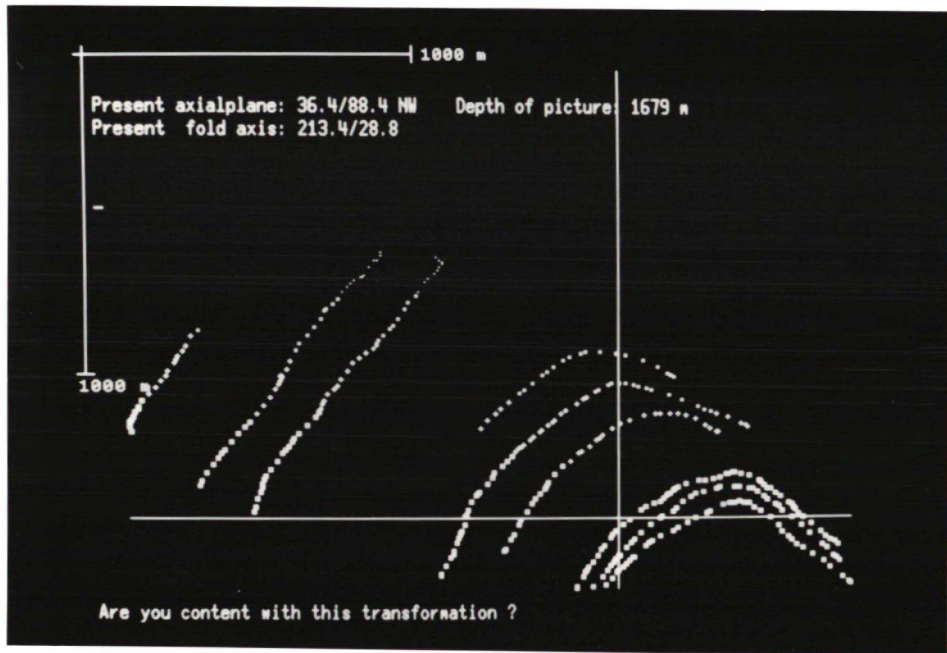


Fig. 4.4

Projection of points measured for the surfaces of the KAP OSWALD fold segment. The fold segment is viewed down the fold axis, and the axialplane is shown vertical. The horizontal line crosses it at the position of the centerpoint of the fold segment. The surfaces shown are, from bottom to top: Bed group 17, bottom and horizon A; bed group 18, bottom, horizon A and horizon B; bed group 19, bottom; Ulvesø, Arena and Storeelv Formations (all bottoms). The points are shown with smaller symbols, the farther down the fold axis they lie.

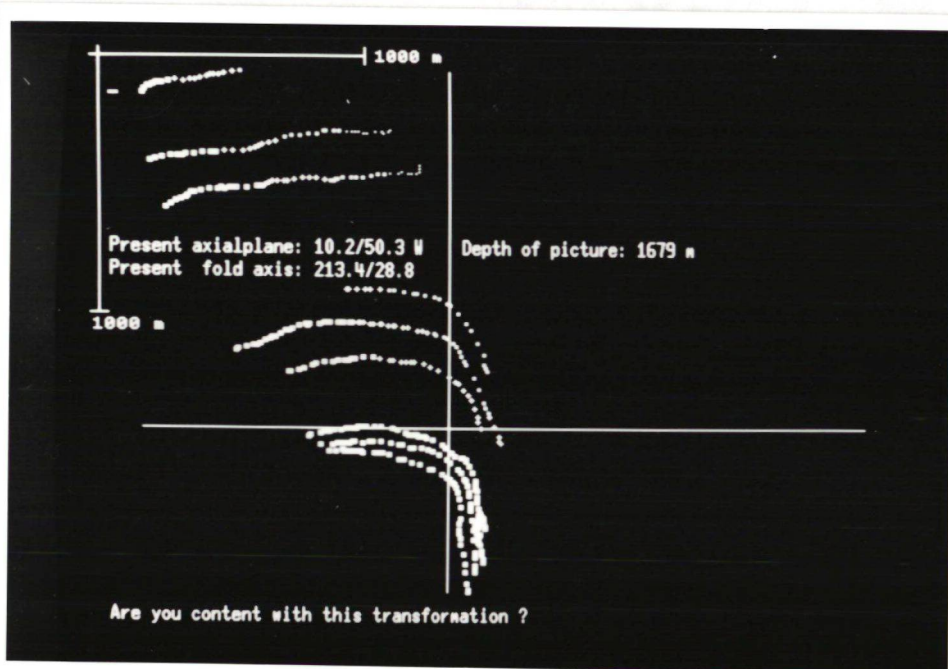


Fig. 4.5

Accepted projection of the KAP OSWALD fold segment.

4.5. Here the axial plane is 5-50 W, while the fold axis is unchanged. The fold is seen to be a monocline with an unexpected, moderately west-dipping axial plane, which is most unusual for the Eleonore Bay anticline.

This projection was accepted, and the next step was to fit the individual surfaces with a polynomial each. One example is shown on fig. 4.6; this surface (the bottom of bed group 19) has a broad, rounded hinge,

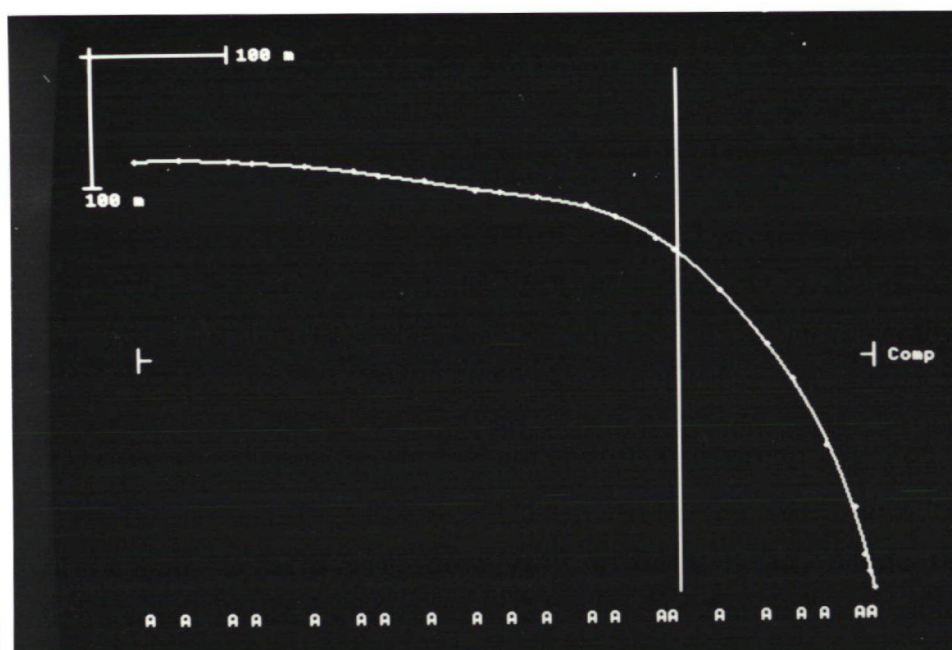


Fig. 4.6

Fitting a polynomial to the bottom of bed group 19. For explanation see fig. 4.7.

which is fitted with an 10-term polynomial without complications. Another example is shown on fig. 4.7; this surface (the bottom of bed group 18) has a more angular hinge and a very steep western flank. Here it was necessary to give a high weight to the points in the hinge zone, and a somewhat smaller weight to the points on the flat flank to get a good fit. The polynomial has 10 terms in this case too.

After polynomials had been fitted to all surfaces of interest, a deformation mechanism analysis could be carried out. The surfaces selected for this was bed group 19 (bottom), bed group 18 (bottom, horizon A and horizon B) and bed group 17 (bottom). Horizon A of bed group 17 is left out, since it seems to represent a surface that was not originally parallel to the other surfaces. The deformation mechanism analysis was not set to find a single 'guiding surface' (section 3.8) for the similar part of the

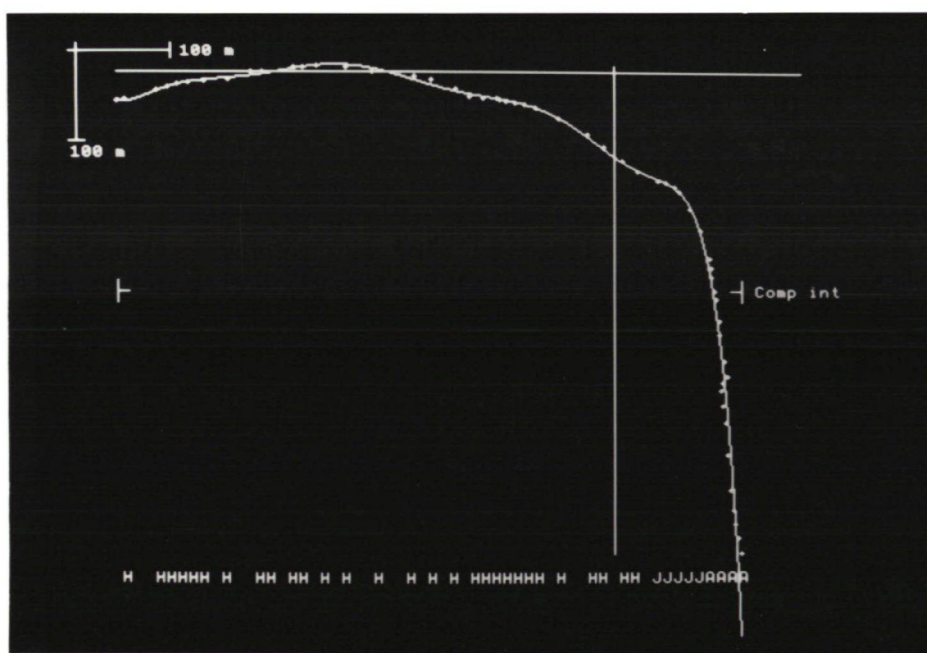


Fig. 4.7

Fitting a polynomial to the bottom of bed group 18. The vertical line is the trace of the axialplane, the horizontal line crosses it at the position of the centerpoint of the fold segment. 'Comp int' = computation interval; the polynomial is only fitted to points within this (user definable) interval. The letters at the bottom indicate the mean weight given by the user to the points in the interval covered by the letter. 'A' corresponds to a mean weight between 1 and 1.4, 'B' = 1.4 - 2.0, 'C' = 2.0 - 2.8 etc; 'a' = 1.0 - 0.7, 'b' = 0.7 - 0.5, 'c' = 0.5 - 0.35 etc.

folding, but calculated a proportion of flexural slip folding (ϕ) for each surface pair. The deformation mechanism analysis resulted in the best fitting deformation parameters shown in table 1.

The correlation coefficients between the calculated thicknesses and the homogeneous compression lie in the range - 0.98 - 0.99, showing that the values are strongly dependent on each other. The two other correlation coefficients, between ϕ and the compression, and between ϕ and the undeformed thickness, lie in the range $\pm 0.2 - 0.7$.

The calculated best fitting thickness (74 m for bed group 17, 396 m for bed group 18) are in good agreement with the thickness of these bed groups reported from less deformed areas in the vicinity (Eha, 1953). The ϕ value of 1 for bed group 17, indicating that all the folding was by flexural slip, is what would be expected for this thin unit of competent dolomite. Bed group 18 has a more variable lithology; the interval between horizon A and horizon B could be seen on the air photographs to be rather

Table 1.

 Homogeneous compression $1,37 \pm 0.01$

| | Undeformed thickness (meter) | Phi (Proportion of flex- ural slip folding) |
|------------------------|---------------------------------|---|
| Bed grup 19, bottom | 99 ± 1 | 0.61 ± 0.01 |
| Bed grup 18, horizon B | 102 ± 1 | 0.42 ± 0.01 |
| Bed grup 18, horizon A | 195 ± 2 | 0.98 ± 0.00 |
| Bed grup 18, bottom | 74 ± 1 | 1.00 ± 0.00 |
| Bed grup 17, bottom | | |

soft and recessive. In accordance with this, it has a low calculated phi value of 0.42, indicating that 3/5 of the folding took place by similar shear. The calculated homogeneous compression of 1.37 seems rather high, but compression in the area is indicated by a cleavage reported by Montcrieff (1988, p. 98f).

The profile of the analysed surfaces, with strain ellipses drawn on the flanks, is shown on fig. 4.8. It is seen that the fold is strongly asymmetrical, with the western flank steeper and more deformed than the eastern. Such a strong asymmetry relative to the axial plane has not been noted elsewhere along the Eleonore Bugt anticline. The steep fold axis and eastward inclined axial plane at Kap Oswald are also unusual, and seem to require a special explanation. A west-dipping fault east of Kap Oswald, antithetic to the fault limiting the 'D' block to the east, and causing drag on the west flank of the Eleonore Bugt anticline, could be such an explanation, but remains speculative.

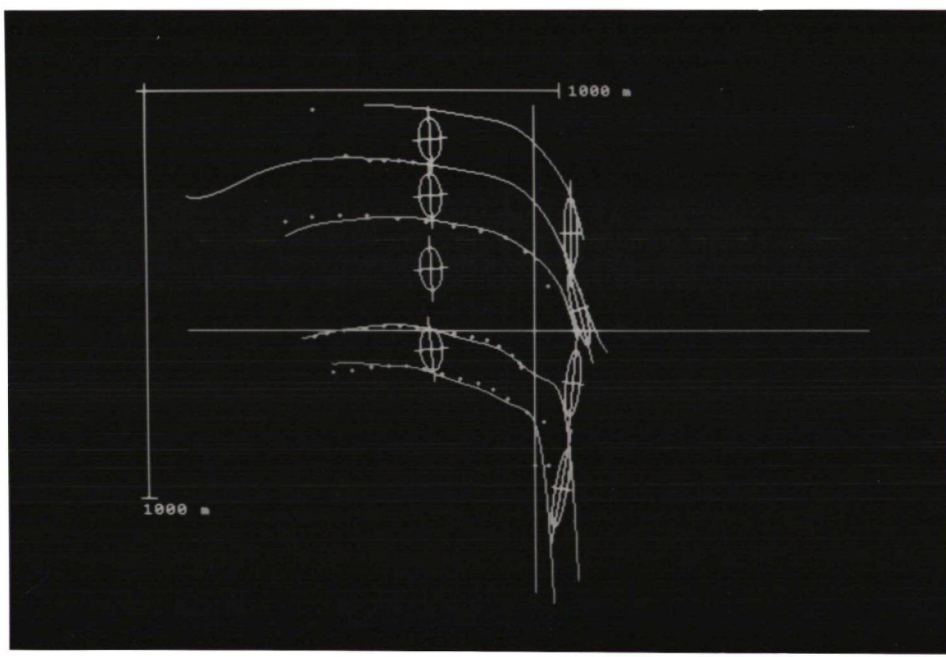


Fig. 4.8

Profile through the KAP OSWALD fold segment with the analysed surfaces shown. The analysed surfaces are bed group 17, bottom; bed group 18, bottom, horizon A and horizon B; bed group 19, bottom. The crossed show points calculated for the surfaces with the best fitting deformation mechanism parameters. Strain ellipses have been drawn on both flanks.

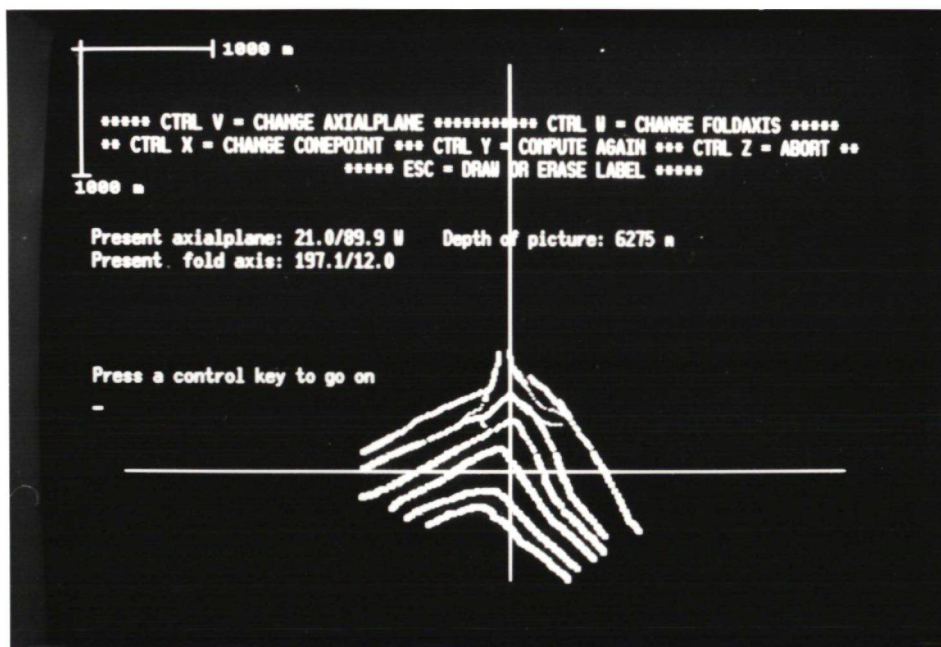


Fig. 4.9

Best obtainable projection for the fold segment ANTIKLINALBUGT. Only selected surfaces are shown; these are the bottoms of the Ulvesø, Arena, Storeelv, Canyon, Kløfteelv and Bastion Formations.

4.2. The Eleonore Bugt anticline in the 'X' fault block

It was first attempted to treat the Eleonore Bay anticline in the 'X' block as a single segment, labelled 'ANTIKLINALBUGT'. The best projection obtainable is shown on fig. 4.9; the hinge of the bottom of the Kløftelv Formation is exposed on both sides of the island, so a precise fold axis could be determined by aligning the two hinges. It is, however, clear from the projection that the segment is not conical or cylindrical; the axial plane is twisted, dipping to the west in the background of the figure and to the east in the foreground. The segment was therefore split in two; only the northern segment, labelled 'ANTIKLINALBUGT N' will be treated further, as the southern segment contained but a single surface hinge.

The accepted projection of the northern segment is shown on fig. 4.10.

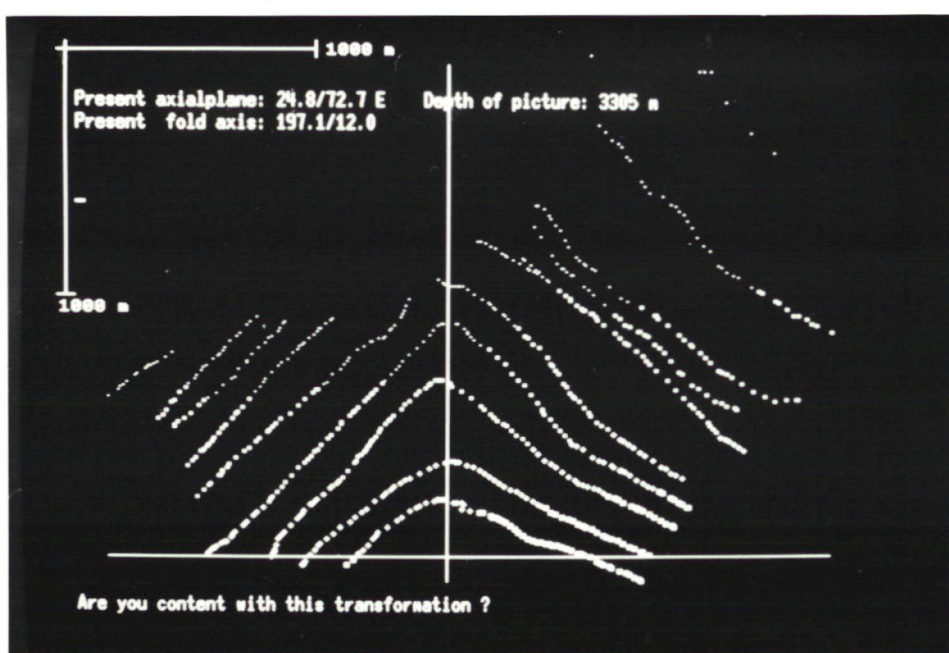


Fig. 4.10

Accepted projection of the fold segment ANTIKLINALBUGT N. Surfaces shown are those of fig. 4,9, plus the bottoms of the Ella Island, Hyolithus Creek, Dolomite Point, Antiklinalbugt and Cape Weber Formations.

Some of the surfaces have very angular hinges; it was necessary to give high weights to the points in the hinge zone, decreasing down the flanks, to get reasonable well fitting polynomiums. An example is shown on fig. 4.11; the fitting polynomium in this case has 15 terms, the maximum accepted by the program.

It is seen from the profile (fig. 4.10), that the segment is

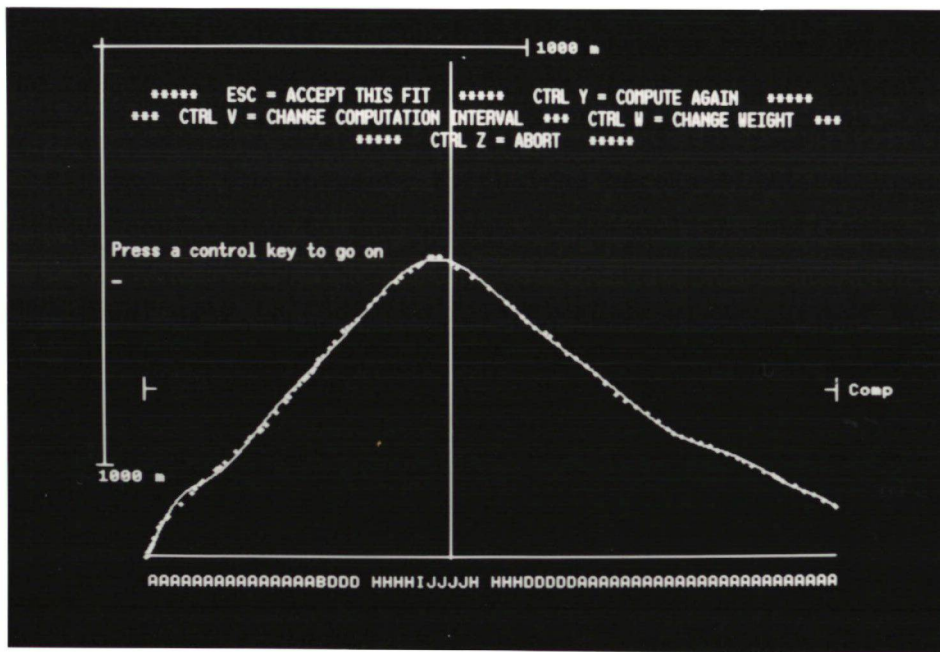


Fig. 4.11

Fitting a polynomial to the bottom of the Storeelv Formation. For explanation, see fig. 4.7.

disharmonically folded. The folding style of the Ulvesø Formation (between the two lowest surfaces) is different from Storeelv Formation (between surface 3 and 4 from below), and the Arena Formation (between the Ulvesø Formation and the Storeelv Formation) merely fills the space between them without conforming to any simple fold model. A shortening computation gave a 13.8% line length shortening for the bottom of the Arena Formation, against 21.3% for the bottom of the Storeelv Formation. The segment is therefore not well suited for deformation mechanism analysis; an attempt failed, since the iterative computation of the best fitting deformation mechanism parameters did not converge. This type of disharmonic folding is a general feature of the Eleonore Bugt anticline (see section 6.2.2.6 and 6.3.1)

4.3. The Central syncline

For this fold a single segment was defined, labelled 'BASTIONEN'. An axial plane could be measured, and a fold axis calculated (fig. 4.12). The best projection obtainable is shown on fig. 4.13. It is obvious that the fold is very disharmonic, being a broad, flat-bottomed syncline in its lower part, and with rather angular folding in its upper part. A

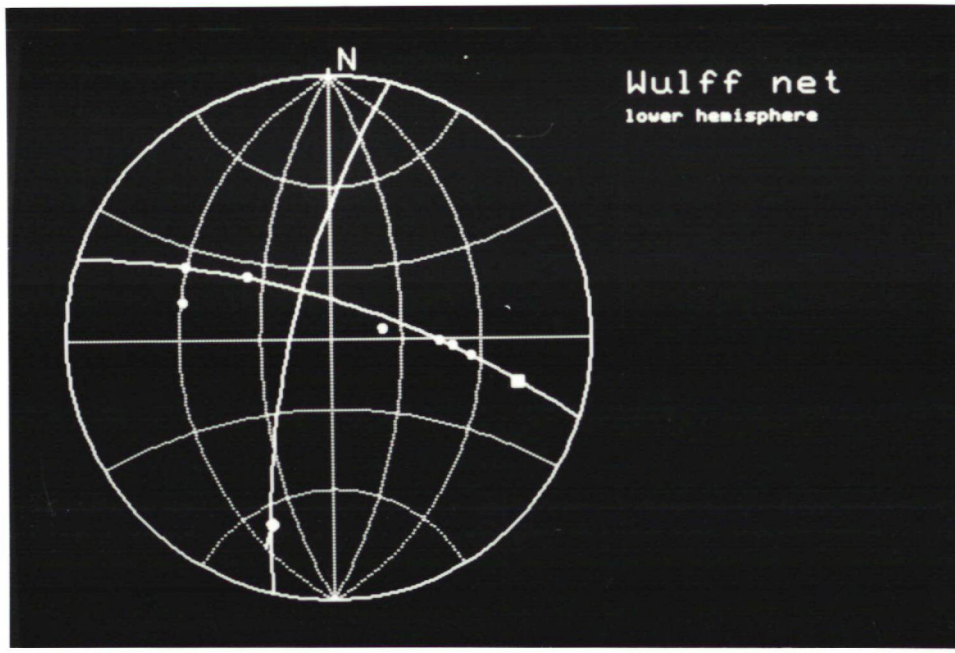


Fig. 4.12

Measured beddingplanes and axialplane (shown with a square and great circle), and calculated fold axis for the fold segment BASTIONEN.

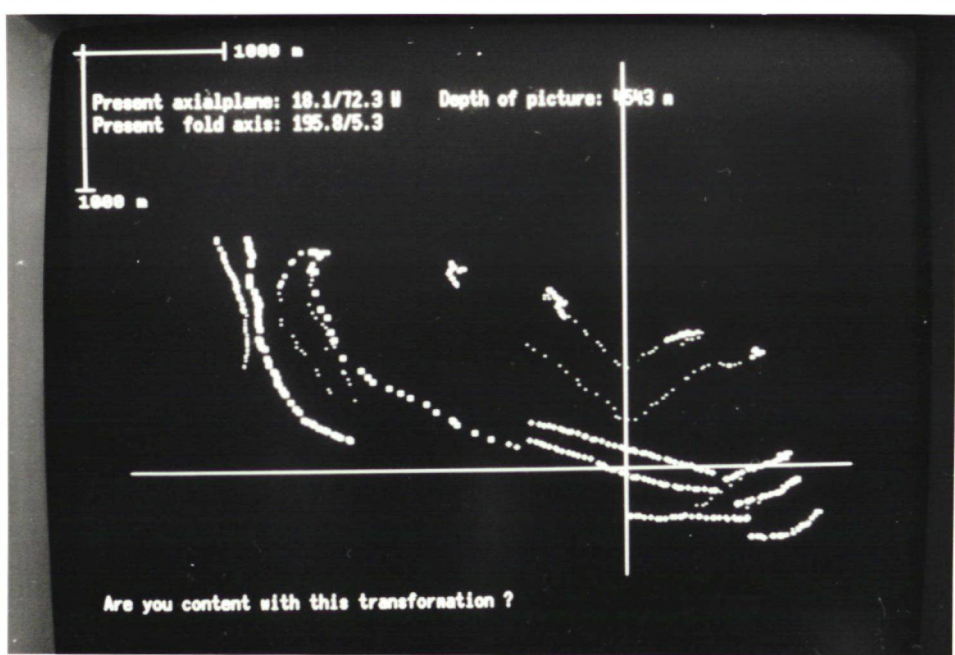


Fig. 4.13

Best obtainable projection for the fold segment BASTIONEN. The surfaces shown are the bottoms of the Dolomite Point, Antiklinalbugt, Cape Weber and Narhvalsund formations, and horizon A of the Narhvalsund Formation.

deformation mechanism analysis was attempted on the two uppermost surfaces (Narhvalsund Formation, bottom and horizon A), but miscarried, since correlations coefficients between the calculated parameters were all close to ± 1 .

On the steep northern wall of Bastionen, which lie in deep shadow on the air photographs, the bottom of the Cape Weber Formation could not be traced with any certainty. On the other hand, the bottom of the Antiklinalbugt Formation could be traced reasonably well, and a polynomial fitted to the surface. The surface representing the bottom of the Cape Weber Formation was therefore modelled using the bottom of the Antiklinalbugt Formation as base, and using a homogeneous compression of 1, 50% flexural slip folding, and an undeformed thickness of 200 m (fig. 4.14). Using the z-guiding feature (see section 7.2) of the PG2 system, the intersection between the modelled surface and topography could be drawn on the map.

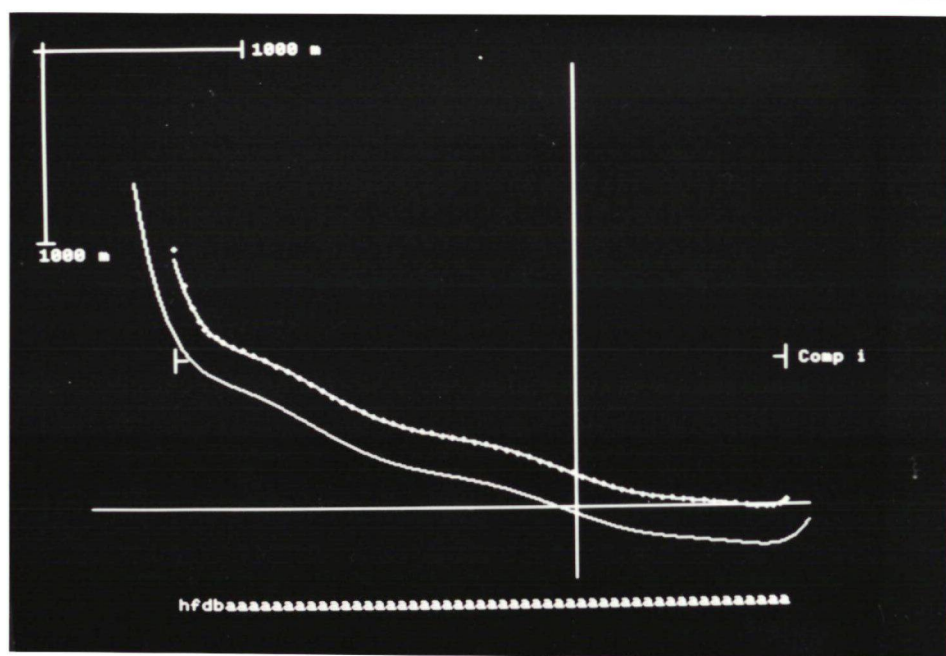


Fig. 4.14

Construction of the bottom of the Cape Weber Formation from the bottom of the Antiklinalbugt Formation. Crosses are points constructed for the Cape Weber Formation, with a polynomial fitted to them.

5. PHOTO-INTERPRETATION OF THE ELEONORE BAY GROUP OF THE FJORD ZONE, CENTRAL EAST GREENLAND

5.1 Introduction

The photo-interpreted area lies between 72°23' and 74°06'N, and between 24°23' and 26°20'W. It covers most of the classic 'Fjord Zone' area of folded Eleonore Bay Group sediments, bordered to the west by crystalline basement rocks and to the east by Devonian clastic sediments. The stratigraphy and photo-geological characteristics of the area is given below in section 5.2.

The photo interpretation was carried out from vertical air photos with a photo scale of 1:150 000. The stereo instrument allows a maximum magnification of 8 x, and the photos are of an excellent quality; nevertheless, less detail is present compared to the old photos with a scale of 1:50 000. The photos are taken with an ultra-wideangle camera; this means that several steep cliffs could not be interpreted, since they fell in the 'dead angle' of one of the photographs of the stereo model.

Otherwise, the interpretation could be carried out with good detail, due to the well differentiated nature of the sedimentary pile investigated. Problematic areas are:

Some steep cliffs, due to the lack of stereo effect mentioned above.

Steep, north-facing cliffs, since they are in deep shadow.

Badly exposed and heavily glaciated areas.

Areas cut by many faults, since the bed groups are difficult to identify in small fault blocks.

Fig. 5.1 shows the areas, where interpretation was difficult.

5.2 Stratigraphy and photo-geological characteristics of the rock of the area

A total thickness of ca. 16 000 m of folded Eleonore Bay Group, Tillite Group and Cambro-Ordovician sediments is present in the area. A stratigraphic column of these rocks is given in fig. 5.2. The folded sediments are underlain with a tectonic boundary by crystalline basement

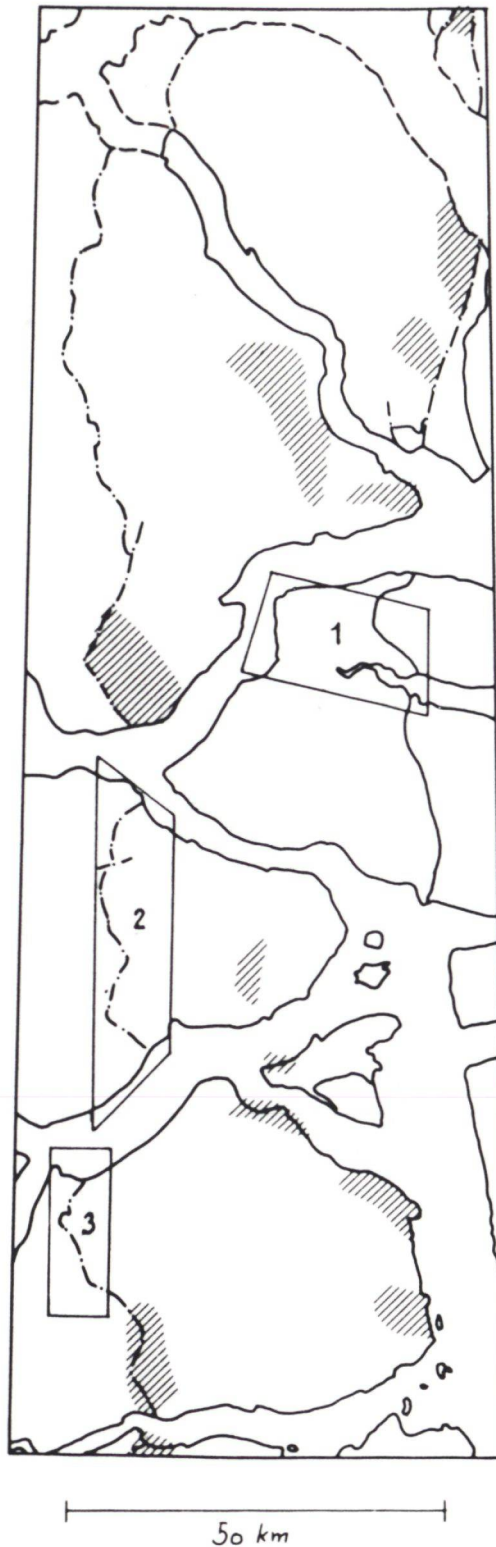


Fig. 5.1

Quality of the photointerpretation. Hatching shows areas where photointerpretation was difficult. The area marked 1 was mapped in the field by the author and J.L. Petersen during four weeks of the summer of 1986. The area marked 2 was interpreted with a mirror stereoscope, and the interpretation transferred manually to the map. The area marked 3 has not been photointerpreted, but is copied from Koch & Haller (1971).

rocks, and overlain with angular unconformity by Devonian continental clastics. No photo-interpretation has been done in the crystalline rocks and the Devonian sediments.

5.2.1 Undivided crystalline rocks

The crystalline rocks below the basal décollement plane of the Eleonore Bay Group mainly comprise Archaen to Lower Proterozoic gneisses, including significant augen gneisses, overlain by Middle Proterozoic (Grenville) metasediments (mica schists and quartzites), migmatites and granites (Higgins et al., 1981; Rex & Gledhill, 1981). Caledonian granites are present to an unknown extent; a large Caledonian granite on the west bank of Granitsø has not been shown.

The boundary to the Eleonore Bay Group sediments is often faulted, in which case it is easily distinguished; where the boundary is the basal décollement plane, distinction is much more difficult. In practice, the basal décollement plane has been drawn where a change occurs from hard rocks with a rugged appearance, to more recessive rocks. Since the lower part of the Eleonore Bay Group is often intruded by granite sheets, the décollement plane is probably placed too high.

5.2.2 Alpefjord series, Eleonore Bay Group

This is a series of quartzites and quartzitic shales, measuring 5500 m in Alpefjord just south of Forsblad Fjord. It was divided by Fränkl (1951) into 16 bed groups, informally named bed group 'a' (lowest) to bed group 'q' (highest). Subdivisions are well visible in the high mountains south of Forsblad Fjord, but their correlation with Fränkl's bed groups (defined at the coast of Alpefjord) is not easy. What is thought to be Fränkl's bed groups 'e' and 'q' have been distinguished on the 1:100 000 map south of Forsblad Fjord.

The uppermost unit of the Alpefjord series, bed group 'q', contains carbonate rocks, and is shown to occur in Jelsdal by Koch & Haller (1971). A thin, light-coloured horizon at this locality has been followed across western Lyell Land as the boundary between the Alpefjord series and the Eremitdal series.

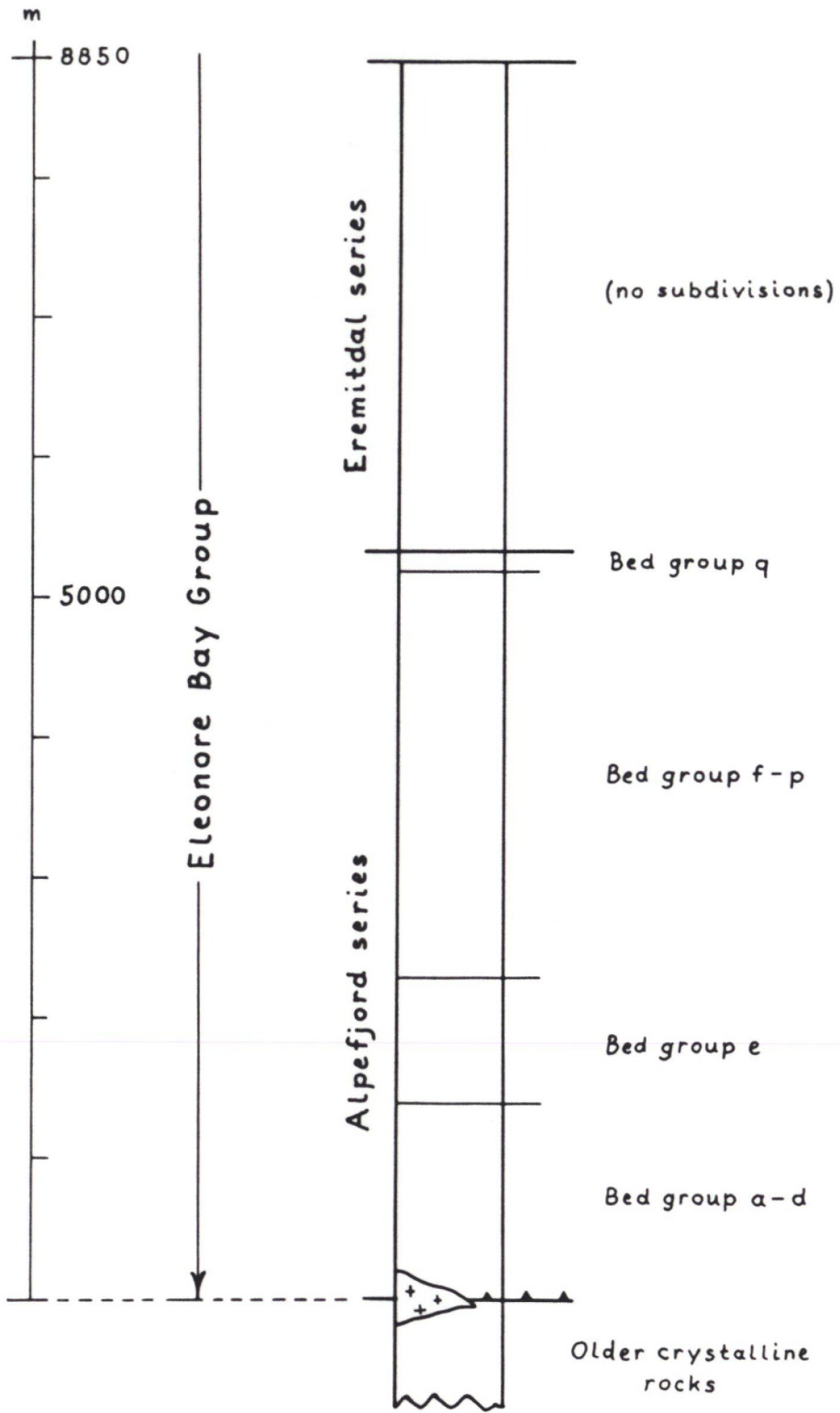


Fig. 5.2 a

Stratigraphic column of the rocks of the photointerpreted area, lower part.

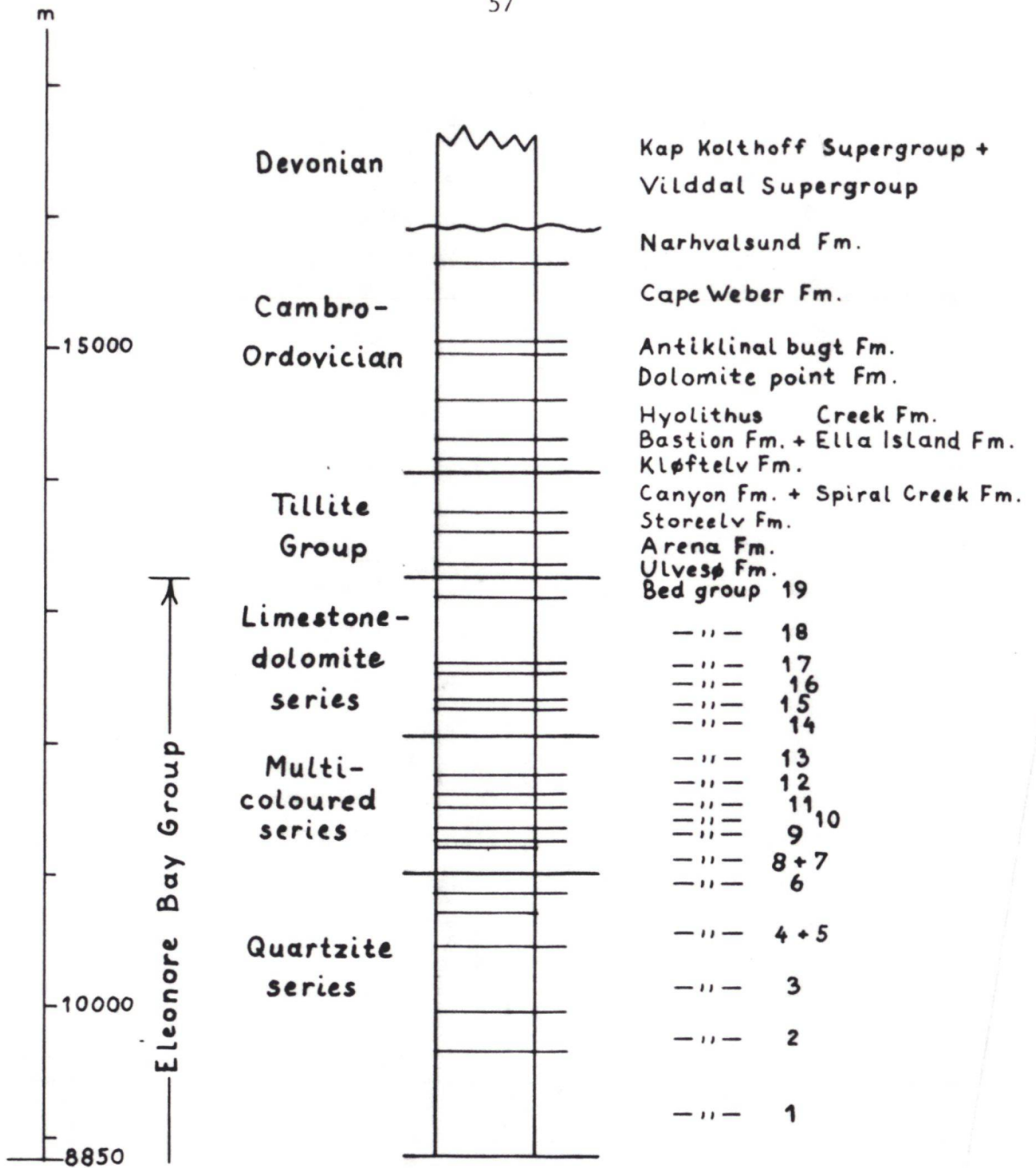


Fig. 5.2 b
Stratigraphic column of the rocks of the photointerpreted area, upper part.

5.2.3 Eremitdal series, Eleonore Bay Group

This unit comprises mainly quartzites and shales, in places with dolomitic lenses. At Forsblad Fjord, where the boundary to the Alpefjord series is preserved, it attains a thickness of 3500 m. Elsewhere up to ca. 2000 m is exposed above the basal décollement plane. It is a recessive unit, in which no subdivisions are visible.

5.2.4 Bed group 1, Quartzite series, Eleonore Bay Group

This unit comprises quartzites and quartzitic shales, with a thickness of 700 - 1000 m. The lower boundary is seen as a change from the dark, recessive rocks of the Eremitdal series to light, cliff-forming quartzites of the lower bed group 1. Upwards bed group 1 usually becomes darker and more recessive.

5.2.5 Bed group 2, Quartzite series, Eleonore Bay Group

This unit comprises light-coloured, thick-bedded quartzites with a thickness of ca. 300 m, which may rise to 500 m in western Lyell Land. It is a light-coloured, fairly resistant unit between the dark, more recessive upper bed group 1 and bed group 3.

6.2.6 Bed group 3, Quartzite series, Eleonore Bay Group

This is a unit of dark, recessive shales with a thickness of 500-700 m, thickest in the western part of the area. It is incompetent and may show significant thickness variations due to deformation.

5.2.7 Bed group 4, Quartzite series, Eleonore Bay Group

Bed group 4 consists of light-coloured, thick-bedded quartzites, upwards with an increasing proportion of rusty shale interbeds. Its thickness is 250-400 m. The lower boundary is marked by thick, resistant, light-coloured quartzites against the dark shales of bed group 3, and is a valuable guiding horizon.

The competent quartzites of bed group 4 often show spectacular folds that are disharmonic to the general fold pattern, and die out in the incompetent bed groups 3 and 5.

5.2.8 Bed group 5, Quartzite series, Eleonore Bay Group

Bed group 5 consists of recessive, dark red or green quartzitic shales with a thickness of 150-200 m. The boundary to bed group 4 is mainly marked by a colour change from rusty black shales to red shales, and is not visible on black-and-white air photographs. The boundary can locally be traced, however, as a change from shales with some quartzitic bands to shales with no quartzitic bands.

5.2.9 Bed group 6, Quartzite series, Eleonore Bay Group

This unit is 100-150 m thick and consists of thick-bedded, white and light red quartzites. The lower boundary is often marked by a band of white quartzites and is a good guiding horizon.

5.2.10 Bed group 7, Multicoloured series, Eleonore Bay Group

Bed group 7 comprises ca. 200 m of dark red, dolomitic shales. It is a recessive and incompetent unit that may show significant thickness variations due to deformation.

5.2.11 Bed group 8, Multicoloured series, Eleonore Bay Group

Bed group 8 comprises 20-50 m of yellow-weathering, thin-bedded dolomites. This light-coloured unit between the dark bed groups 7 and 9 is a good guiding horizon.

5.2.12 Bed group 9, Multicoloured series, Eleonore Bay Group

This unit comprises 100-150 m of dark, rather massive limestone. It is distinguished by its resistant nature, but especially the upper boundary may be difficult to see.

5.2.13 Bed group 10, Multicoloured series, Eleonore Bay Group

This unit comprises 100-200 m of dark red dolomitic shales with some yellow-weathering dolomite bands and lenses. It is mainly distinguished as a recessive unit between the resistant limestones of bed group 9 and 11, but the boundaries may be hard to pinpoint. The unit is incompetent and may show strong thickness variations due to deformation.

5.2.14 Bed group 11, Multicoloured series, Eleonore Bay Group

Bed group 11 consists of 100-150 m of dark limestone. It is distinguished from bed group 10 by its resistant nature, and sometimes also by its very dark colour.

5.2.15 Bed group 12, Multicoloured series, Eleonore Bay Group

Bed group 12 consists of 100-200 m of white, thick-bedded dolomites. Its competent, resistant nature and its light colour makes it an excellent guiding horizon.

5.2.16 Bed group 13, Multicoloured series, Eleonore Bay Group

Bed group 13 consists of ca. 300 m of quartzitic shales with some thick-bedded quartzites, and in its upper part with yellow-weathering dolomitic bands. It is of a spectacular rusty weathering colour, which is unfortunately not visible on the black-and-white aerial photographs, where bed group 13 is best distinguished by its recessive nature.

5.2.17 Bed group 14, Limestone-dolomite series, Eleonore Bay Group

This unit comprises 150-250 m of dark limestone. It is distinguished by its dark colour and its resistant nature compared to the underlying bed group 13. The exact position of the boundary may be difficult to pinpoint, however, since spectacular yellow-weathering dolomite bands occur both in the upper bed group 13 and lower bed group 14. Where possible, the boundary has been drawn at the lowest black horizon between the dolomitic bands.

5.2.18 Bed group 15, Limestone-dolomite series, Eleonore Bay Group

Bed group 15 comprises 50-150 m of white, massive dolomite. With its light colour it is easily distinguished between the dark bed groups 14 and 16. Its thickness varies strongly within short distances, and in some places it probably wedges out and is replaced by dolomites at an other level in the dark, uniform limestones of bed group 14 and 16. In Strindberg Land, it is replaced by limestones (Katz, 1952), which may be distinguished with some difficulty as lighter and more recessive than the bed group 14 and 16 limestones.

5.2.19 Bed group 16, Limestone-dolomite series, Eleonore Bay Group

This unit comprises ca. 200 m of dark, usually recessive limestones. Occasionally it contains light, dolomitised bands, that may be mistaken for bed group 15 or 17.

5.2.20 Bed group 17, Limestone-dolomite series, Eleonore Bay Group

Most of the description of bed group 15 applies to bed group 17 as well, exchanging bed Group 14 and 16 with bed Group 16 and 18. It is not replaced by limestones in Strindberg Land, however. In eastern Ymer \emptyset it is absent or very weakly developed, and here the distinction of bed group 16 and 18 is very difficult.

5.2.21 Bed group 18, Limestone-dolomite series, Eleonore Bay Group

Bed group 18 comprises 350-600 m of dark limestones, occasionally with white, dolomitised bands. It may locally be subdivided.

5.2.22 Bed group 19, Limestone-dolomite series, Eleonore Bay Group

Bed group 19 comprises 150-200 m of variegated dolomitic shales. It may be distinguished from bed group 18 by its more recessive nature, and sometimes by a banded appearance in its lower part. Since bed group 18 is also rather recessive, the exact position of the boundary may be difficult to see.

5.2.23 Bed group 20, Limestone-dolomite series, Eleonore Bay Group

Bed group 20 comprises 0-70 m of thin-bedded limestones. It is only present from Ymer \emptyset northwards, where it is distinguished from bed group 19 by its lighter colour and more resistant nature. It cannot, however, be distinguished photo-geologically from the overlying Ulves \emptyset Formation, and on the maps it is included in this unit. Recently, Moncrieff (1988) has described it as the lateral equivalent of the Ulves \emptyset Formation.

5.2.24 Ulves \emptyset Formation ('lower tillite') Tillite Group

This unit comprises 5-100 m of glacial sediments, mainly tillites. As noted above, the boundary to bed group 20 of the Eleonore Bay Group could not be seen. The Ulves \emptyset Formation is thick, where bed group 20 is thin (Moncrieff, 1988) and together they show a relatively constant thickness of 50-100 m.

5.2.25 Arena Formation ('inter tillite beds'), Tillite Group

This unit comprises 100-300 m of laminated shales with some packets of thin-bedded quartzites. It is distinguished by its recessive nature and dark colour.

5.2.26 Storeelv Formation ('upper tillite'), Tillite Group

This unit comprises 100-200 m of glacial sediments, mainly tillites. It is distinguished by its resistant nature compared to the shales of the Arena Formation and Canyon Formation, but it is often difficult to recognise.

5.2.27 Canyon Formation, Tillite Group

The Canyon Formation comprises 250-300 m of dolomitic and silty shales, with light-coloured limestones and dolomites in the upper part. It is distinguished by its recessive nature.

5.2.28 Spiral Creek Formation, Tillite Group

The Spiral Creek Formation comprises 25-50 m of dark red sandstones and shales. Where visible, it is a good guiding horizon, but it is often covered by scree.

5.2.29 Kløftelv Formation, Lower Cambrian

The Kløftelv Formation comprises 50-100 m of light-coloured, thick-bedded sandstones. It is distinguished by its resistant nature, but may in places be difficult to recognise. Where the Spiral Creek Formation is not visible, the lower boundary to the likewise light-coloured parts of the upper Canyon Formation is very difficult to locate accurately.

5.2.30 Bastion Formation, Lower Cambrian

The Bastion Formation comprises 100-150 m of dark shales. It is distinguished by its dark colour and recessive nature.

5.2.31 Ella Island Formation, Lower Cambrian

The Ella Island Formation comprises ca. 50 m of sandstones. It could not be distinguished photogrammetrically and may unsystematically have been included in either the Bastion Formation or the Hyolithus Creek Formation.

5.2.32 Hylolithus Creek Formation, Lower Cambrian

The Hylolithus Creek Formation comprises ca. 300 m of dark, massive dolomite. It is distinguished by its dark colour and resistant nature.

5.2.33 Dolomite Point Formation, Lower Cambrian - Lower Ordovician

The Dolomite Point Formation comprises 300-400 m of light yellow-weathering dolomites. It is distinguished by its resistant nature and its light colour; the Hylolithus Creek Formation is, however, also resistant and the exact position of the colour change may be difficult to locate.

5.2.34 Antiklinalbugt Formation, Lower Ordovician

The Antiklinalbugt Formation (formerly the Cass Fjord Formation) comprises 100 to 300 of muddy limestones. It is distinguished by its recessive nature. Both the upper and lower boundary are difficult to locate accurately.

5.2.35 Cape Weber Formation, Lower Ordovician

The Cape Weber Formation comprises ca. 600 of massive limestones. It is distinguished by its massive, resistant nature and relatively dark colour compared to the Antiklinalbugt and Dolomite Point Formations.

5.2.36 Narhvalsund Formation, Lower Ordovician

The Narhvalsund Formation is the youngest preserved part of the Caledonian Upper Proterozoic - Lower Palaeozoic sedimentation in the map area. 200 m of dolomite and limestone has been preserved here; the lowest part is slightly lighter coloured than the Cape Weber Formation, but the units are difficult to distinguish photogeologically.

5.2.37 Undivided Devonian sediments

The Devonian sediments of the map area comprise continental sandstones and conglomerates of the Kap Kolthoff, the Kap Graah and the Vilddal Supergroup (Friend et al., 1983; P. H. Larsen & H. Olsen, pers. comm.) These units have not been distinguished by this project. A photogeological and field study of the Devonian sediments of Central East Greenland is presently being undertaken by P. H. Larsen and H. Olsen, Grønlands Geologiske Undersøgelse.

The lowest Devonian sediments of the area are generally brecciose or conglomeratic; they are distinguished from the underlying, older sediments by their lack of structure.

5.2.38 ?Devonian melange (Skyggedal conglomerate)

This unit, described by Sommer (1957) and in section 6.4.1, only occurs at the south coast of Narhvalsund. Its boundaries are taken from Sommer (1957), as it could not be distinguished photogrammetrically in the deep shadow of the steep, north-facing coast.

5.2.39 Upper Ordovician to Devonian granite

These are usually medium- to coarsegrained, two-mica granites to quartz-monzonites (Higgins et al. 1981; Rex & Gledhill 1981). They are distinguished by their light colour and their lack of structure.

5.2.40 Dykes of uncertain age

A few, narrow east-west trending lineaments at the east end of Antarctic Sund have been interpreted as dykes. They have not been noted by Eha (1953).

5.3. Ages of the rocks of the photo-interpreted area

The Eleonore Bay Group and the Tillite Group have been dated using acritarchs by Vidal (1979). Vidal concluded that the Eleonore Bay Group was of Upper Riphean age, while the Tillite Group was of Vendian age. A significant hiatus between the two Groups was postulated. A recent investigation of the glacial sediments of the Tillite Group (Montcrieff 1988) concludes, however, that sedimentation was continuous from the Eleonore Bay Group to the Tillite Group. This is in agreement with Bertrand-Sarfati & Caby (1976), who dated the Limestone-dolomite series of the Eleonore Bay Group as Vendian using stromatolites.

The Kløftelv Formation has not been dated, but it is regarded as Cambrian because of its transgressive nature. The overlying formations have been dated by macrofossils (summary in Henriksen & Higgins, 1976) and microfossils (Vidal, 1979; Smith, 1982) as Lower Cambrian (Bastion Formation, Ella Island Formation, Hyolithus Creek Formation); Lower Cambrian to Lower Ordovician (Dolomite Point Formation); and Lower

Ordovician (Antiklinalbugt Formation, Cape Weber Formation, Narhvalsund Formation).

Vertebrate macrofossils bracket the Devonian sediments of the map area as Givetian to Famennian (Summary in Friend et al., 1983). The Skyggedal conglomerate has not been dated.

The crystalline rocks and the granites have been dated by radiometric methods. A summary of the results is given by Rex & Gledhill (1981). Important individual ages are discussed in the structural analysis (section 6).

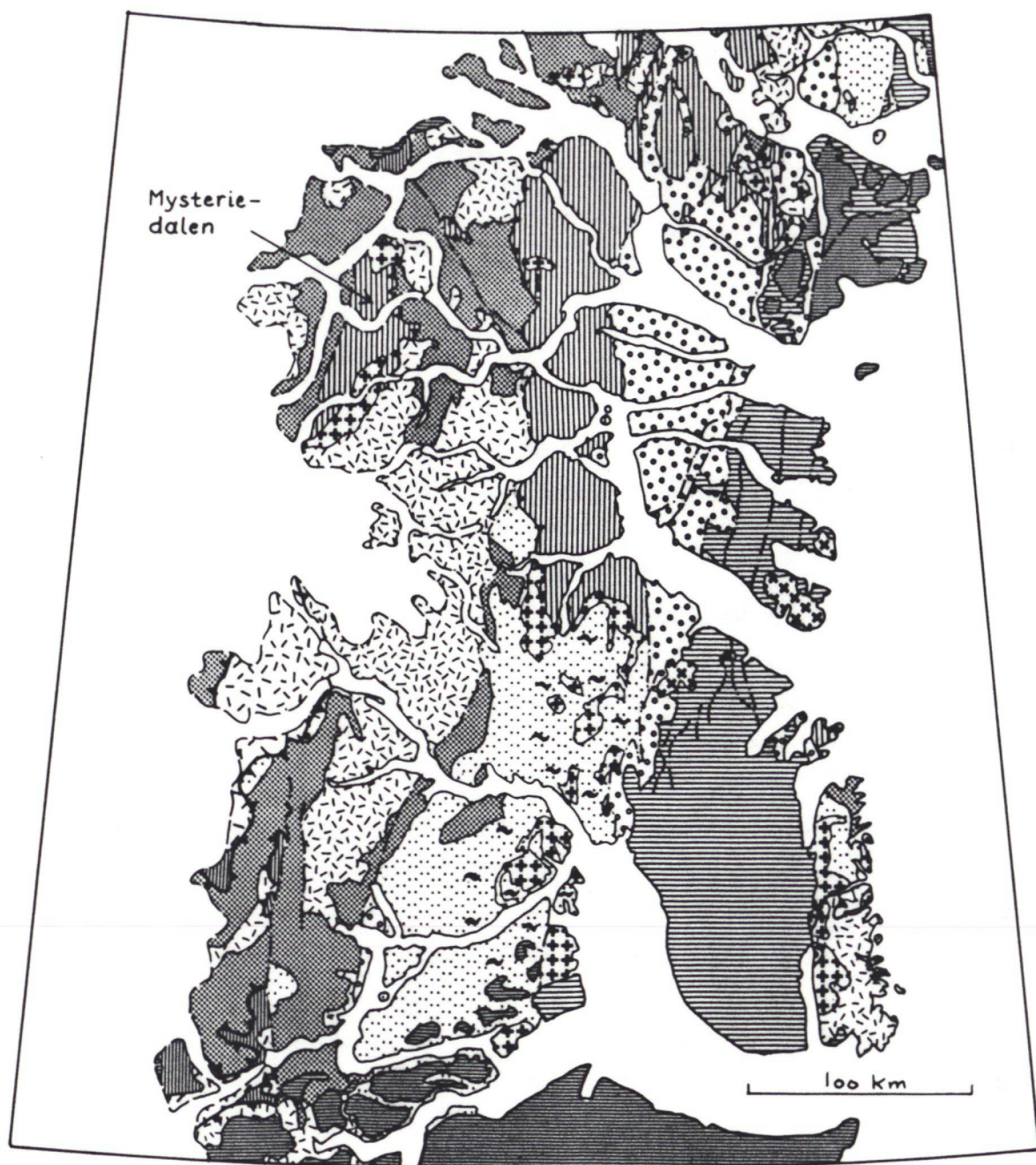
6 STRUCTURAL ANALYSIS OF PHOTO-INTERPRETED AREA

6.1 Introduction

A structural analysis has been carried out of the photo-interpreted area. The results of the analysis have been compiled into a structural map 1:250 000, reproduced here as plate II and covering the photo-interpreted area. This area will in the following be referred to as 'the map area'. The map area is situated in central East Greenland between 72° and 74°N. The geology of this region was investigated by a series of expeditions led by Lauge Koch in the years 1929 - 1958. An early synthesis of the structural evolution was given by Wegmann (1935), who created the 'stockwerk model'; this was further developed by J. Haller, who published a synthesis of the geology of the region (1971) and of the tectonic evolution (1970). Also a geological map at a scale of 1:250 000 was published (Koch & Haller, 1971). Detailed descriptions based on field work in the map area are given by Eha (1953), Fränkl (1953a, 1953b), Katz (1952) and Sommer (1957).

The 'stockwerk model' regards the pre-Devonian rocks of the region as almost exclusively Caledonian. A sequence of geosynclinal sediments (the Eleonore Bay Group, Tillite Group and the overlying Cambro-Ordovician sediments) more than 16 km thick was during the Caledonian orogenesis migmatized and granitized in its deeper parts; the resulting, highly mobile quartzo-feldspathic rocks (the lower 'stockwerk') was separated from the stiffer, low metamorphic upper part of the sedimentary sequence (the upper 'stockwerk') by a strongly deformed zone of high metamorphic sediments (the middle 'stockwerk'). Folding in the upper 'stockwerk' is thought to be largely a reflection of (mainly vertical) movements in the lower 'stockwerk'. Very little of the original basement to the Eleonore Bay Group has survived in a recognisable state, according to the 'stockwerk model'.

Later investigations by Grønlands Geologiske Undersøgelse in the Scoresby Sund region in the years 1968-1972, and in the 72°-74°N region from 1975 to 1978, and especially the isotopic dating programmes carried out in connection with these investigations (see Steiger et al., 1979; Rex & Gledhill, 1981), and Hansen & Henriksen (in prep.) for summaries) has cast doubt on the 'stockwerk model'. Most of the quartzo-feldspathic rocks of the 'lower stockwerk' appear to be Lower Proterozoic or older gneisses, or migmatites of Grenville (1200-900 Ma) age; significant Caledonian

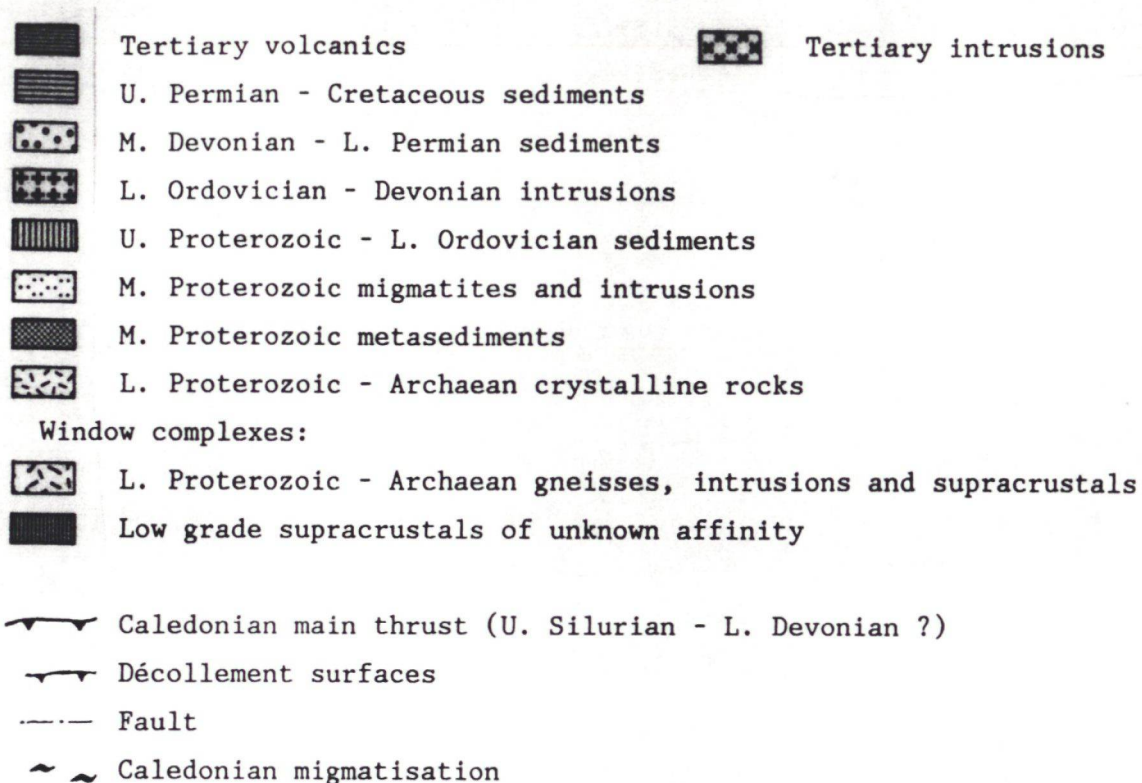


migmatisation has only been described from the Stauning Alper - eastern Renland area. Most of the high-grade metasediments of the 'middle stockwerk' appear to be of Grenville age. The rocks of the middle and lower 'stockwerks' thus seem to be the basement of the Upper Proterozoic (Upper Riphean, Vidal 1979) Eleonore Bay Group.

The basement contact is described (Higgins et al., 1981) as a border zone between high grade, strongly recrystallised metasediments of Grenville age, and lower grade, less recrystallised Eleonore Bay Group sediments. The zone is frequently intruded by granite sheets, and contains frequent shear

Fig. 6.1

Geologic map of Central East Greenland



zones and dislocations pointing to movements along it. The zone is interpreted by Higgins et al. as a décollement zone between deforming Eleonore Bay Group sediments and a relative inert basement; in Mysteriedalen in Louise Boyd Land a major, recumbent fold lies immediately above the décollement zone, pointing to a westward movement of the Eleonore Bay Group of at least 25 km at this locality.

A late- to postkinematic granite, intruded into the décollement zone at the north coast of Forsblad Fjord, has given a Rb/Sr whole rock isochron age of 445 ± 5 Ma (Rex et al., 1976), thus giving an Upper Ordovician minimum age for the movement on the décollement zone.

Very little activity in the 72° - 74° N region can be dated to the interval between the Upper Ordovician and the Middle Devonian, though other parts of the Caledonian fold belt in East Greenland were the site of important thrusting and plutonism in this period.

In the Middle and Upper Devonian the region became the site of important continental sedimentation with accompanying deformation and volcanism. The stratigraphy of the Devonian sediments were investigated by Bütler (summary in Haller, 1971), who divided them into five 'series'. The 'series' were

distinguished by their ages relative to four deformational events, the 'Hudson Land phases I-IV'. Friend et al. (1983) investigated the sedimentology of the Devonian sediments. They retained Bütler's subdivision into five 'series', but concluded that only the four younger are extensively exposed north of 72°N. The oldest of these, which were named the Vilddal Supergroup, had been deposited in an ill-defined basin east of the map area, while the second oldest, named Kap Kolthoff Supergroup, had been deposited in a well-defined, ca. 60 km wide north-south oriented basin. This basin, whose western margin coincides with the eastern boundary of the map area, was named the Gauss basin. The basin fill had been partially supplied by rivers entering the basin from the west and building up huge alluvial fans into the basin. The Devonian conglomerates at Ella Ø were thought to have been deposited by such a river. Outside the fans, the Gauss basin was filled up by sandstones, deposited from south-flowing rivers.

Recent investigations of the central East Greenland Devonian, carried out by the Grønlands Geologisk Undersøgelse from 1986 onwards, have led to modifications of this model (P.H. Larsen & H. Olsen, pers. comm.). The conglomerates at Ella Ø, and similar conglomerate occurrences along the west margin of the Gauss basin, are referred to the Vilddal Supergroup; active movements on the basin margins and resulting high relief are thus earlier than the deposition of the Kap Kolthoff Supergroup. The Kap Kolthoff Supergroup shows no signs of a western Gauss basin margin of marked relief.

In the map area, only structures dating from the Upper Ordovician and from the Middle to Upper Devonian are present. No younger structures have been identified; post-Devonian deformation, if present, could have been reactivation of earlier structures.

6.2 Upper Ordovician structures

The following structural elements are from stratigraphic and radiometric evidence thought to be of Upper Ordovician age (fig. 6.2):

Basal décollement zone

Folds of a general north-south axial direction

East-west striking faults between Kejser Franz Joseph Fjord and Narhvalsund

Low angle tension faults

6.2.1 Basal décollement zone

The basal décollement zone can be followed from Forsblad Fjord across Lyell Land until Kap Hedlund, where it is cut off by the Kap Hedlund fault; and from Granitsø across northern Strindberg Land and Andrée Land to Lucia Gletscher, where it is cut off by the Blomsterbjerg fault. It is difficult to recognise photogrammetrically, and the photo-interpretation has given no new information on it.

6.2.2 Folds of general north-south axial direction

The area is deformed by a set of large folds, some of which can be followed for 150 km along the axis. They are generally rather open structures, and with rapidly changing profiles along the axis. The largest folds will be described individually in some detail; these are:

- I. The Border Syncline
- IIa. The Kap Alfred anticline and
- IIb. The Nunatakletscher anticline
- IIIa. The Central syncline and
- IIIb. The Eremitdal syncline
- IVa. The Eleonore Bugt anticline and
- IVb. The Agard Bjerg anticline
- V. The Gletscherpas syncline
- VI. The Brogetdal anticline

Profiles through the folded area are given in plate III. In the description below, numbers in parantheses refer to profile numbers.

6.2.2.1 The Border Syncline runs just east of the present-day outcrop of the basal décollement zone from Nunatakletscher to ca. 5 km north of Grejsdal. North of Eremitdal it is a well developed box fold with a south-plunging axis (15); south of Eremitdal it flattens out (14), and at Grejsdal it seems to dissolve into several smaller folds (13).

6.2.2.2 The Kap Alfred anticline can be followed from the present-day margin of the Eleonore Bay Group at Jelsdal, Lyell Land, and northwards until Kempe Fjord. It is a very large fold with an amplitude of ca. 4 km at Jelsdal (2); northwards it seems to diminish (3), and north of Kempe Fjord/Narhvalsund it is replaced by tension faults.

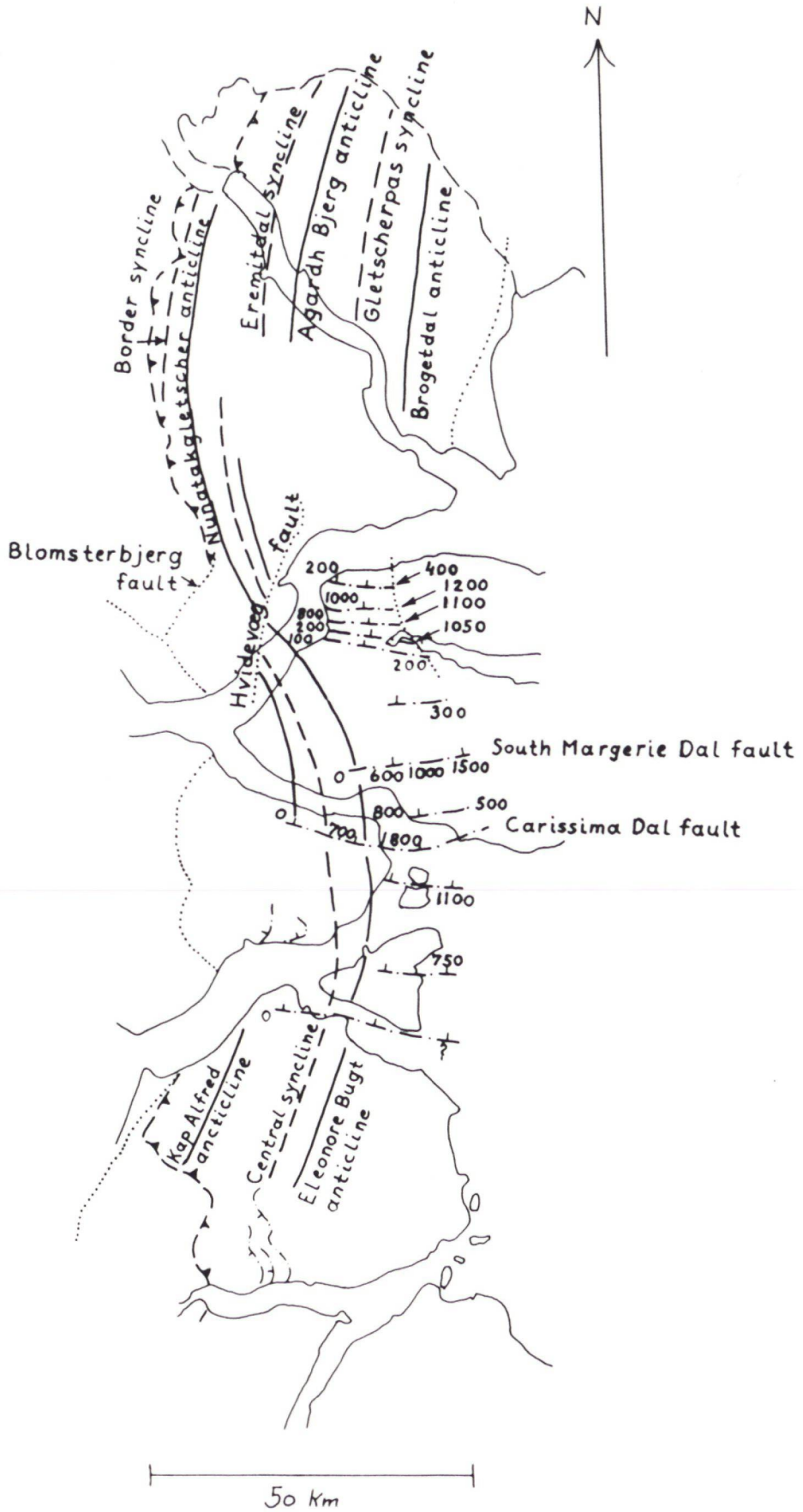


Fig 6.2

Structures regarded as upper Ordovician.

- ▼ — ◀ — Basal décollement surface
- Major anticline
- Major syncline
- — — — — ⁵⁰⁰ Fault with dip direction and throw indicated

6.2.2.3 The Nunatakglletscher anticline can be followed from Nunatakglletscher, where it is a well developed, broad box fold (15), across Eremitdal to the ice field between Eremitdal and Grejsdal. Here it flattens very much and almost loses its identity (13); south of Grejsdal it tightens somewhat again, and can be followed as an open, rounded anticline across Andrée Land (9-11). All this way, it is exposed in the Quartzite series; east of the Hvidevæg fault, where it is shifted ca. 4 km dextrally, it is exposed in the Limestone-dolomite series and Tillite Group, and here it assumes a more angular, though still open form (8). It can be followed across Ymer Ø to northern Suess Land, where it ends abruptly at the Carissima Dal fault. The area between the southern end of the Nunatakglletscher anticline and the northern end of Kap Alfred anticline is virtually unfolded (5).

6.2.2.4 The Central syncline can be followed from Grejsdal in Andrée Land to Jelsdal in central Lyell Land; south of Jelsdal it is replaced by tension faults (1). North of Jelsdal the syncline first appears as an open fold in bed groups 4-7 (2); the axis is north-plunging, and in northern Lyell Land bed group 18 is exposed in the core. Here the syncline has developed an almost flat bottom (3). North of the large faults in Narhvalsund (sections 6.2.3, 6.4.1), the Narhvalsund Formation is exposed in the core; the syncline is still flat-bottomed (4), though angular, disharmonic folds are present in the core (section 4.3). The axis ascends rapidly northwards, flattening out in Suess Land, where the fold is mainly exposed in the Limestone-dolomite series and the Tillite Group. The structure flattens out here, and is almost indistinguishable at the Carissima Dal fault (6). Northwards the axial plane becomes east-dipping, and across Ymer Ø the fold tightens again, until it at Kiledal is an almost isoclinal, overturned fold in the Limestone-dolomite series and the Tillite Group (8).

North of Kejser Franz Joseph Fjord, the Central syncline is cut obliquely by the Hvidevæg fault, which shifts it dextrally ca. 4 km. The shape of the fold just north of the fjord is difficult to establish, due to disturbances from the fault, but north of Benjamin Dal it is an open structure with east-dipping axial plane in the lower Quartzite series (9). Northwards it tightens, giving rise to overturned, subisoclinal parasitic folds in bed group 4, which constitutes the core of the fold in northern Blåbærdal. North of Blåbærdal the axial plane steepens; at Grejsdal the fold is still prominent and fairly tight (11, 12), but northwards it flattens quickly and disappears (13). It does not link up with the Eremitdal syncline as shown by Fränkl (1953a).

6.2.2.5 The Eremitdal syncline can be followed from northern Strindberg Land to Endelø's Gletscher south of Eremitdal in Andrée Land. Further to the south it splits into smaller folds and dies out. At Eremitdal the fold is a broad structure with a steep western flank (14). The core is occupied by the upper Quartzite series, and bed group 4 is folded into a spectacular series of smaller box folds. In southern Strindberg Land the syncline is a broad, open structure in the Quartzite series (16).

6.2.2.6 The Eleonore Bugt anticline can be followed along the Central Syncline from central Lyell Land, where it is replaced to the south by tension faults, to Grejsdal in Andrée Land, where it dies out. In central Lyell Land it is an open, upright, rather angular structure (2). Further North in Lyell Land, the fold becomes asymmetrical by the decrease in the dip of the eastern flank (3); it thereby assumes the form of a monocline, limiting the large, non-folded area east of Polhem Dal. Just south of Narhvalsund the flat, eastern flank starts to dome, but north of the large faults in Narhvalsund, in the Cambro-Ordovician of Ella Ø, the fold is again upright and symmetrical (4). Northwards across Ella Ø the dip of the eastern flank decreases again, and the fold retains a monoclinial form (5) until just south of the Carissima Dal fault. Here the eastern flank starts to dome, and the crest of the fold moves from the hinge of the monocline to the dome (6). The doming is cut off by the Carissima Dal fault; north of this fault the crest is at the hinge of the fold, which is asymmetrical, but with a fairly steep (25°) eastern flank. On the north side of Antarctic Sund, this flank is again low dipping and has developed a dome, which in

turn is cut off by the south Margerie Dal fault. North of this the Agardh Bjerg anticline is monoclinic, with a flat eastern flank (7) that starts to dome in central Ymer Ø. This doming is obscured by Kejser Franz Joseph, but does not seem to be cut off by the east-west faults in Noa Dal; it may possibly be traced as far as Eleonore Bugt, diverging in trend from the direction of the monocline hinge of the fold. This follows the Central Syncline to the Hvidevæg fault, with disharmonic folding in the Multicoloured series at Kiledal (8). At the Hvidevæg fault it is shifted 4 km dextrally; northwards of the fault it can be followed as a monocline as far as Grejsdal, all the way with a domed eastern flank (9, 10). The doming can actually be followed further to the north than the monocline hinge, being accentuated by faulting at Grejsdal (11), but north of Grejsdal it splits into smaller folds and dies out (12). It does not link up with the Agardh Bjerg anticline as shown by Fränkl (1953a).

6.2.2.7 The Agardh Bjerg anticline can be followed east of the Eremitdal syncline from northern Strindberg Land to Endeløs Gletscher in Andrée Land. It is a broad, open structure (15, 16), whose southern end is obscured by the Hvidevæg fault.

6.2.2.8 The Gletscherpas syncline and

6.2.2.9 The Brogetdal anticline are only present in Strindberg Land. They are both broad, open structures, but superimposed later folding (section 6.4.2) makes it difficult to ascertain their true profile.

Besides the large folds described above, folds on a smaller scale have been recognised in several areas, namely west of the Nunatakletscher anticline between northern Sues Land and Blomsterbjerg fault; in a zone east of the Agardh Bjerg anticline and Eleonore Bugt anticline, between Noa Dal and northern Strindberg Land; and in central Andrée Land, in the transition zone between the central syncline/Eleonore Bugt anticline and Eremitdal syncline/Agardh Bjerg anticline. The Eleonore Bay Group east of the Eleonore Bugt anticline seems to be non-folded, but is gently east-dipping.

6.2.3 East-west striking faults

Between Noa Dal and Narhvalsund, a group of east-west striking faults have relationships to the major folds indicating a common age for both. It comprises the south Margerie Dal fault and the Carissima Dal fault, and a fault that is interpreted positioned in Narhvalsund; across these faults, the Eleonore Bugt anticline changes profile abruptly (section 6.2.2.6). These three faults all die out towards the west, and attain their greatest exposed throw at their eastern ends (fig. 6.2). The same applies to most of the other east-west striking faults between Noa Dal and Narhvalsund, and it is therefore assumed that they are all of the same generation. Together they have resulted in an extension in a north-south direction of at least 4 km along the eastern margin of the Eleonore Bay Group outcrop, decreasing to zero towards the west. A bending of the area, with the outside of the bend to the east, is necessary to explain this (see section 6.3).

According to Fränkl (1953a), the medium scale fold pattern in the Morænedal area in Andrée Land changes abruptly across the east-west faults in the area. This could not be confirmed photogrammetrically, since much of the area is badly exposed, but it would indicate that the faults were active during the folding. They have probably been reactivated during the Devonian deformation (section 6.4.2).

The faults of the Morænedal area probably extends into the heavily glaciated area between Endeløs Gletscher and Grejsdal, where the pattern of the major folding changes rather quickly. The glaciation makes this difficult to ascertain.

6.2.4 Low angle tension faults

West dipping, low angle (20° - 40°) extension faults occur in the southern part of Suess Land and in south-western Lyell Land. In Lyell Land they set in where the Central Syncline and the Eleonore Bugt anticline die out, and grow more prominent to the south; at Forsblad Fjord the extension amounts to ca. 500 m. They continue south of the mapped area.

In southern Suess Land they lie to the south of a weakly folded area, but north of the northern end of the Kap Alfred anticline. They may, however, extend further to the north into the badly exposed Ørkendal area. At Kempe Fjord, the extension amounts to ca. 1500 m.

The tension faults may be due to rotational strain at the end of large folds, in the manner shown in fig. 6.3.

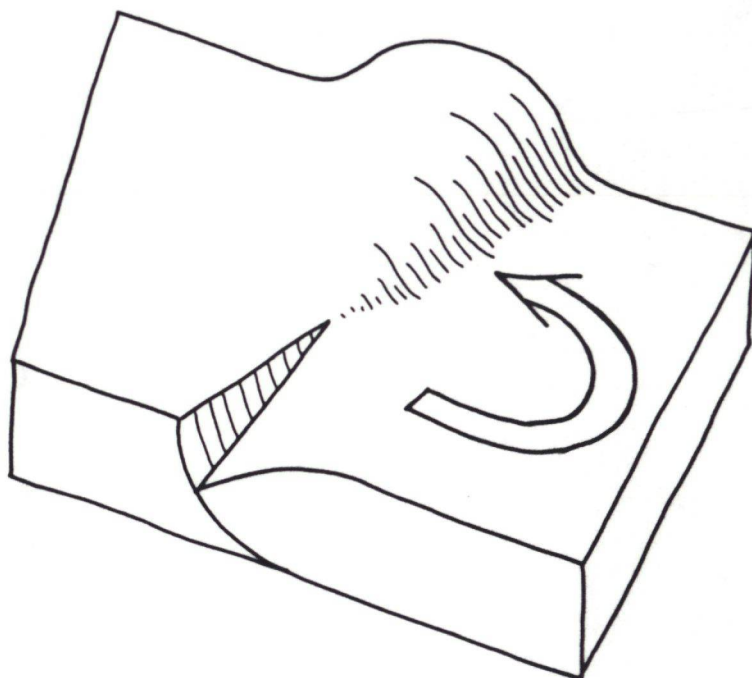


Fig. 6.3

Model for the development of tension faults at the end of a conical fold.

6.3 Discussion of the upper Ordovician deformation

6.3.1 General westward translation of the Eleonore Bay Group

As stated in the introduction (section 6.1), the boundary between the Eleonore Bay Group and the underlying crystalline rocks is now interpreted as a décollement surface (Higgins et al., 1981) with at least locally a westward movement of 25 km or more. Bengaard (1985) assumed this movement to be a general feature of the deformation of the Eleonore Bay Group. The main arguments for the assumption of a general westward movement of the whole Eleonore Bay Group, and not just a local westward movement of the Eleonore Bay Group around Mysteriedalen, are as follows:

a) The Central Syncline/Eleonore Bay anticline fold pair has a distinct westward vergence over most of their length. The other major folds of the area show no clear vergence, and thus apparently speak against movement; the same is the case in the Mysteriedalen area, however, where non-verging folds are present at stratigraphic levels above the large, recumbent fold (Higgins et al., 1981, fig. 18).

b) The deformation varies at different heights in the sediment pile. This is prominent at Kiledal (profile 8), where the steep but uncomplicated monocline in the Quartzite series develops upwards through the disharmonic folding in the Multicoloured series into the tight, overturned fold in the Limestone-dolomite series and Tillite Group. Here the line length shortening is much greater than in the Quartzite series. Further upwards shortening must decrease again, as there is not room for much Cambro-Ordovician in the core of the Central Syncline (fig. 6.4). The folding at

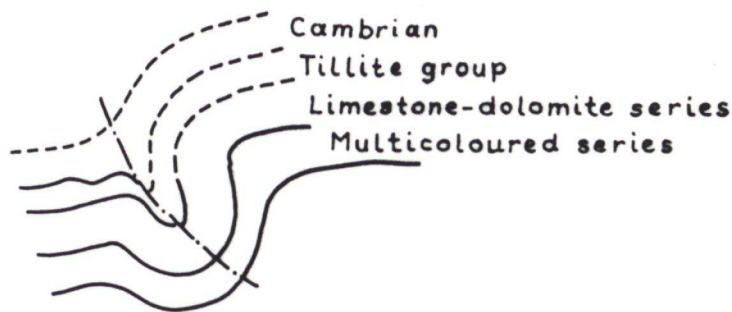


Fig. 6.4

Profile through the Central Syncline and the Eleonore Bugt Anticline at Kiledal, with the effects of the Kiledal fault removed.

this place is thus partly of an intrafolial nature with westward translation of the upper part of the folded sediments. A folding style like this makes shortening calculations of the type made by Eha (1953) meaningless.

Disharmonic folding with different shortening at different levels can be seen at other places along the Eleonore Bay anticline, and at the Eremitdal syncline. Here the translation direction is not clear, however.

During the field mapping of the north-western part of Ymer Ø, several minor (100 m scale) thrusts were found in incompetent units (bed group 1, 3, 13). The thrusts had westward displacement, and point to westward beddingplane-parallel translations in this otherwise mainly unfolded area. Thrusts like these are too small to be recognised by photogrammetry on a photo scale of 1:150 000. Small thrusts with an eastward displacement were also seen, but they were steeper and seem to be associated with the east limbs of box folds in bed group 4 of the Quartzite series (see also Higgins et al., 1981, fig. 16).

c) There is a large difference in the stratigraphy of the Eleonore Bay group in the area around Mysteriedalen, and its assumed correlatives in the eastern part of the map area (Haller, 1971). Today the areas are separated by ca. 50 km of basement rocks; if the 25 km westward movement of the Mysteriedalen Eleonore Bay group only applies to this area, the original separation would have been but ca. 25 km. This is a rather short distance for such large stratigraphical changes to occur, especially as the sediments of the two areas appear to be of the same general facies type. The original separation would have been even shorter, if it is assumed that the Eleonore Bay group of the map area has moved eastwards, sliding down the basement uplift to the west.

6.3.2 Dynamic models for the translation

Three dynamic models can be proposed to account for the westward translation of the Eleonore Bay group across the basement:

- a) The Eleonore Bay group may have been pushed by a compressive force acting from the east.
- b) The basement may have moved eastward below the Eleonore Bay group scraping the Eleonore Bay group off in a 'thin-skinned' fashion. In this case the compressive forces in the Eleonore Bay group would have been acting from the west to the east, in contrast to model a).
- c) The Eleonore Bay group may have slid down a westward dipping basement driven by gravity. In this case the driving force would not have been acting from any particular direction, but would have attacked dispersed in the whole mass of the Eleonore Bay group.

Model a) and b) implies the existence of a regional stress field in the large block of the Eleonore Bay Group during deformation. This stress field would have been fairly homogeneous, since there is no regional thrusting and generally only moderate folding to take up the stress. The assumption of a fairly homogeneous stress field is not in accordance with the fact that the deformation in the Eleonore Bay group varies in an unsystematical way in a north-south direction. Segments with fairly strong folding (northern Ymer \emptyset) alternate with less folded segments (northern Strindberg Land, southern Ymer \emptyset) and almost unfolded segments (central Andrée Land).

One segment (Lyell Land + southern Suess Land) combines tensional and compressional structures in an apparently rotational deformation (sect. xx).

This observed variability of deformation agrees better with the assumption of a large slab of Eleonore Bay Group, sliding down a sloping basement and beginning to disintegrate into a mosaic of smaller blocks, each with its own local stress field and resulting local deformation. Therefore the gravity gliding model c) is preferred.

The two compressional models a) and b) implies the existence of Upper Ordovician shortening in the basement below or east of the Eleonore Bay Group, presumably in the form of thrusts. The gravity gliding model c) implies the non-existence of such shortening. A major Caledonian basement thrust exists in central East Greenland, but it lies west of the Eleonore Bay Group. It is badly dated, but is probably younger than the deformation of the Eleonore Bay Group (Bengaard, 1985).

It is seen from the structural map that the direction of the fold axes vary systematically within the map area, describing a large, open 'S'. The southern bend of the 'S' lies in the area of the east-west faults described in sect. 6.2.3, and may be due to the bending deduced from them.

The mechanism behind the bedding remains obscure. It is tempting to imagine that the basement uplift in central Suess Land (of Devonian age, see sect. 6.4.1) were initiated in the Upper Ordovician, and represented an obstacle to the westward gliding of the Eleonore Bay Group, which then bended around it. This agrees not, however, with the weak folding in most of the Eleonore Bay Group in Suess Land.

An interesting feature of the deformation is the domes developed on the flat eastern flank of the Eleonore Bugt anticline (fig. 6.5). The domes at Grejsdal, Noa Dal and south Margerie Dal/Carissima Dal, are spaced regularly at 25-30 km intervals along a lineament striking ca. 150° , and are each elongated in a north-south direction. The culmination of the Nunatakgløtsher anticline at Eremitdal lies where the next dome would be expected to the north-northwest; together, the domes are arranged as en échelon domes. En échelon domes form, where two blocks of cover rocks, parted from a rigid basement by a décollement zone, move differentially to each other in a horizontal direction (Wilcox et al., 1973). This generally happens over a strike-slip fault in the basement, but could also happen by differential movements in a sheet of gravity gliding cover rocks. It cannot be determined, which mechanisms were active, but in any case the block

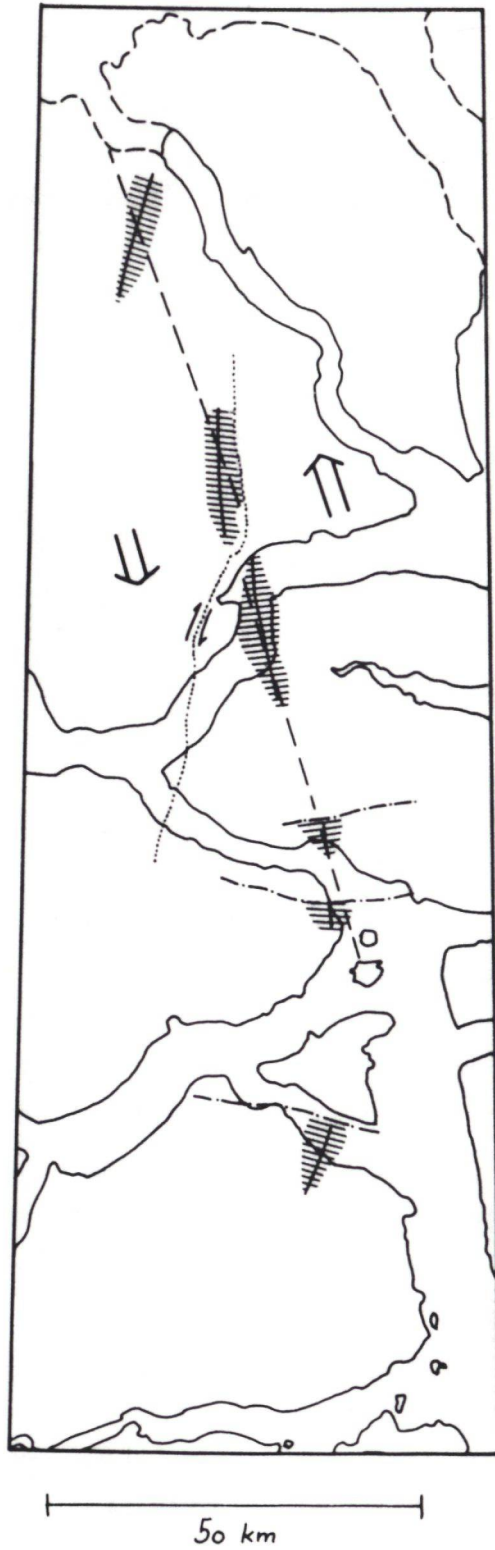


Fig. 6.5

Doming on the eastern flank of the Eleonore Bugt Anticline. Hatching indicates domed areas. Thick arrows shows inferred differential movement in the Eleonore Bay Group to account for the doming.

east-northeast of the dome lineament must have moved to the north-northwest relative to the other block west-southwest of the domes.

The southernmost dome, at the northern end of Polhem Dal, is not aligned with the others. It may have been shifted to the west by the bending discussed above.

6.4 Devonian deformation

Two systems of structures in the map area can be dated as Middle to Upper Devonian; both consist mainly of faults. One is connected with the western margin of the Eleonore Bay Group outcrop of the map area, the other with the western margin of the Gauss basin, which coincides with the eastern margin of the Eleonore Bay Group outcrop.

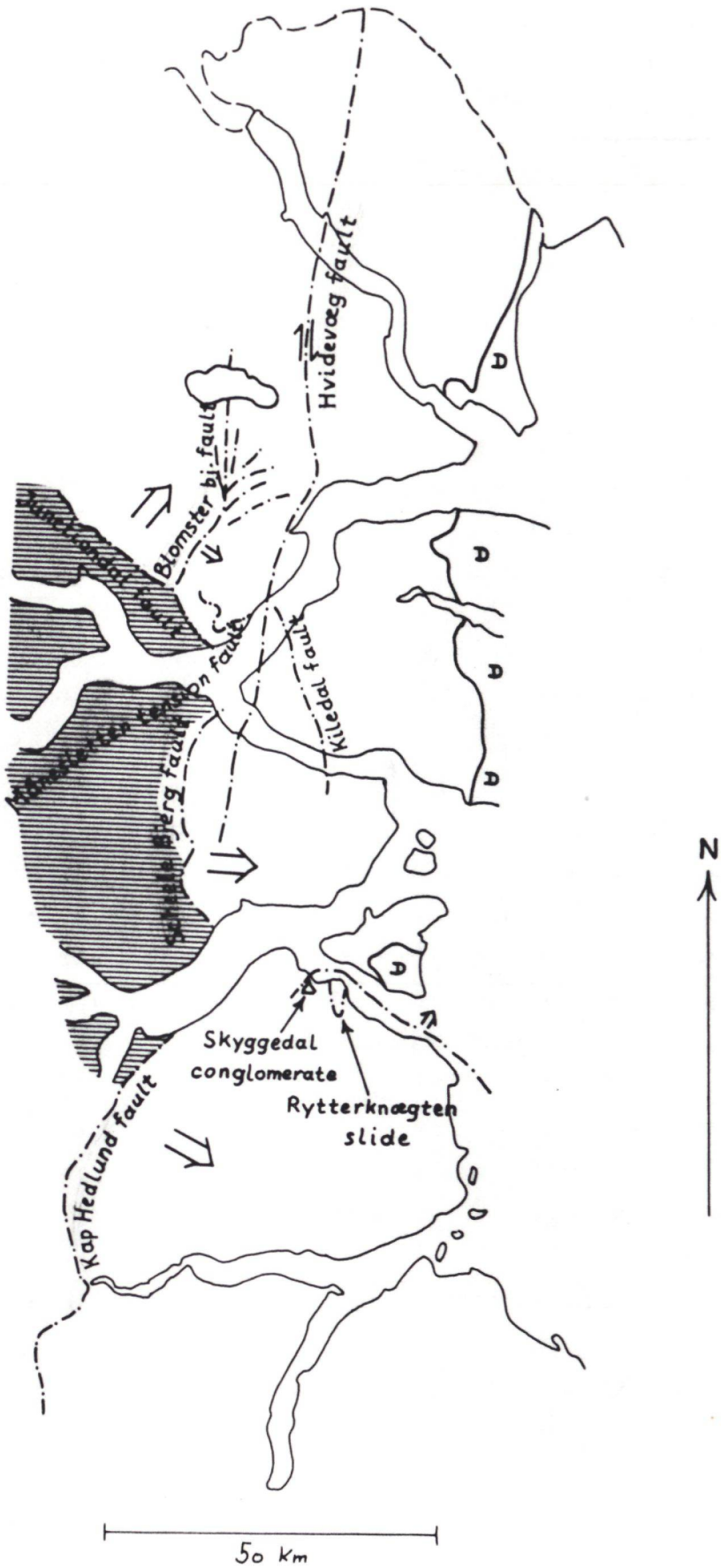
6.4.1 Fault system associated with the western margin of the Eleonore Bay group in the map area.

This system comprises the Junctiondal fault, the Scheele Bjerg fault, the Kap Hedlund fault, the Blomsterbjerg fault, the Hvidevæg fault and a fault in Narhvalsund (fig. 6.6). It probably also comprises the Månesletten tension fault, the Kiledal fault and northwest-southeast striking faults in eastern Lyell Land. The Junctiondal fault, the Scheele Bjerg fault and the Kap Hedlund fault together limit a block of crystalline rocks to the west. This block is characterised by K/Ar mineral ages, interpreted as cooling ages, of down to 370 Ma, while the surrounding rocks have cooling ages of 410-430 Ma (Rex & Higgins, 1985). The crystalline block thus seems to be a basement uplift of Middle Devonian age; this age must also pertain to the surrounding faults.

The Junctiondal fault and the Scheele Bjerg fault both have very large throws, with the crystalline rocks to the west uplifted at least 5000 m. A synclinal area with Limestone-dolomite series and Tillite Group runs along them to the east; it is possible that this synclorium lies on the west flank of a large 'roll-over' anticline, developed during the faulting.

Fig. 6.6

Devonian structures associated with a basement uplift to the west of the map area. Hatching indicates the area with low cooling ages. Thick arrows show the relative movement of the fault blocks. D = Devonian sediments.



No such effect is seen along the Kap Hedlund fault, however, whether this is due to a smaller throw or different fault geometry in depth.

The Junctional fault, Scheele Bjerg fault and Kap Hedlund fault are not parallel, and down-slope movement on them must have resulted in differential movements in the Eleonore Bay Group block to the east. These movements were taken up by other faults. A large fault in Narhvalsund has taken up much of the differential movement from the Scheele Bjerg fault and Kap Hedlund fault (an Upper Ordovician fault is probably also present in Narhvalsund, see section 6.2.3). The presence of Devonian faulting in Narhvalsund is supported by the presence of the 'Skyggedal conglomerate' (Sommer, 1957). This is a conglomerate of locally derived blocks, some rounded and some angular, in a matrix of red-brown sandstone. The conglomerate is preserved below an apparently old slide consisting of the incompetent bed group 19 of the Limestone-dolomite series of the Eleonore Bay Group. Sommer (1957) compares the conglomerate to the Devonian conglomerates of the area. On Ella Ø, on the downthrown side of the Narhvalsund fault, is found a major occurrence of continental clastics. This is dated as upper Middle Devonian from vertebrate fossils (Friend et al., 1983) and may have been deposited in a valley governed by the fault. The Skyggedal conglomerate, and the large slide at Rytterknægten, may have developed at the side of this valley. The fault throw across Narhvalsund is very large, ca. 6000 m at Ella Ø, but part of the movement occurred on the Upper Ordovician east-west fault. In eastern Lyell Land, Many faults parallel the strike of Narhvalsund and may be contemporaneous with the Narhvalsund fault.

The Blomsterbjerg fault takes up some of the differential movements between the Junctional fault and the Scheele Bjerg fault. It feathers out to the north, where it is cut by the Grejsdal granite. This has been dated to 377 ± 89 Ma (Rb/Sr whole rock isochron, but the isochron is in reality located by two points; Rex & Gledhill, 1981). Another part of the differential movement of the Junctional fault/Scheele Bjerg fault is taken up by the Hvidevæg fault. This fault has a dextral strike-slip movement of ca. 4 km; this reflects the northward component of the movement of the block northeast of the Junctional fault.

6.4.2 Devonian structures associated with the western margin of the Gauss basin

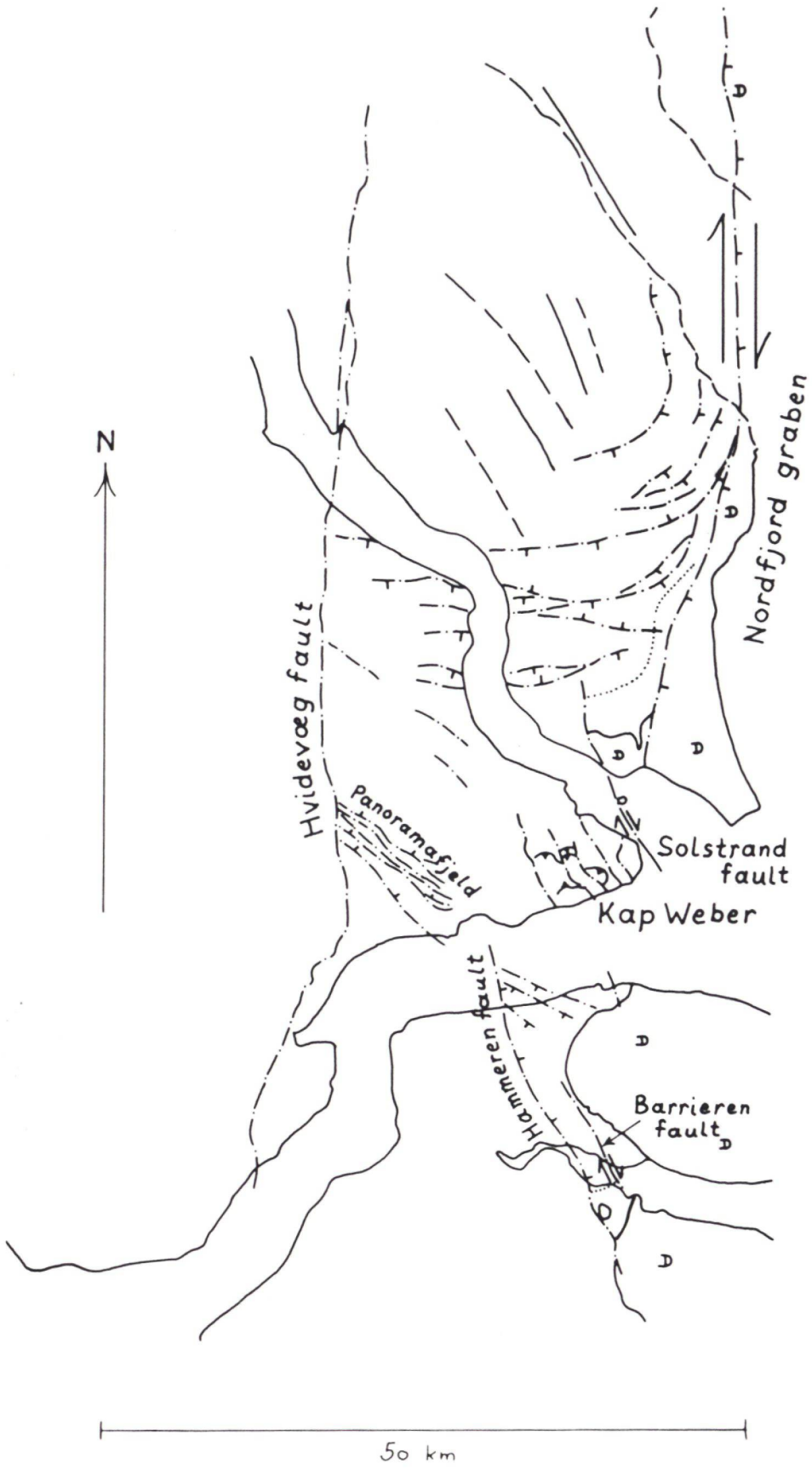
In the map area, the western margin of the Gauss basin can be divided into a northern, a central and a southern segment with different structural characteristics.

In the southern segment, from Narhvalsund southwards, a marginal flexure and north-south striking faults run along the margin on the east coast of Lyell Land, as described by Sommer (1957).

In the central segment, from ca. 73°13' N southwards to Narhvalsund, the sediments of the Gauss basin oversteps the Upper Ordovician structures of the Eleonore Bay Group without apparent deformation. Any structures associated with the formation of the basin must lie east of the present Eleonore Bay Group outcrop, possibly buried beneath the Devonian sediments.

In the northern segment, from Strindberg Land to ca. 73°13'N, structures of several types are present and may be combined into a model, pointing to dextral strike-slip movement along the margin of the Gauss basin. Other structures are connected with the formation of the Nordfjord graben, a narrow graben structure developed after the deposition of the Kap Kolthoff Supergroup. The structures are (fig. 6.7):

- a) In most of central Strindberg Land, the north-south running Brogetdal anticline and Gletscherpas syncline is superposed by folds with axial direction between 135° and 155°. The superposition gives rise to domes and basins, e.g. the large dome exposing the Eremitdal series along Waltershausen Gletscher, already described by Katz (1952). The folds die out a few km east of Hvidevæg fault, giving an en échelon arrangement of the folds. It is difficult to ascertain, whether the folds are present on the badly exposed plateau of southern Strindberg Land. Further south, in the eastern part of Andrée Land and on Ymer Ø north of Noa Dal, the few medium scale folds probably belong to the Upper Ordovician folding, whose axis here is directed north-northwest. South of Noa dal, the folding in the eastern part of the Eleonore Bay Group dies out, irrespective of its age.
- b) In the south-eastern part of Strindberg Land, many crescent-shaped faults are present. They strike east-west at Geologfjord, but swing to the north as they are followed eastward, until they parallel or join the Gauss basin margin. The faults generally have downthrow to the south and east, but antithetic faults also occur, creating small, but spectacular horst and graben structures along the east coast of Strindberg Land.



c) At the south side of Brogetdal the Tillite Group and the Cambrian sediments, together normally ca. 2000 m thick, have been sheared out to a thickness of 5-600 m (Katz 1952, fig. 39). To the south and west of this locality they are not exposed, but must be thinned to find room between the exposed Limestone-dolomite series and the Ordovician. The thinning is not present north of Brogetdal; to the west the thinned zone is cut off by the Solstrand fault.

A similar thinning of the Tillite Group and Cambrian is present at the south coast of Dusen Fjord; here the thinning is cut off to the west by the Hammeren fault, and to the east probably by the Barrieren fault.

d) The Nordfjord graben is bounded to the west by a prominent north-south striking fault running from Solstrand at the south coast of Strindberg Land, across the mouth of Brogetdal to Waltershausen Gletscher, and from there northward out of the map area. North of Brogetdal, it is accompanied by a strong marginal flexure.

The structures mentioned under a-c above may be combined into a structural model of dextral strike-slip movement along the western margin of the Gauss basin, if this is assumed to have followed the western boundary fault of the Nordfjord graben. The northern part of this fault runs north-south, but in Strindberg Land it strikes ca. 18° ; this bend creates an obtuse promontory of Eleonore Bay Group rocks into the Gauss basin at Strindberg Land. Dextral movement on a fault of this shape will cause compression on the stoss side of the Promontory, accounting for the en echelon folds in central Strindberg Land, and cause tension of the lee side. Here the curved faults are tensional structures, possibly also with a minor amount of sinistral strike-slip. Further south, the thinned zones may be viewed as slides, limited to the sides by small strike-slip faults, and creating small pull-apart basins.

Fig. 6.7

Devonian structures associated with the western margin of the Gauss Basin.

-  Anticline
-  Syncline
-  Fault with dip direction indicated
-  Minor thrusts at Cape Weber
-  Sliding in the Tillite Group and the Cambrian sediments

The complicated, northeast-directed thrust system at Kap Weber is here interpreted as gravity slides into the basin created by the Solstrand fault; the thrusts do not seem to extend below the level of the Tillite Group. The interpretation is based on Fränkl's (1952a) description of Kap Weber, since the structures are too small to be investigated by photogrammetry based on 1:150 000 photos.

A group of northwest-southeast striking faults occur at Panoramafjeld and at the north coast of Hammeren. The faults at Panoramafjeld stop at the Hvidevæg fault, and have downthrow to the northeast; they may be associated with the dextral movement of the Hvidevæg fault. The faults at Hammeren have downthrow to the southwest, and seem to be connected with the dying-out of the Hammeren fault to the north. The junction is, however, covered by the Kejser Franz Joseph Fjord. Those northwest-southeast faults could thus provide a link between the two Devonian structure systems of the map area.

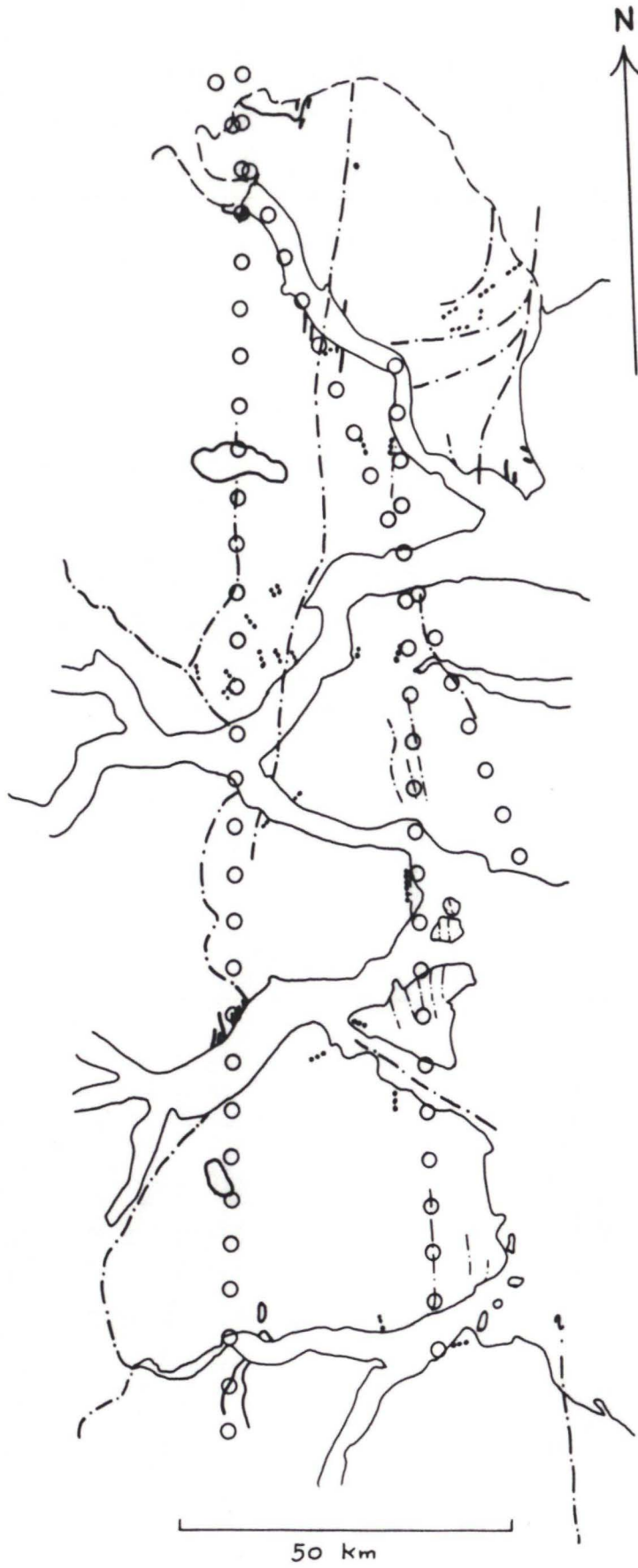
6.5 Deep-seated fractures

Many of the structures treated above are shallow structures, which deform the Eleonore Bay Group but do not extend below the basal décollement surface of the Eleonore Bay Group. Fractures, which extend down into the underlying crystalline basement below are of interest, since they may provide pathways for mineralizing agents. Such fractures would also be expected to be the site of intrusive activity. Besides the major Upper Ordovician and Devonian granite intrusions, several Tertiary and pre-Tertiary dykes are shown within the map area by Koch & Haller (1971); more may be present in the less accessible areas. A new occurrence of ultrabasic dykes were found in Noa Dal during the field mapping in 1986 (fig. 6.8). In the map area any basement fractures will often be buried beneath several km of Eleonore Bay Group sediments; therefore their surface

Fig. 6.8

Deep-seated fractures and lineaments in the map area.

- Tertiary dyke
- ... Pre-Tertiary dyke
- ◊ Granite intrusion
- ○ ○ Lineament



expressions may occur as fairly broad zones. The fractures, which may be expected to extend into the basement, are (fig. 6.8):

a) Obviously most of the Devonian faults associated with the western margin of the Eleonore Bay Group outcrop, namely the Junctiondal fault, the Scheele Bjerg fault, the Kap Hedlund fault, the fault in Narhvalsund and the Hvidevæg fault. Tertiary dykes are present at the north coast in Kempe Fjord, close to the Kap Hedlund fault; pre-Tertiary dykes are common in the area between the Blomsterbjerg fault, the Junctiondal fault and the Hvidevæg fault. Tertiary dykes are further present where the Hvidevæg fault crosses Geologfjord, and in Alpedal close to the Hvidevæg fault a small, pre-Tertiary intrusion occurs. The Blomsterbjerg fault and the Scheele Bjerg fault are probably the surface expressions of a larger lineament that also governs the emplacement of the Forsblad Fjord granite, the Argand Gletscher granite, the Grejsdal granite and the Nunatakletscher/Granitsø granite, and the apparent flexure of the basal décollement surface at Eremitdal (profile 14, 15). The present western margin of the Eleonore Bay Group outcrop of the map area, which runs in a general north-south direction, may also be a reflection of this lineament.

b) The major fractures associated with the western margin of the Gauss basin, i.e. the Nordfjord graben marginal fault and the crescent-shaped fault system. Pre-Tertiary dykes are present in central Strindberg Land, in the area of the latter; Tertiary dykes are present northwest of Kap Ovibos near the former.

Two less obvious lineaments are present, which may also be the surface expressions of deep-seated fractures. One may be followed as a zone of north-south striking faults along 25° W longitude from the south coast of Lyell Land to immediately south of Noa Dal. Further north it may be represented by the north-south trending valley on Ymer Ø opposite Grejsdal, by the valley between Grejsdal and Geologfjord, and the north-south trending segment of Geologfjord. Pre-Tertiary dykes are present in this lineament at Noa Dal, eastern Suess Land and at Geologfjord. Some of the east-west faults of assumed Upper Ordovician age terminates at north-south faults of this lineament; this would mean that they were active during the westward gliding of the Eleonore Bay Group across the basement. In accordance with this the zone of north-south faults defining the lineament is very broad, 5-10 km.

The other less obvious lineament runs in a 160° - 340° direction from the south-eastern Fladedal, along the Hammeren fault and lower Grejsdal. From there it runs across eastern Andrée Land, dividing the topographically rather flat area south-west of Morænedal from the mountaneous area to the west; then it runs along inner Geologfjord and across the basement rocks of north-western Strindberg Land, where its direction is clearly seen in the valleys. Tertiary dykes are present where this lineament crosses the Hvidevæg fault; a single pre-Tertiary dyke is present in eastern Andrée Land. The southern, and most distinct, half of this lineament runs parallel to the Central Syncline - Eleonore Bugt anticline fold pair, but separated some 20-25 km from them. It is tempting to imagine that the fold pair were initiated above the basement fracture postulated to account for the lineament.

7. SUMMARY AND CONCLUSIONS

As described in the introduction (section 2), this paper is the final report of the project 'geometric and geological analysis of photogrammetrically measured folded surfaces'. The aim of this project was to make computer treatment of folded surfaces, measured with the Kern PG2 stereo restitution instrument of the photogrammetric laboratory of the Grønlands Geologisk Undersøgelse, possible; and to carry out a photogeological mapping and structural analysis of an area of folded sediments in central East Greenland. The results obtained by the project may be summarised thus:

7.1 Mathematical modelling of folded surfaces

A mathematical modelling of folded surfaces had to be developed, to make computer calculations possible. The modelling used involves the splitting up of a folded area into single forms, i.e. single antiforms and synforms, and the splitting up of each single form along its length into approximately cylindrical or conical segments. Each fold segment is then treated individually (section 3.1). The folded surfaces of each segment are projected onto a profile plane perpendicular to the segment's fold axis (section 3.3), and the projection of each surface is modelled by a polynomial (section 3.4).

With the aid of this modelling, it is possible to compute the line length shortening of the folded surface (section 3.5).

A simple deformation mechanism model has also been developed (section 3.6). The model regards the fold as having formed in three steps; the first involves flexural slip folding, the second similar shear folding with the same axial plane, and the last homogeneous compression perpendicular to the axial plane. Equations have been derived, that describe the relationship between points on two different surfaces of such a fold.

Using these equations, it is possible to construct a new folded surface from an old, given the deformation mechanism parameters (section 3.7). It is furthermore possible to calculate the best fitting deformation mechanism parameters for a fold, where two or more surfaces have been modelled (section 3.8); and, when the deformation mechanism parameters are known, to calculate the strain ellipse for arbitrary points between the surfaces (section 3.9).

7.2 Computer implementation of the mathematical models

Computer programs have been written that implement the mathematical modelling summarized above. The programs are designed to run as part of the 'PG2 system' on a HP 1000 mini computer. The 'PG2 system' has been developed by H.F. Jepsen, Grønlands Geologiske Undersøgelse, for computer processing of the data collected with the Kern PG2 stereo restitution instrument. The programs allow calculation of the fold parameters mentioned above. Also, a routine for computation of the distance from an arbitrary point to a folded surface has been developed, and a routine allowing 'z-guiding' on a folded surface. The latter feature involves motor setting of the height of the measuring mark of the PG2 instrument, so that the measuring mark follows the surface when moved around in the stereo model. The program texts (ca. 700 pages) are available from Grønlands Geologiske Undersøgelse on request.

The western part of Ella^Ø was photo-interpreted using 1:50 000 air photos and analysed, using the programs, in greater detail than the larger photo-interpreted area (see below). This analysis is treated in section 4; the rather diverse shapes of the folded surfaces on the western part of Ella Ø could be modelled successfully using the method described in section 3. The fold manipulation routines (fold construction, z-guiding on folded surfaces) and the analytical routines (shortening computation, deformation mechanism analysis) were valuable tools in the photo-interpretation and structural analysis of the area, though the folding proved more disharmonic than expected.

7.3 Photo-interpretation of an area of folded sediments

Using the program developed, and the other programs of the 'PG2 system', an area of folded sediments has been photo-interpreted using air photos with a scale of 1:150 000 (section 5). The area is situated in the fjord zone of central East Greenland between 72°23'N and 74°06'N, and between 24°23'W and 26°20'W. It comprises mainly Upper Proterozoic to Lower Palaeozoic sediments, deformed during the Caledonian orogeny. A 1:250 000 geological map of the area has been compiled and is included in this report as plate I. Also, three geological maps 1:100 000 have been compiled; these maps are available from Grønlands Geologiske Undersøgelse on request.

7.4 Structural analysis of the photo-interpreted area

A structural analysis of the photo-interpreted area has been carried out (section 6), and a structural map 1:250 000 compiled (plate II). It is concluded that structures from two well separated periods during the Palaeozoic are present in the area, apart from the deformation in the crystalline rocks of the basement.

7.4.1. Upper Ordovician structures

The earlier structures, thought from radiometric and stratigraphical evidence to be the Upper Ordovician, comprises:

- 1) A basal décollement zone between the Eleonore Bay Group and the basement;
- 2) Major folds of a general north-south direction;
- 3) East-west striking faults;
- 4) West dipping, low angle tension faults.

The structures are interpreted as having formed while the Eleonore Bay Group moved at least 25 km in a westward direction by gravity gliding. Local differences in movement gave rise to local variations in the stress field, accounting for a marked, unsystematical variation in deformation intensity within the area. The low-angle tension faults are thought to be the result of local horizontal rotation, where conical folds die out and give rise to tension at their ends (fig. 6.3). The east-west faults are thought to be the result of tension on the outer arc of a zone of horizontal bending in the southern part of the area.

7.4.2 Devonian structures

The younger structures are from radiometrical and stratigraphical evidence thought to be of Middle to Upper Devonian age. A set of faults developed as a result of the rising of a basement uplift to the west of the central part of the area. Another set of structures comprises en échelon folds, crescent-shaped faults, and slides in the north-eastern part of the area. This set of structures are thought to have developed as a result of dextral strike-slip movement on the western margin of the Gauss Basin, a major Devonian sedimentary basin to the east of the area. These two sets of structures seem to have influenced the deposition of the Vilddal Supergroup of Upper Middle Devonian age. Younger ?Devonian structures are related to

the formation of the Nordfjord Graben, a narrow graben structure at the north-eastern margin of the area. These are the youngest structures identified within the area.

7.4.3. Deep-seated fractures

An attempt has been made to determine which of the above-mentioned structures that penetrate into the basement. Three basement lineaments have been identified from the occurrence of faults and magmatic intrusions (fig. 6.8).

ACKNOWLEDGEMENTS

The project was carried out at the photogeological laboratory of the Grønlands Geologiske Undersøgelse, led by H.F. Jepsen, who introduced me to the PG2 system. The project was financed by a grant from the Carlsberg Foundation.

I am grateful to J.L. Petersen for giving me the opportunity to visit Ymer Ø and for good companionship in the field; and to P.-H. Larsen and H. Olsen for valuable information on the Devonian sediments of East Greenland.

REFERENCES

- Bengaard, H.-J. 1985: Beskrivelse til et geologisk, et metamorft og et strukturelt kort i målestokken 1:1000 000 over Østgrønland 70°-82°N. Unpubl. dissertation, Geologisk Centralinstitut, Københavns Universitet.
- Bertrand-Sarfati, J. & Caby, R. 1976: Carbonates et stromatolites du sommet du Groupe d'Eleonore Bay (Précambrien terminal) au Canning Land (Groenland oriental). *Bull Grønlands geol. Unders.* 119, 51 pp.
- Eha, S. 1953: The pre-Devonian sediments of Ymers Ø, Suess Land, and Ella Ø (East Greenland) and their tectonics. *Meddr Grønland* 111(2), 105 pp.
- Fränkl, E. 1951: Die untere Eleonore Bay Formation in Alpefjord. *Meddr Grønland* 151(6), 15 pp.
- Fränkl, E. 1953a: Geologische Untersuchungen in Ost-Andrées Land (Nordostgrønland). *Meddr Grønland* 113(4), 160 pp.
- Fränkl, E. 1953b: Die geologische Karte von Nord-Scoresby Land (Nordostgrønland). *Meddr Grønland* 113(6), 56 pp.
- Friend, P.F., Alexander Marrack, P.D., Allen, K.C., Nichol森, J. & Yeats, A.K. 1983: Devonian sediments of East Greenland VI. Review of results. *Meddr Grønland* 206(6), 96 pp.
- Haller, J. 1970: Tectonic map of East Greenland (1:500 000). An account of tectonism, plutonism and volcanism in East Greenland. *Meddr Grønland* 171(5), 286 pp.
- Haller, J. 1971: *Geology of the East Greenland Caledonides*. Interscience publishers, New York, 413 pp.
- Hansen, B.T. & Henriksen, N. (in prep).
Bull. Grønlands geol. Unders.

- Henriksen, N. & Higgins, A.K. 1976: East Greenland Caledonian fold belt. In Escher, A. & Watt, W.S. (edit.) *Geology of Greenland*, 182-246. Geol. Surv. Greenland, Copenhagen.
- Higgins, A.K., Friderichsen, J.D. & Thyrsted, T. 1981: Precambrian metamorphic complexes in the East Greenland Caledonides (72°-73°N) - their relationships to the Eleonore Bay Group, and Caledonian orogenesis. *Rapp. Grønlands geol. Unders.* 104, 46 pp.
- Jepsen, H.F. & Dueholm, K.S. 1978: Computer supported geological photo-interpretation. *Rapp. Grønlands geol. Unders.* 90, 146-150.
- Katz, H.R. 1952: Zur Geologie von Strindbergs Land (Nordostgrønland). *Meddr Grønland* 111(1), 150 pp.
- Koch, L. & Haller, J. 1971: Geological map of East Greenland 72°-76°N Lat. (1:250 000). *Meddr Grønland* 183, 26 pp., 13 map sheets in portfolio.
- Moncrieff, A.C.M. 1988: The Vendian stratigraphy and sedimentology of East Greenland. Unpubl. Ph.D. dissertation, University of Cambridge.
- Poulsen, C. & Rasmussen, H.W. 1951: Geological map (scale 1:50 000) and description of Ella Ø. *Meddr Grønland* 151(5), 25 pp.
- Rex, D.C., Gledhill, A.R. & Higgins, A.K. 1976: Progress report on geochronological investigations in the crystalline complexes of the East Greenland Caledonian fold belt between 72° and 74°N. *Rapp. Grønlands geol. Unders.* 80, 127-133.
- Rex, D.C. & Gledhill, A.R. 1981: Isotopic studies in the East Greenland Caledonides (72°-74°N) - Precambrian and Caledonian ages. *Rapp. Grønlands geol. Unders.* 104, 47-72.
- Rex, D.C. & Higgins, A.K. 1985: Potassium-argon mineral ages from the East Greenland Caledonides between 72° and 74°N. In: Gee, D.G. & Sturt, B.A. (edit.) *The Caledonide orogen - Scandinavia and related areas*, 1115-1124. Wiley & Sons Ltd., London.

- Smith, M.P. 1982: Conodonts from the Ordovician of East Greenland. *Rapp. Grønlands geol. Unders.* 108, p. 14.
- Sommer, M. 1957: Geologie von Lyells Land (Nordostgrønland). *Meddr Grønland* 155(2), 157 pp.
- Steiger, R.H., Hansen, B.T., Schuler, C. Bär, M.T. & Henriksen, N. 1979: Isotopic age determination revealing the polyorogenic nature of the southern Caledonian fold belt in East Greenland. *J. Geol.* 87, 475-495.
- Wegmann, C.E. 1935: Preliminary report on the Caledonian orogeny in Christian X's Land (North-east Greenland). *Meddr Grønland* 103(3), 59 pp.
- Vidal, G. 1979: Acritarchs from the Upper Proterozoic and Lower Cambrian of East Greenland. *Bull. Grønlands geol. Unders.* 134, 40 pp.
- Wilcox, R.E., Harding, T.P. & Seely, D.R. 1973: Basic wrench tectonics. *AAPG Bull.* 57(1), 74-96.

This bag contains:

H.-J Bengaard, 1989: Geometrical and geological analysis of photogrammetrically measured deformed sediments of the fjord zone, central East Greenland. Grønlands geologiske Undersøgelse Open File Series No. 89/6, 101 pp.

Plate Ia:

Geological map 1:250 000 of the U. Proterozoic - L. Palaeozoic sediments of the fjord zone, central East Greenland.

Plate Ib:

Geological map 1:250 000 of the U. Proterozoic - L. Palaeozoic sediments of the fjord zone, central East Greenland. Legend.

Plate IIa:

Structural map 1:250 000 of the U. Proterozoic - L. Palaeozoic sediments of the fjord zone, central East Greenland.

Plate IIb:

Structural map 1:250 000 of the U. Proterozoic - L. Palaeozoic sediments of the fjord zone, central East Greenland. Legend.

Plate III:

Profiles 1:250 000 through the U. Proterozoic - L. Palaeozoic sediments of the fjord zone, central East Greenland.

Plate IVa:

Geological map 1:50 000 of western Ella Ø, central East Greenland.

Plate IVb:

Geological map 1:50 000 of western Ella Ø, central East Greenland. Legend.

Hans-Jørgen Bengaard, 1989:

Geometrical and geological analysis of photogrammetrically measured deformed sediments of the Fjord Zone, Central East Greenland.

Grønlands Geologiske Undersøgelse.

Plate Ia:

Geological map 1:250 000 of the U. Proterozoic - L. Palaeozoic sediments of the Fjord Zone, Central East Greenland.



Hans-Jørgen Bengaard, 1989:

Geometrical and geological analysis of photogrammetrically measured deformed sediments of the Fjord Zone, Central East Greenland.
Grønlands Geologiske Undersøgelse.

Plate Ib:

Geological map 1:250 000 of the U. Proterozoic - L. Palaeozoic sediments of the Legend.

GEOLOGICAL MAP 1:250.000 OF THE U. PROTEROZOIC - L. PALAEOZOIC
SEDIMENTS OF THE FJORD ZONE, CENTRAL EAST GREENLAND
LEGEND



 $\frac{1}{12}$ Strike and dip of bedding

 $\frac{1}{14}$ Direction and plunge of fold axis

 $\frac{1}{27}$ Fault with dip indicated

 Basal decollement

 Slide

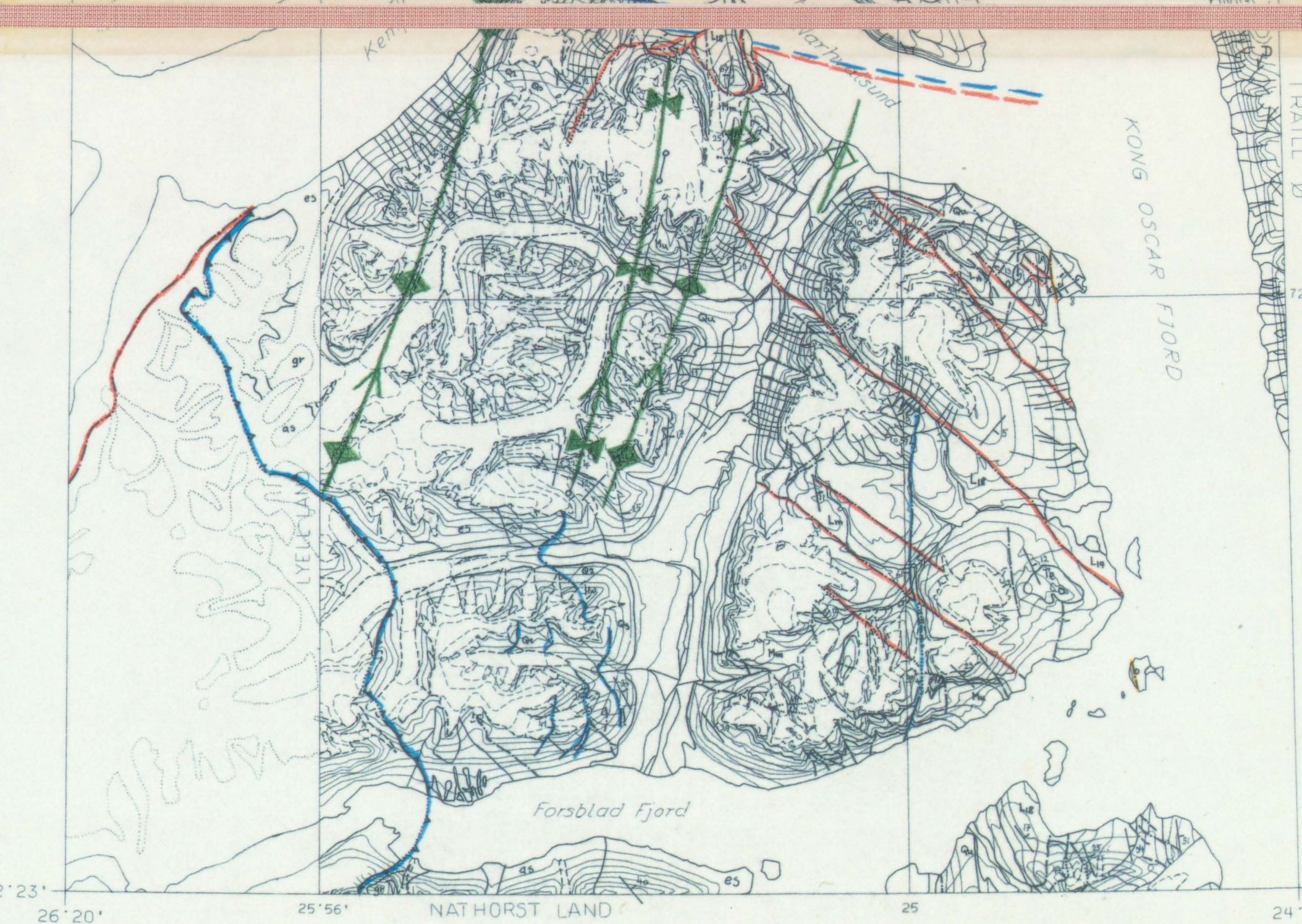
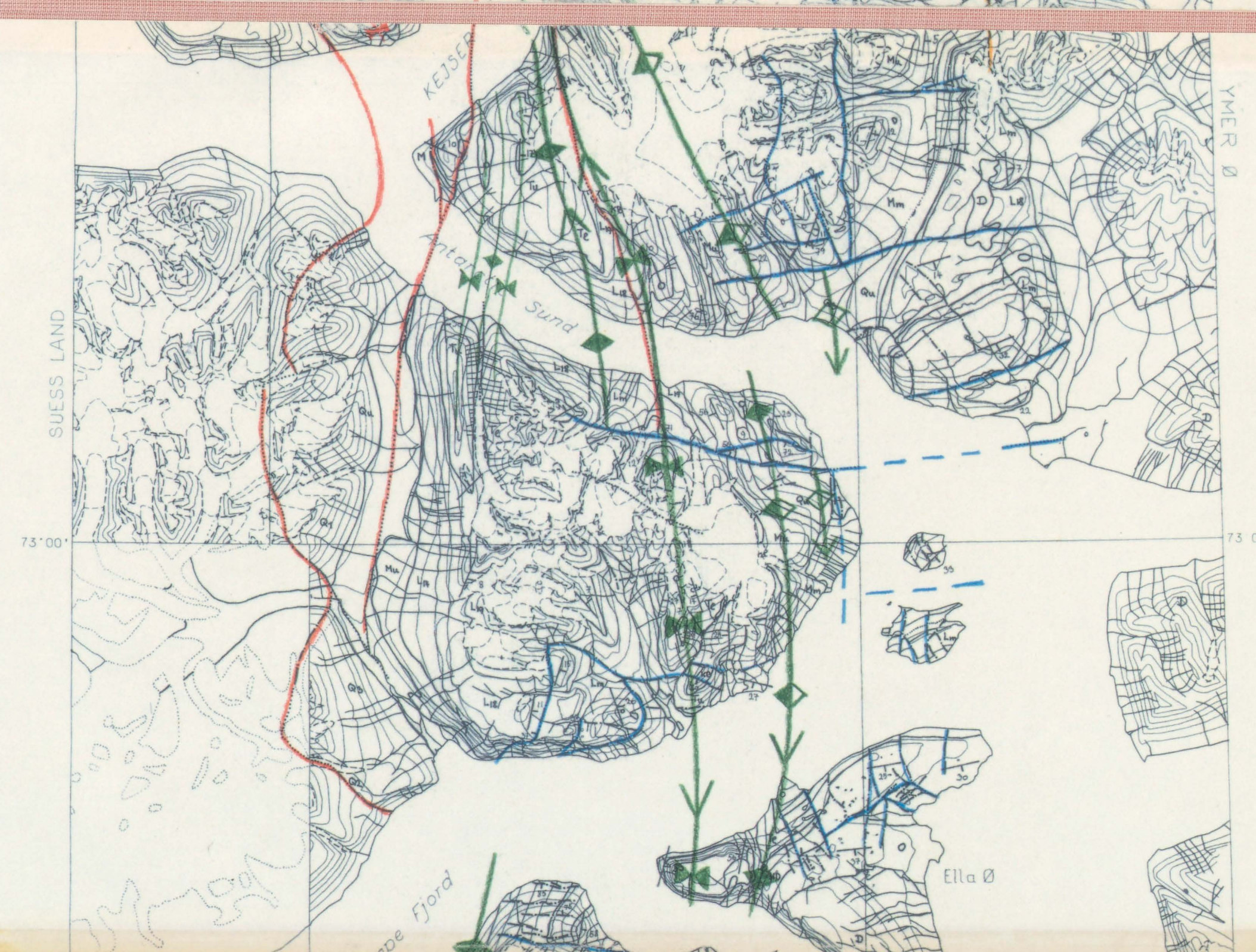
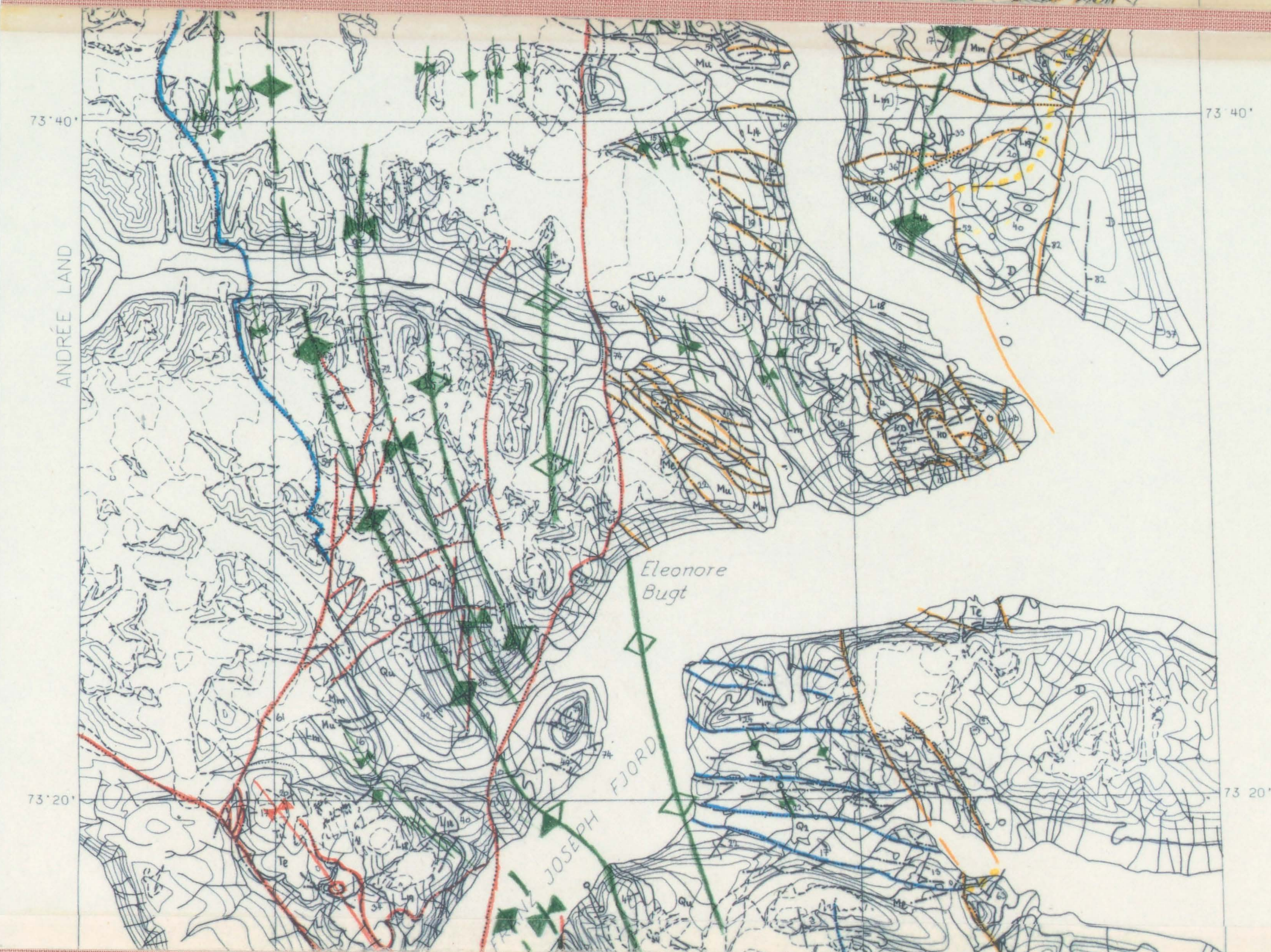
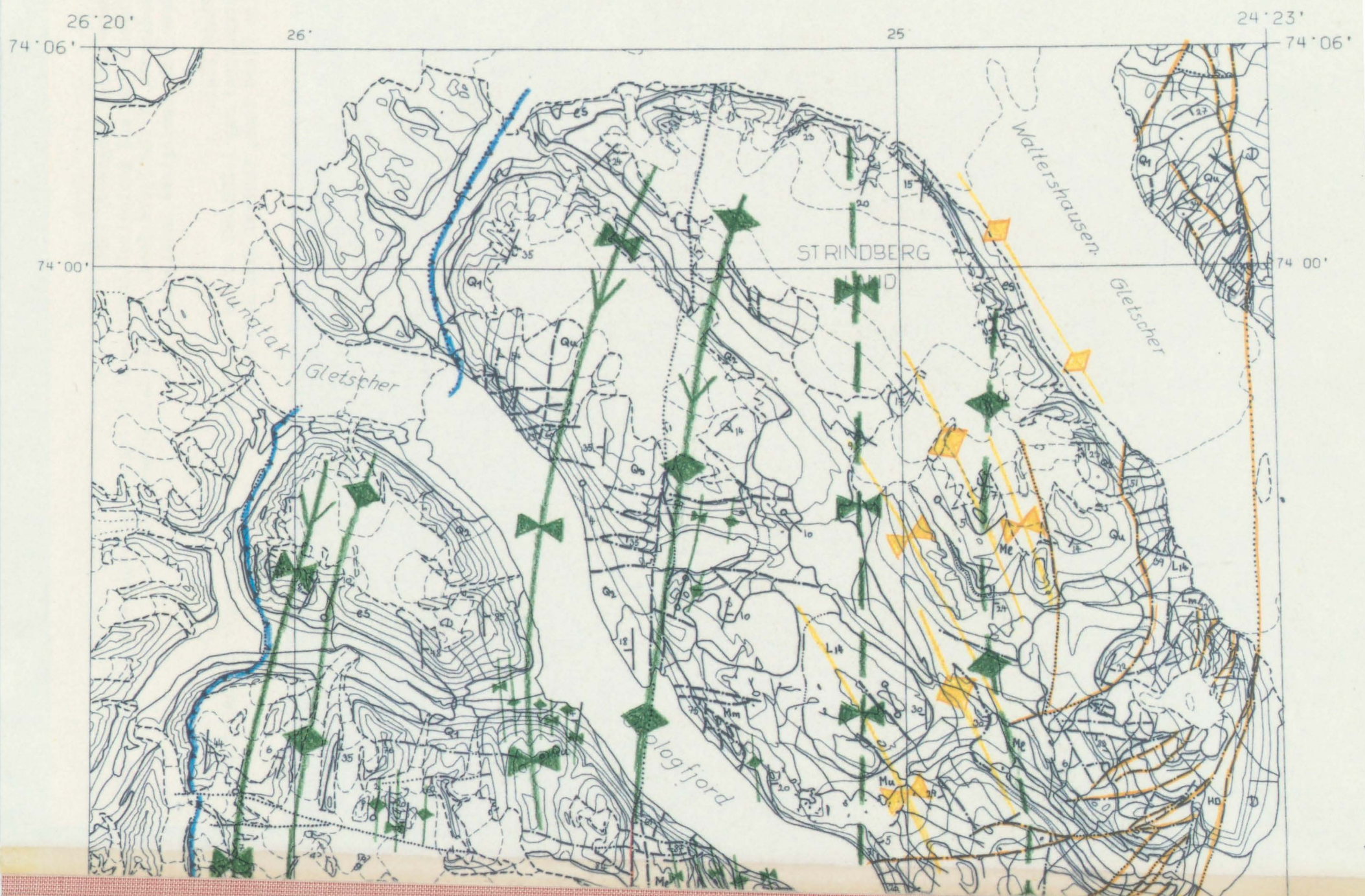
Hans-Jørgen Bengaard, 1989:

Geometrical and geological analysis of photogrammetrically measured deformed sediments of the Fjord Zone, Central East Greenland.

Grønlands Geologiske Undersøgelse.

Plate IIa:

Structural map 1:250 000 of the U. Proterozoic - L. Palaeozoic sediments of the Fjord Zone, Central East Greenland.



Hans-Jørgen Bengaard, 1989:

Geometrical and geological analysis of photogrammetrically measured deformed sediments of the Fjord Zone, Central East Greenland.
Grønlands Geologiske Undersøgelse.

Plate Iib:

Structural map 1:250 000 of the U. Proterozoic - L. Palaeozoic sediments of the Fjord Zone, Central East Greenland.

Legend.

STRUCTURAL MAP 1:250.000 OF THE U. PROTEROZOIC - L. PALAEOZOIC
 SEDIMENTS OF THE FJORD ZONE, CENTRAL EAST GREENLAND
 LEGEND

U. ORDOVICIAN STRUCTURES

-  *Syncline, major, well-defined, axial plunge indicated*
-  *—"—, —"—, ill-defined or inferred*
-  *—"—, minor*
-  *Anticline, major, well-defined, axial plunge indicated*
-  *—"—, —"—, ill-defined or inferred*
-  *—"—, minor*
-  *Anticlinal monocline*
-  *Axis of doming*
-  *Basal décollement surface*
-  *Fault*

DEVONIAN STRUCTURES ASSOCIATED WITH A BASEMENT UPLIFT
 WEST OF THE MAP AREA

-  *Fault*
-  *Syncline*

DEVONIAN STRUCTURES ASSOCIATED WITH THE WESTERN MARGIN
 OF THE GAUSS BASIN

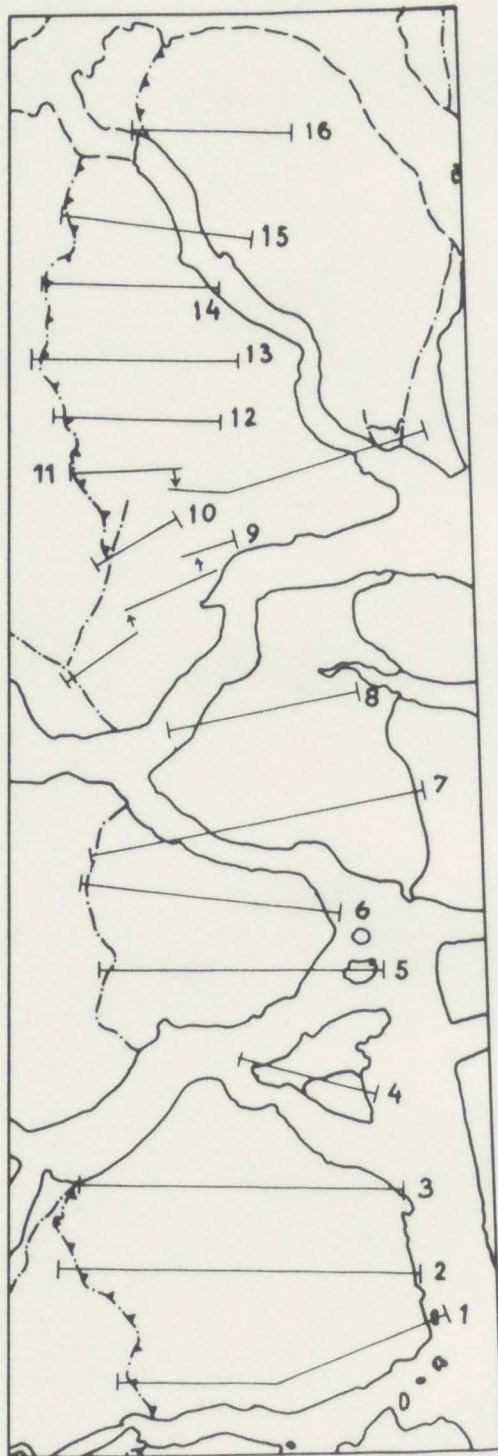
-  *Syncline*
-  *Anticline*
-  *Thrust*
-  *Fault*
-  *Slide*

Hans-Jørgen Bengaard, 1989:

Geometrical and geological analysis of photogrammetrically measured deformed sediments of the Fjord Zone, Central East Greenland.

Plate III:

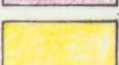
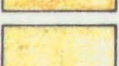
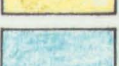
Profiles 1:250 000 through the U. Proterozoic - L. Palaeozoic sediments of the Fjord Zone, Central East Greenland.

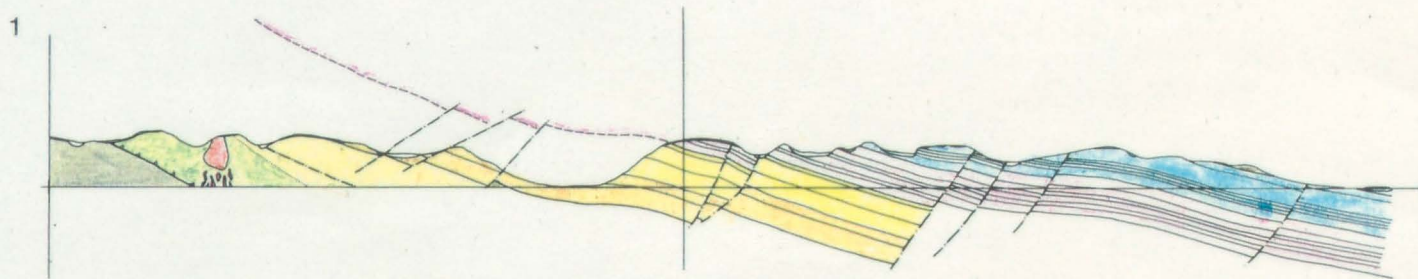
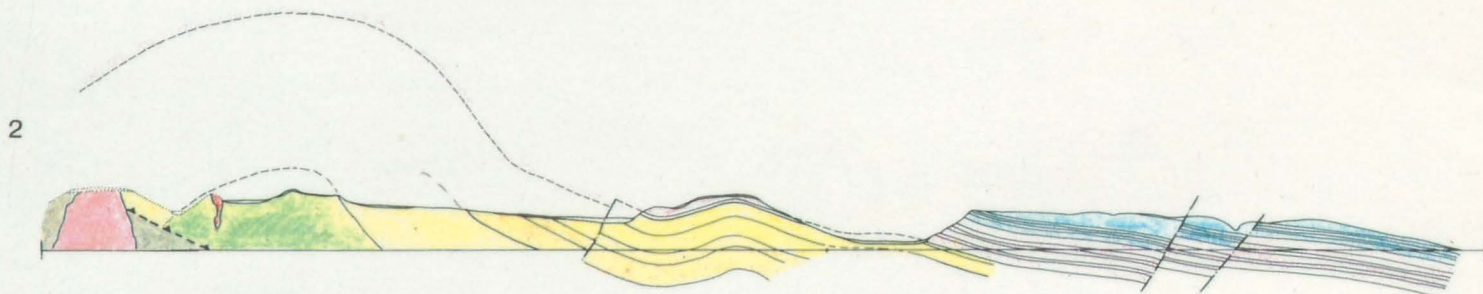
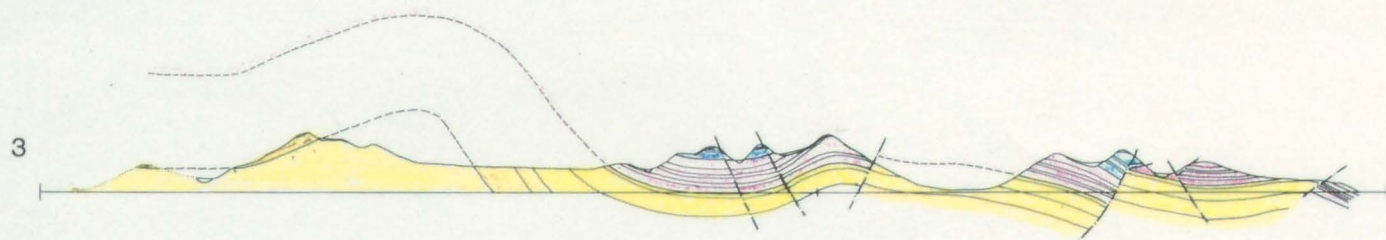


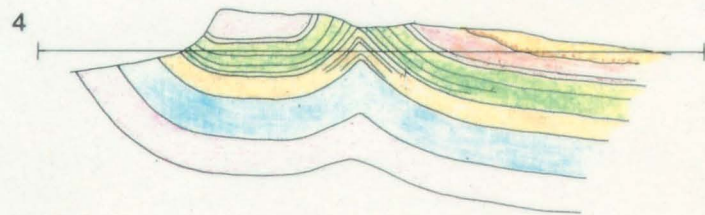
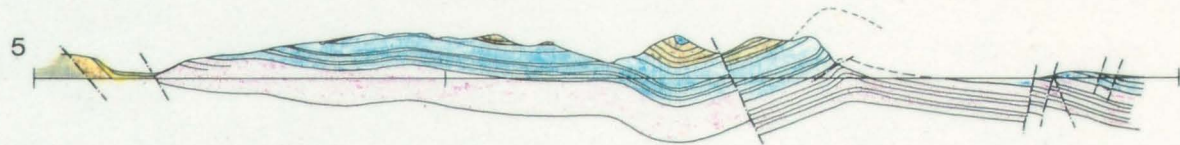
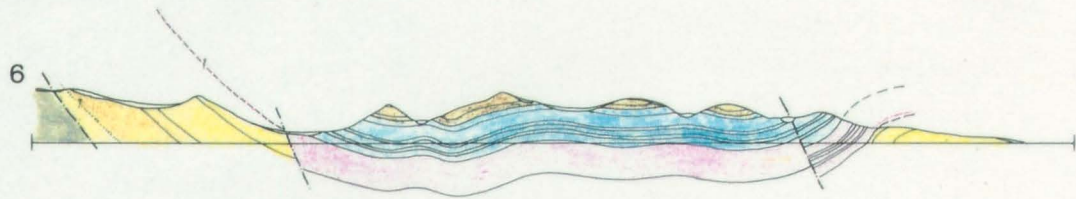
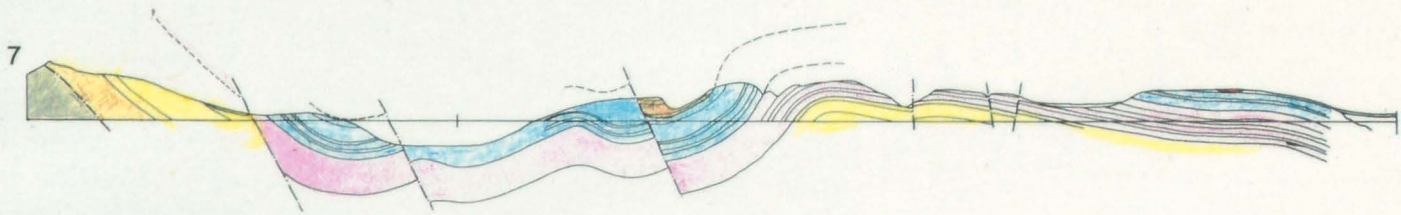
50 km

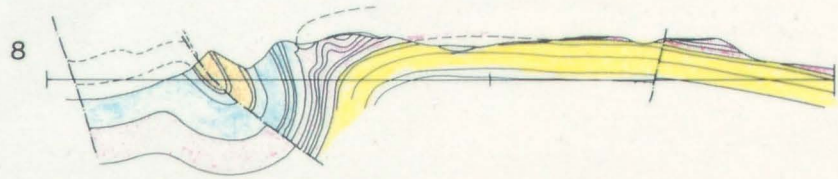
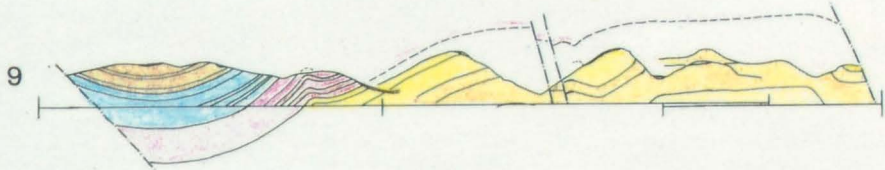
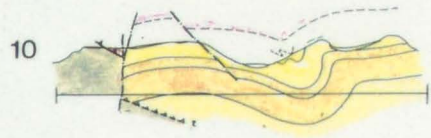
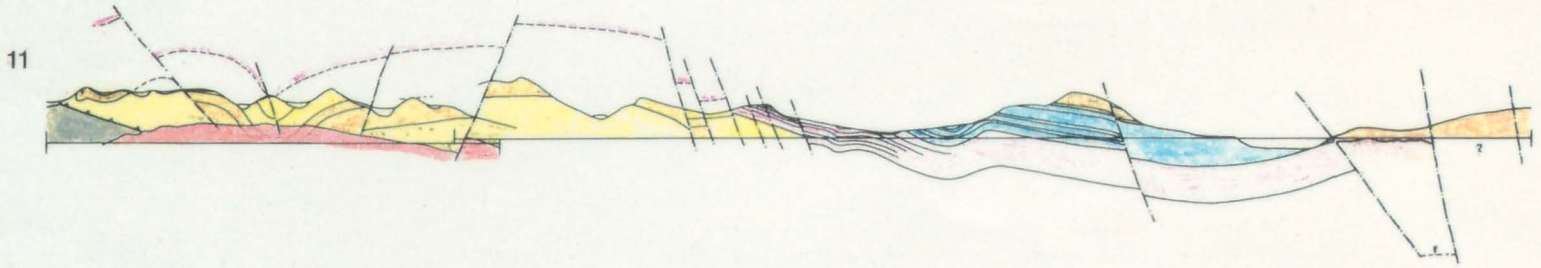
PROFILES 1:250.000

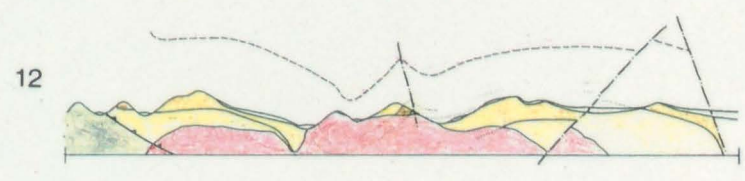
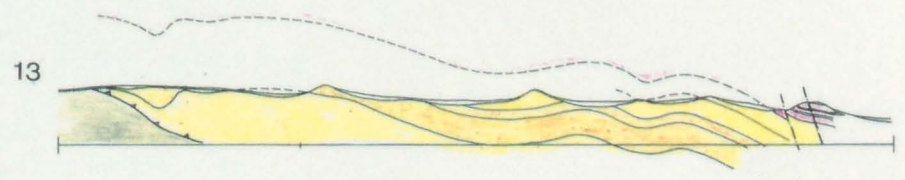
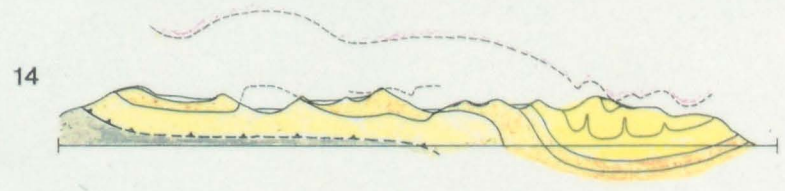
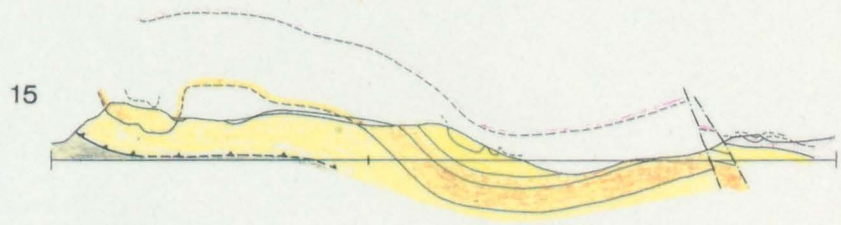
LEGEND

| | |
|---|--|
|  | <i>Granite intrusions</i> |
|  | <i>Devonian sediments</i> |
|  | <i>Antiklinalbugt Fm. - Narhvalsund Fm.</i> |
|  | <i>Kløftelv Fm. - Dolomite Point Fm.</i> |
|  | <i>Tillite Group</i> |
|  | <i>Eleonore Bay Group, Limestone - dolomite series</i> |
|  | ————— " —————, <i>Multicoloured series</i> |
|  | ————— " —————, <i>Quartzite series, bed group 3-6</i> |
|  | ————— " —————, ————— " —————, ————— " ————— 1-2 |
|  | ————— " —————, <i>Eremitdal series</i> |
|  | ————— " —————, <i>Alpefjord series</i> |
|  | <i>Older crystalline rocks</i> |









Hans-Jørgen Bengaard, 1989:

Geometrically and geological analysis of photogrammetrically measured deformed sediments of the Fjord Zone, Central East Greenland.

Grønlands Geologiske Undersøgelse.

Plate IVa:

Geological map 1:50 000 of Western Ella Ø, Central East Greenland.

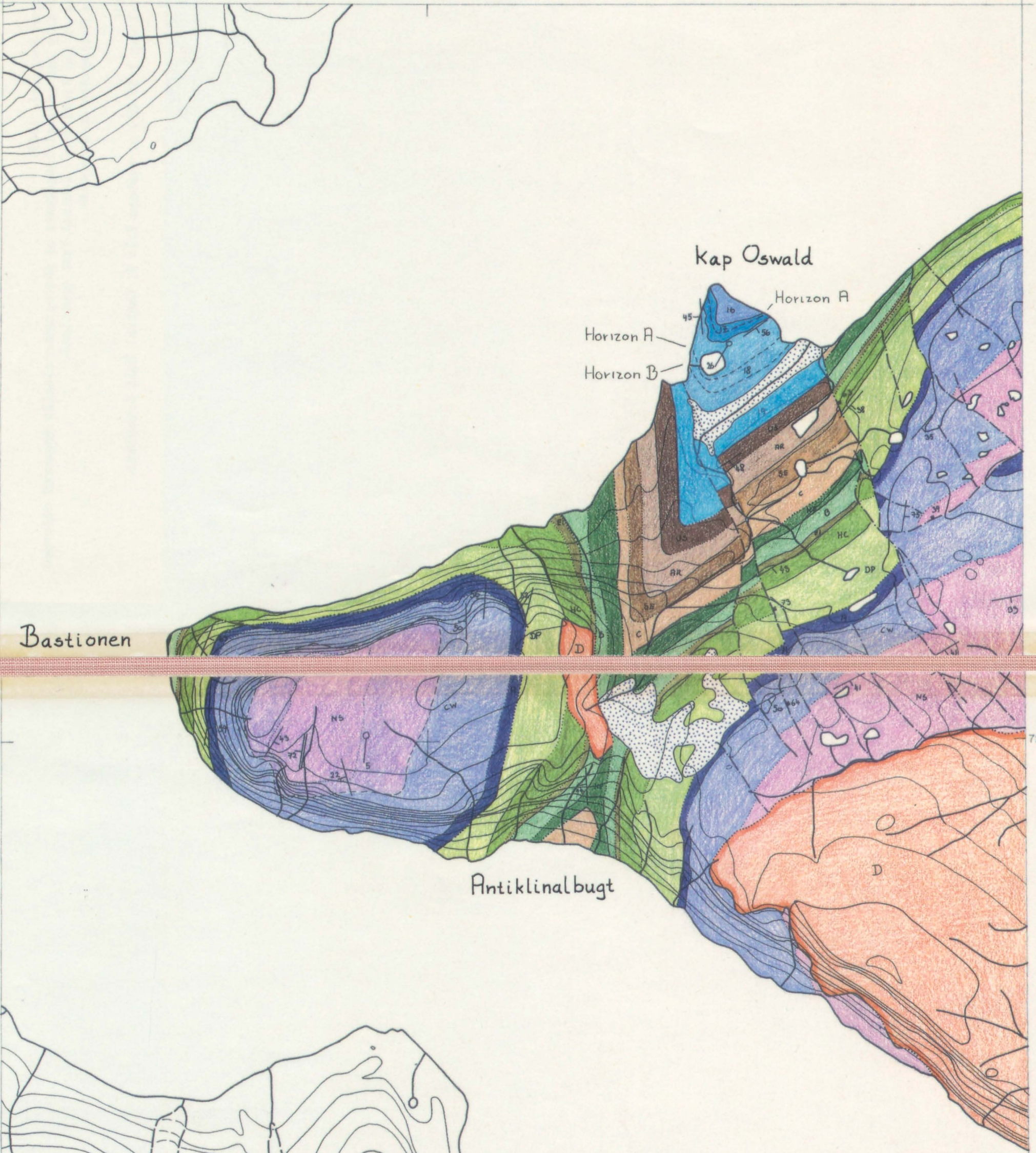
25° 25'

25° 15'

25° 01'

72° 55'

72° 51'



72° 50'

72° 50'

Antiklinalbugt

2° 46'

25° 25'

25° 15'

25° 01'

72° 4

Hans-Jørgen Bengaard, 1989:

Geometrical and geological analysis of photogrammetrically measured deformed sediments of the Fjord Zone, Central East Greenland.

Grønlands Geologiske Undersøgelse.

Plate IVb:

Geological map 1:50 000 of Western Ella ϕ , Central East Greenland.

Legend.

GEOLOGICAL MAP 1:50.000 OF WESTERN ELLA Ø,
CENTRAL EAST GREENLAND
LEGEND

